TESIS DE LA UNIVERSIDAD DE ZARAGOZA

2020 100

Cruz Octavio Robles Rovelo

Riego por aspersión a baja presión en coberturas totales y máquinas de riego

Departamento
Ciencias Agrarias y del Medio Natural

Director/es
Zapata Ruiz, Valvanera
Burguete Tolosa, Javier

ISSN 2254-7606

Prensas de la Universidad
Universidad Zaragoza

ISSN 2254-7606

Universidad Zaragoza
1542

Tesis Doctoral

RIEGO POR ASPERSIÓN A BAJA PRESIÓN EN COBERTURAS TOTALES Y MÁQUINAS DE RIEGO

Autor

Cruz Octavio Robles Rovelo

Director/es

Zapata Ruiz, Valvanera
Burguete Tolosa, Javier

UNIVERSIDAD DE ZARAGOZA

Ciencias Agrarias y del Medio Natural

2019

UNIVERSIDAD DE ZARAGOZA

FACULTAD DE VETERINARIA

DEPARTAMENTO DE CIENCIAS AGRARIAS
Y DEL MEDIO NATURAL

T E S I S D O C T O R A L

RIEGO POR ASPERSIÓN A BAJA PRESIÓN EN COBERTURAS TOTALES Y MÁQUINAS DE RIEGO

LOW-PRESSURE SPRINKLER IRRIGATION IN SOLID-SET AND CENTER PIVOT SYSTEMS

Presentada por

Cruz Octavio Robles Rovelo

En satisfacción de los requisitos necesarios para obtener el grado de Doctor

Directores: **Dra. María Valvanera Zapata Ruiz**
Dr. Javier Burguete Tolosa

ESTACIÓN EXPERIMENTAL DE AULA DEI
CSIC
CONSEJO SUPERIOR DE INVESTIGACIONES CIENTÍFICAS

Zaragoza, España
Abril 2019

La **Dra. María Valvanera Zapata Ruiz** y el **Dr. Javier Burguete Tolosa** ambos Científicos Titulares del grupo de investigación "Riego, Agronomía y Medio Ambiente" de la Estación Experimental de Aula Dei del CSIC (EEAD-CSIC),

CERTIFICAN

Que la Tesis Doctoral que lleva por título: "Riego por aspersión a baja presión en coberturas totales y máquinas de riego", ha sido realizada por el Ingeniero Civil de nacionalidad mejicana **CRUZ OCTAVIO ROBLES ROVELO** en el departamento de Riego, Agronomía y Medio Ambiente (EEAD-CSIC) bajo nuestra dirección.

Asimismo, informamos que la Tesis Doctoral corresponde con el Plan de Investigación que en su momento fue aprobado por el Departamento de Ciencias Agrarias y del Medio Natural de la Universidad de Zaragoza y que, a nuestro juicio, reúne las condiciones necesarias para optar al grado de Doctor del mismo.

Dra. María Valvanera Zapata Ruiz

Dr. Javier Burguete Tolosa

Zaragoza España, Abril de 2019

Avda. Montañana, 1005
Apdo. 13034, 50080
Zaragoza, España
Tel: (+34) 976 716 080

A Carmen† y Luis†

AGRADECIMIENTOS

Este trabajo no habría sido posible sin el apoyo de muchas personas a quienes quiero expresar mi más sincero agradecimiento en estas líneas:

A mis directores de tesis, Nery Zapata y Javier Burguete, por su disponibilidad y tan oportunos consejos, por la constante motivación y excelente dirección. Llevaré siempre presente sus enseñanzas, su amistad y apoyo incondicional. Gracias por las críticas y las discusiones científicas que me han permitido crecer profesionalmente. Gracias por su confianza, por hacerme sentir como en casa.

Gracias también a Borja Latorre, por tu valiosa ayuda y contribución al desarrollo de mi tesis, tu optimismo y consejos siempre tan alentadores. Para mí, como un director de tesis.

Al Ministerio de Economía, Industria y Competitividad del Gobierno de España por la financiación de mi beca predoctoral dentro del proyecto AGL2013-48728-C2-1-R.

Al grupo de "Riego, Agronomía y Medio Ambiente". A Enrique Playán por la amistad, su apoyo, su confianza y los consejos. A José Cavero por los consejos y por compartirme su conocimiento en este periodo de tesis, por echarme un cable cuando lo necesité. A Eva Medina, Pilar Paniagua y Miguel Millán, echaré de menos esas risas y esas salidas en especial a los "juepingos", gracias por estar siempre disponibles por ayudarme en el desarrollo de mi tesis, gracias por compartir sus conocimientos. A Juan Herrero, Carmen Castañeda, César Romano, gracias a todos por la ayuda, por la compañía, los consejos y los buenos momentos juntos. A todo el grupo, gracias amigos por acogerme en éste, por estar siempre dispuestos a ayudarme en lo laboral y en lo personal.

A todo el personal de la Estación Experimental de Aula Dei (EEAD-CSIC) que de alguna manera ha puesto su granito de arena para realizar este trabajo. Gracias a Miguel Izquierdo, Vicente Villarroya, Valero Pérez y Pablo García por el apoyo técnico.

A mis amigos y compañeros del CITA por la ayuda, los alegres momentos, las aventuras, las excursiones: Wafa Malik, Beatriz Moreno, María Jiménez, María Lorenzo, Daniel Isidoro, Farida Dechmi, Raquel Salvador, Daniel Crespo, Dolores Quílez, Ramón Isla, Rosa Gómez, Eva Herrero, Javier Tapia.

A mis amigos y compañeros que han pasado por el despacho 0.7, gracias por esas risas y momentos juntos: Estela Luna, David Carmona, El Habib El Malki, Ramiro Félix, Francisco Montoya, Mario Morales, Sophia Bahddou.

A mis amigos y compañeros por los momentos juntos, las fiestas, las excursiones, las cenas y el apoyo incondicional, los echaré de menos: Irene, Iván, Jorge, Brenda, Adrián, Samuel, María, Najla, Chesco, Carlos, Nick, Miriam, Fran, Alejandro, Pierre, Valerie, Arantxa, Edgar, Miquel, Yuri y Álvaro, Jorge, Juan, Tamara, Nacho y Adrián. Incluidos también los salseros: Mariela, Sara, Ernesto, Mirna, Carmen, Dida, Karen, Yeni y Aracely.

Al casero Paco y a su familia por hacerme sentir parte de ella, por abrirme las puertas de casa. Gracias a todos por el apoyo moral, los consejos para la vida diaria y los buenos ratos.

I wish to acknowledge the hospitality of the Land Air and Water Resources Department from the University of California Davis, especially to my supervisor Daniele Zaccaria for his kindly acceptance in his group. Thanks to Giulia Marino, Michael Whiting, Cayle Little, Rick Snyder, Mahesh Maskey, and Octavio Lagos for sharing their knowledge and good times together. To all the personnel of the department from whom I´ve learned.

A mis padres que, aunque no estuvieron presentes para ver concluido este logro, los he llevado siempre en mis pensamientos, algún día nos encontraremos de nuevo. A mis hermanos Eber y Zaira y al pequeño Alex. Gracias familia por ser mi mayor motivación cada día.

A mis amigos y mi familia en México por el apoyo y ánimos a la distancia.

¡Muchas gracias a todos!

ÍNDICE

Índice de tablas

Índice de figuras

CAPÍTULO I. INTRODUCCIÓN

Introducción

De acuerdo a la Organización de las Naciones Unidas en el reporte del año 2017 sobre la población mundial existen 7600 millones de personas en la actualidad, y se pronostican 8600 millones para el año 2030 y 9800 millones para el año 2050, con una tasa de incremento aproximada de 83 millones de personas por año. Este 29% de incremento poblacional al año 2050 supone incrementar la producción de cultivos para abastecer la demanda mundial. A su vez, la producción agrícola está limitada por la creciente escasez del recurso agua y la adaptación al cambio climático (FAO, 2009; ONU, 2017; FAO, 2018).

Como alternativa de solución, en 2015 la asamblea General de la ONU aprobó la Agenda 2030 en la cual se especifican 17 objetivos de desarrollo sostenible. De los anteriores, 12 están relacionados con acciones de cambio climático. Por ejemplo, el número dos establece: "poner fin al hambre siguiendo entre otros hitos el de aumentar la productividad agrícola, la producción y los ingresos de los productores a pequeña escala, así como aumentar en la investigación y servicios de extensión agrícola". Los planes estratégicos anteriores junto con el Acuerdo de Paris de 2016 proveen oportunidades de adaptación y acciones de mitigación de cambio climático en agricultura (ONU, 2015; FAO, 2016).

El cambio climático repercute negativamente en las cosechas y en el rendimiento de cultivos. De los sectores de la economía, el energético es el primer contribuyente en las emisiones de gases de efecto invernadero (GEI) seguido por el sector agrícola (FAO, 2018). La producción de energía se ha incrementado en 2,5 veces desde 1971 al año 2016 (IEA, 2018) contribuyendo proporcionalmente al incremento de los GEI, mientras que el sector agrícola ha incrementado los GEI un 1,1% anual en el periodo entre 2000-2010 (Tubiello y col., 2013).

De acuerdo con el informe de Alexandratos y Bruinsma (2012) sobre la proyección mundial de la agricultura al año 2050, se estima una tasa de crecimiento anual de 0,8% en la producción de cultivos entre el año 2030 y 2050, de la cual el 90% se llevará a cabo en países en desarrollo contribuyendo en un 74% de la producción mundial. Para lograr este crecimiento, los autores reportan que es necesario incrementar tres aspectos: el rendimiento de cultivos en un 80%, la superficie de tierra cultivable en un 10% y la intensidad de cultivos en un 10%. La expansión de la tierra cultivable será una clave importante para países en desarrollo de América Latina y África Subsahariana en donde se utiliza menos del 20% de la tierra para producción de cultivos. La tierra mundial cultivable se estima en 1661 millones de hectáreas para el año 2050, con una tasa de crecimiento anual de 0,1% sobre los 1592 millones registrados en el año 2005. Alexandratos y Bruinsma (2012) proyectan que la expansión de tierra equipada para riego en términos netos es de 20 millones de hectáreas para el año 2050 (6,6%) pasando de 302 millones (año 2005) a 322 millones en 2050. Para lograr un incremento en la tierra cultivada es necesaria

una regeneración en los sistemas de riego actuales. Se estima que anualmente el 2,5% del regadío actual deberá sustituirse o rehabilitarse por nuevos sistemas de riego suponiendo una vida útil de los mismos de 40 años.

La modernización de regadíos pretende mejorar el uso de los recursos y el servicio a los usuarios mediante la transformación de las infraestructuras de riego y la mejora de la gestión del agua de riego. En España, desde los años 90, una parte importante de la inversión en modernización se ha destinado a cambiar las redes de canales abiertos usados en riego por superficie, por redes de distribución colectivas de riego presurizado, para riego por aspersión o goteo (Playán y Mateos, 2006). Estos planes de modernización aúnan la iniciativa privada con fondos públicos nacionales y europeos, y son los responsables del cambio de las infraestructuras de aproximadamente 2 millones de los 3,7 millones de hectáreas regadas actualmente en España, siendo ahora el riego localizado el mayoritario con un 50% de la superficie regada, en segundo lugar el riego por gravedad con un 25%, en tercero el riego por aspersión con un 16% y finalmente los sistemas automotrices con un 9% (ESYRCE, 2017). La transición de un sistema de riego a otro depende de las condiciones locales y sobre todo del cultivo al que se oriente.

En contraste, en China, a pesar del crecimiento poblacional, del incremento de sus zonas áridas y la sequía de las últimas décadas, se presentan diversos problemas para adoptar las medidas para la mejora en la gestión del agua que el gobierno ha propuesto. Estos problemas, se deben en parte a la falta de apoyo por parte de los agricultores y las asociaciones de usuarios del agua (Hu y col., 2014). En China, de los 69,8 millones de hectáreas equipadas para riego, el 85% se encuentra bajo sistemas de riego superficial, el 4% con riego por aspersión y 1% con riego localizado, no hay registro del 10% faltante. El 62% del agua de riego en China proviene de fuentes superficiales y el 5% de aguas residuales (AQUASAT, 2017). En Estados Unidos de América, de los 26,7 millones de ha equipadas para riego, el 45% se encuentran bajo riego superficial, el 47% con riego por aspersión y 7% bajo riego localizado. El 64% del agua de riego proviene de fuentes subterráneas y el 35% de fuentes superficiales (AQUASAT, 2017).

Las modernizaciones de los sistemas de riego por superficie a riego presurizado han supuesto una disminución del uso del agua por superficie, pero también un incremento en la demanda eléctrica. En España, Corominas (2009) reporta una reducción del 21% en el uso de agua y un aumento de 657% en la demanda de electricidad entre los años 1950 y 2007. Además, con la derogación de la tarifa eléctrica para el sector agrícola en el año 2008, la energía se ha convertido en un coste de producción muy importante en la agricultura de regadío. Rodríguez y col. (2011) reportan un incremento de 120% en el coste eléctrico en los dos años posteriores a esta derogación. Esta situación ha forzado a las comunidades de regantes a optar por medidas como reorganizar los riegos inicialmente diseñados para regar a la demanda por el riego en periodos de energía más barata. Considerando estos retos, muchos trabajos de investigación se han enfocado en optimizar el uso de la energía buscando alternativas para disminuir su consumo y sus costes. Una de

las líneas de trabajo ha sido la optimización de los equipos de bombeo y metodologías de sectorización de las redes de riego (Rodríguez-Díaz y col., 2009; Moreno y col., 2010; Fernández García y col., 2013; Córcoles y col., 2016). Sin embargo, es necesario seguir avanzado en la optimización de la energía en el contexto general de la agricultura de regadío prestando atención al riego en parcela, al cultivo, a su rendimiento y a los beneficios económicos.

En el riego en parcela, se han propuesto diversas alternativas para regar con menor energía usando diversos sistemas de riego:

- A partir de los años 60, comienzan los primeros trabajos de investigación con el sistema de riego por goteo sub-superficial (RGS) en países como Israel y Estados Unidos, particularmente en el estado de California. De estos estudios se detectaron problemas que impidieron el uso del RGS, tales como la obturación en los emisores y baja distribución de uniformidad (Lamm y col., 2012). No fue sino hasta los años 80 que la metodología de RGS fue adoptada como parte del riego agrícola moderno, con el uso de materiales de mejor calidad y mejores diseños de emisores (Camp y col., 2000). El RGS se presenta como una alternativa para incrementar la eficiencia en producción y reducir la tasa de aplicación, además de requerir una baja presión de operación en los emisores (100 kPa-150 kPa). Sin embargo, estos sistemas no se adaptan a cualquier tipo de suelo, debido a la percolación profunda. También es importante tener en cuenta que el agua de RGS asciende por capilaridad y que, en suelos arenosos, esta propiedad se complica (Salvador y Aragüés, 2013). Otro problema es que, dependiendo del tipo de suelo, puede haber dificultad para localizar las fugas y repararlas, el tiempo de reparación y la mano de obra son también dos inconvenientes. Además, debe considerarse una importante inversión inicial para el sistema de filtrado y su mantenimiento para evitar acumulación de sales en los emisores (Zaccaria y col., 2017).

- Por otra parte, en 1952 se creó el sistema de riego automotriz de tipo pivote central o lateral (Splinter, 1976) usado para regar superficies de gran tamaño. Inicialmente, equipados con aspersores de impacto que operaban a altas presiones de hasta 550 kPa que después fueron sustituidos por los hoy conocidos aspersores spray de plato fijo (FSPS) y los aspersores spray de plato de rotación (RSPS) cuyas presiones de operación se limitan a 206 kPa. Diversas formas de riego con pivote central han surgido como el sistema de aplicación de precisión de baja energía (LEPA) (Lyle y Bordovsky, 1981), el sistema de aplicación de spray de elevación media (MESA) o el de aplicación de spray de baja elevación (LESA). El sistema MESA usa aspersores que riegan a presiones de entre 100 kPa y 140 kPa, mientras que la presión usada en LEPA y LESA es de entre 40 kPa y 70 kPa. El sistema LEPA limita su uso respecto a los otros debido a un tratamiento especial en la siembra (circular) y en el suelo (bacheo).

- Los sistemas de riego por aspersión en cobertura total implementan aspersores de impacto que operan a presiones entre 300 kPa y 400 kPa. Sin embargo, estudios recientes sobre eventos de riego individuales sin cultivo, indican que es posible reducir esta presión a 200 kPa sin afectar demasiado a la calidad de riego en términos de uniformidad (Playán y col., 2006; Paniagua, 2015). Diversas variables afectan el patrón de distribución de agua en los sistemas de riego de cobertura total como el espaciamiento entre aspersores y laterales, velocidad y dirección de viento, tipo de aspersor, presión de operación, tamaño de boquillas y altura del aspersor (Tarjuelo y col., 1999; Playán y col., 2005).

Los beneficios netos de los agricultores son el mayor criterio para determinar la aceptación de cambios en diseño u operación en los sistemas de riego al disminuir su presión de trabajo. Por lo tanto, es de suma importancia evaluar los efectos de disminuir la presión de operación en los aspersores de impacto de cobertura total y en los aspersores de los sistemas pivote central, analizando las variables que afectan a la distribución de agua, su repercusión en la calidad de riego y en la producción de cultivo.

Además, los modelos de simulación de redes colectivas de riego y de simulación de riego por aspersión en parcela, se presentan como una alternativa para la mejora del diseño de los mismos. Diversos modelos de simulación se han presentado para la optimización del diseño de redes colectivas de riego, optimizando el diseño de la red desde el punto de vista económico e hidráulico (Aliod y col., 1998; Roosman, 2000; Lamaddalena y Sagardoy, 2000). Otros autores analizan las implicaciones de la meteorología y del diseño en parcela de la red general (Zapata y col., 2007; Kadraa y Lamaddalena, 2010).

Por otro lado, Delirhasannia y col. (2010) reportan que, desde los años 60, diversos autores han trabajado en el desarrollo de modelos de simulación en pivote central que se basan en: 1) el análisis de diferentes curvas radiales de aplicación de agua de aspersores individuales, 2) el análisis del espaciamiento entre aspersores individuales y el solapamiento de sus pluviometrías, 3) valoración de la calidad del riego en términos estadísticos del solapamiento en pivote central y 4) la simulación del movimiento de sistemas autopropulsados y su distribución de agua en el suelo. Como parte de los esfuerzos de modelización en máquinas de riego, Ouazaa y col. (2014) proponen un modelo balístico que simula la distribución de agua de emisores tipo RSPS y FSPS combinando diferentes presiones, boquillas y condiciones meteorológicas. Posteriormente Ouazaa y col. (2016) analizan para una configuración de boquillas sobre un pívot con aspersores FSPS, el efecto de la alineación de sus torres y de la variabilidad meteorológica en la calidad de los riegos aplicados y en la producción de un cultivo de maíz.

En cuanto a los modelos de simulación de riego por aspersión en cobertura total y aspersores aislados, surgen en los años 80 y se basan en la segunda Ley de Newton utilizando la teoría balística para describir la trayectoria de gotas individuales (Fukui y

col., 1980). Estos modelos consideran diversos factores como: la distribución de los tamaños de gotas, el rango de diámetros de las mismas, la simulación de su trayectoria mediante métodos numéricos (considerando las mayores fuerzas que actúan sobre ellas, como el peso y la resistencia aerodinámica). Con estas consideraciones, los modelos pronostican el patrón de aplicación de agua considerando los efectos del viento, las pérdidas por evaporación y arrastre y finalmente la lámina de riego aplicada en una superficie dada (von Bernuth y Gilley, 1984; Vories y col., 1987; Seginer y col., 1991; Carrión y col., 2001; Playán y col., 2006). Otros trabajos como el de Dechmi y col. (2004) combinan la simulación balística de riego por aspersión con la simulación del desarrollo de un cultivo de maíz. Zapata y col. (2017) presentan un modelo de riego por aspersión aplicado a una zona regable incorporando la simulación balística, el desarrollo del cultivo y la simulación hidráulica de la red colectiva.

Es necesario continuar con los esfuerzos para mejorar la simulación del reparto de agua en riego por aspersión en cobertura total y máquinas de riego a nivel de parcela, generalizando los modelos para implementarlos con diversos tipos de aspersores y bajo diversas condiciones de operación como la presión de operación, las condiciones meteorológicas, los espaciamientos en aspersores, entre otros. Es también necesario realizar mejoras numéricas a los modelos de simulación que permitan corregir los errores de simulación actuales y el tiempo de cálculo en procesos de calibración y simulación. La automatización de los procesos anteriores y su integración en una herramienta, supondría reproducir, bajo cualquier escenario, el riego de los diferentes tipos de aspersores de manera más eficiente.

Una de las primeras propuestas del riego por aspersión a baja presión en aspersores de impacto fue desarrollada por Kincaid (1991). Dicho autor propuso incorporar una placa deflectora al brazo de impacto del aspersor para mejorar el reparto de agua cuando trabajan a baja presión. Esta modificación permitió que las gotas llegaran a caer en la parte intermedia del radio mojado, mejorando ligeramente el patrón de aplicación de los aspersores a baja presión, pasando de una forma de rosquilla a una forma triangular. El patrón de aplicación de forma triangular en sección trasversal, mejora el coeficiente de uniformidad de Christiansen (1942) –CUC– respecto al patrón de rosquilla al solapar el riego de un conjunto de aspersores. En la actualidad, con los desarrollos tecnológicos de la iniciativa privada, han surgido nuevos aspersores de impacto que adoptan los desarrollos de Kincaid para operar a baja presión.

En el trabajo de Playán y col. (2006), se desarrollaron estudios técnicos caracterizando y simulando el riego de dos aspersores de impacto de manera individual y en cobertura total. Sus resultados fueron alentadores al notar pequeñas diferencias (< 5%) en la distribución de uniformidad entre el riego de 300 kPa y 200 kPa en cobertura total utilizando espaciamientos convencionales. En un estudio más reciente, Paniagua (2015) analizó este efecto de reducción de presión (de 300 kPa a 200 kPa) usando aspersores en cobertura total con las modificaciones sugeridas por Kincaid (1991). Ella concluye que, los

aspersores modificados operando a 200 kPa producen un riego adecuado (con patrones de riego triangular en su sección transversal) con CUC de hasta 92% en cobertura total.

Los estudios anteriores sugieren que disminuir la presión en un tercio respecto a la convencional es técnicamente posible cumpliendo con los estándares de calidad de riego por aspersión. Sin embargo, es necesario evaluar el efecto estacional de esta reducción de presión y analizar desde el punto de vista agronómico el efecto que tiene sobre el desarrollo y producción de un cultivo. Es importante tener en cuenta que pueden existir mermas en la producción de cultivo. De ser así, es también necesario valorar si estas diferencias de producción respecto al riego convencional pueden ser amortizadas por el ahorro energético que supone disminuir la presión.

En esta tesis se realiza un estudio experimental para analizar la viabilidad técnica y agronómica de la disminución de un tercio de la presión convencional en aspersores de impacto. Se propone trabajar sobre un cultivo de maíz, pues ante alguna deficiencia de riego, ésta puede ser fácilmente visible ya que es un cultivo sensible al estrés hídrico. También se analizará la viabilidad técnica del riego a baja presión en sistemas autopropulsados de riego por aspersión. Además, se desarrollarán modificaciones a un modelo balístico para poder aplicar dicha teoría a la simulación del riego por aspersión tanto en coberturas totales como en máquinas de riego.

Referencias

AQUASAT, 2017. AQUASTAT. Area equiped for irrigation; prepared by AQUASTAT, FAO's Global Information System; Food and Agriculture Organization of the United Nations: Roma, Italy, 2014 (http://www.fao.org/nr/water/aquastat/data/irrs/readPdf.html?f=CHNIRR_ eng.pdf).

Alexandratos, N., Bruinsma, J., 2012. World agricultural towards 2030-2050: the 2012 revision. FAO, ESA Working Paper No. 12–03.

Aliod, R., Eizaguerri, A., Estrada, C., Guillén, J., 1998. Development and validation of hydraulic modeling tools for pressurized irrigation networks. Hydroinformatics 98, Horsholm, Denmark. 545–552.

Carrión, P., Tarjuelo, J.M., Montero, J., 2001. SIRIAS: a simulation model for sprinkler irrigation: I. Description of the model. Irrig. Sci. 20, 73–84.

Camp, C. R., Lamm, F.R., Evans, R.G., Phene, C.J., 2000. Subsurface drip irrigation: Past, present and future. In proc. of the 4th Decennial Nat'l Irrigation Symp., Phoenix, AZ, Nov. 14-16. pp. 363–372.

Christiansen, J.E., 1942. Irrigation by sprinkling. Agric. Exp. Stn. Bull. 670. Univ. of California, Berkeley.

Corominas, J., 2009. Agua y energía en el riego en la época de la sostenibilidad. Ingeniería del Agua, 17(3), 219–233.

Córcoles, J.I., Tarjuelo, J.M., Moreno, M.A., 2016. Pumping station regulation in on-demand irrigation networks using strategic control nodes. Agric Water Manag 163, 48–56.

Dechmi, F., Playán, E., Cavero, J., Martínez-Cob, A., Faci, J.M., 2004. A coupled crop and solid-set sprinkler simulation model: I. Model development. J. Irrig. Drain. Eng. ASCE. 130 (6), 499–510.

Delirhasannia, R., Sadraddini, A.A., Nazemi, A.H., Farsadizadeh, D., Playán, E., 2010. Dynamic model for water application using centre pivot irrigation. 105, 476─485.

ESYRCE, 2017. Encuesta de superficies y rendimientos de cultivos en España. Ministerio de Agricultura y Pesca Alimentación y Medio Ambiente -MAPAMA. p 101.

FAO, 2009. High Level Expert Forum - How to Feed the World in 2050. Global agriculture towards 2050. Rome 12-13 October 2009. p.4. (http://www.fao.org/fileadmin/templates/wsfs/docs/Issues_papers/HLEF2050_Global_Agriculture.pdf).

FAO, 2016. Coping with water scarcity in agriculture, a global framework for action in a changing climate. p.12. (http://www.fao.org/3/a-i6459e.pdf).

FAO, 2018. The future of food and agriculture – Alternative pathways to 2050. Summary version. Rome, Italy, p. 68. (http://www.fao.org/3/ca1553en /CA1553EN.pdf).

Fernández García, I., Rodríguez Díaz, J.A., Camacho Poyato, E., Montesinos, P., 2013. Optimal operation of pressurized irrigation networks with several supply sources. Water Resour. Manag. 27, 2855–2869.

Fukui, Y., Nakanishi, K., Okamura, S., 1980. Computer evaluation of sprinkler irrigation uniformity. Irrig. Sci. 2, 23–32.

Hu, X.J.; Xiong, Y.C.; Li, Y.J.;Wang, J.X.; Li, F.M.;Wang, H.Y.; Li, L.L., 2014. Integrated water resources management and water users' associations in the arid region of northwest China: A case study of farmers' perceptions. J. Environ. Manag. 145, 162–169.

IEA, 2018. World energy balances: overview. Statistics. International Energy Agency. p. 24.

Khadra, R., Lamaddalena, N., 2010. Development of a decision support system for irrigation systems analysis. Wat. Resour. Manag. 24, 3279–3297.

Kincaid, DC 1991. Impact sprinkler pattern modification. Transaction of the ASAE 34(6), 2397–2403.

Lamaddalena, N., Sagardoy, J.A., 2000. Performance analysis of on-demand pressurized irrigation systems. Irrig. and Drain. paper, 59. FAO. Rome, Italy.

Lamm, F.R., Bordovsky, J.P., Schwankl, L.J., Grabow, G.L., Peters, R.T., Colaizzi, P.D., Trooien, T.P., Porter, D.O., 2012. Subsurface drip irrigation: status of the technology in 2010. Am. Soc. Agric. Biol. Eng. 55, 483–491.

Lyle, W.M., Bordovsky, J. P., 1981. Low energy precision application (LEPA) irrigation system. Trans. of ASAE. 24(5), 1241–1245.

Moreno, M.A., Ortega, J.F., Córcoles, J.I., Martínez, A., Tarjuelo, J.M., 2010. Energy analysis of irrigation delivery systems: monitoring and evaluation of proposed measures for improving energy efficiency. Irrig. Sci. 28, 445–460.

ONU, 2015. Transformar nuestro mundo: la Agenda 2030 para el Desarrollo Sostenible. Asamblea General de Organización de las Naciones Unidas. Nueva York, Septiembre 2015. p.40. versión en español (http://www.un.org/ga/search/view_doc. asp?symbol=A/RES /70/1&Lang=S).

ONU, 2017. World population 2017. Department of economics and social affairs. Popular division. p.2. (www.unpopulation.org).

Ouazaa, S., Burguete, J., Paniagua, P., Salvador, R., Zapata, N., 2014. Simulating water distribution patterns for fixed spray plate sprinkler using the ballistic theory. Spanish Journal of Agricultural Research, 12(3), 850–863.

Ouazaa, S., Latorre, B., Burguete, J., Zapata, N., 2016. Effect of intra-irrigation meteorological variability on seasonal center-pivot irrigation performance and corn yield. Agric. Water Manage. 177, 201–2014.

Paniagua, M.P., 2015. Mejora del riego por aspersión en parcela. PhD Dissertation. Universidad de Zaragoza, 261 p (in Spanish).

Playán, E., Mateos, L., 2006. Modernization and optimization of irrigation systems to increase water productivity. Agric. Water Manage. 80, 100–116.

Playán, E., Salvador, R., Faci, J.M., Zapata, N., Martínez-Cob, A., Sánchez, I., 2005. Day and night wind drift and evaporation losses in sprinkler solid-sets and moving laterals. Agric. Water Manage. 76 (3), 139–159.

Playán, E., Zapata, N., Faci, J. M., Tolosa, D., Lacueva, J.L., Pelegrín, J., Salvador, R., Sánchez, I., Lafita, A., 2006. Assessing sprinkler irrigation uniformity using a ballistic simulation model. Agric. Water Manage. 84 (1–2), 89–100.

Rodríguez Díaz, J.A., López Luque, R., Carrillo Cobo, M.T., Montesinos, P., Camacho Poyato, E., 2009. Exploring energy saving scenarios for on demand pressurized irrigation networks. Biosyst. Eng. 104, 552–561.

Rodríguez-Díaz J.A., Camacho-Poyato, E. Blanco-Pérez, 2011. Evaluation of water and energy use in pressurized irrigation networks in southern Spain. J. Irrig. Drain Eng., 137(10), 644–650.

Rossman, L.A., 2000. Epanet User Manual. U.S. Environmental protection agency, drinking water research division, risk reduction engineering laboratory, Cincinnati, United States.

Salvador, R., Aragüés, R., 2013. Estado de la cuestión del riego por goteo enterrado: Diseño, manejo, mantenimiento y control de la salinidad del suelo. Información técnica, económica agraria. 109(4), 395–407. http://dx.doi.org/10. 12706/itea.2013.023

Seginer, I., Nir, D., von Bernuth, D., 1991. Simulation of wind distorted sprinkler patterns. J. Irrig. Drain. Eng., ASCE. 117 (2), 285–306.

Splinter, W.E., 1976. Center-pivot irrigation. Sci. Am. 234(6), 90–9.

Tarjuelo, J.M., Montero, J., Honrubia, F.T., Ortiz, J.J., Ortega, J.F., 1999. Analysis of uniformity of sprinkler irrigation in a semiarid area. Agric. Water Manage. 40, 315–331.

Tubiello, F., Salvatore, M., Rossi, S., Ferrara, A., Fitton, N., Smith, P., 2013. The FAOSTAT database of greenhouse gas emissions from agriculture. Environ. Res. Lett. 10 p. Open Access, https://doi.org/10.1088/1748-9326/8/1/015009.

von Bernuth, R.D., Gilley, J.R., 1984. Sprinkler Droplet Size Distribution Estimation from Single Leg Test Data, Trans. of ASAE. 27, 1435–1441.

Vories, E.D., Von Bernuth, R.D., Mickelson, R.H., 1987. Simulating sprinkler performance in wind. J. Irrig. Drain. Eng. 113 (1), 119–130.

Zaccaria, D., Carillo-Cobo, M.T., Montazar, A., Putnam, D.H., Bali, K., 2017. Assessing the viability of sub-surface drip irrigation for resource-efficient alfalfa production in central and southern California. Water, 9, 837. https://doi.org/10.3390/w9110837.

Zapata, N., El Malki, H., Latorre, B., Gallinat, J., Citoler, F.J., Castillo, R., Playán E., 2017. A simulation tool for advanced design and management of collective sprinkler-irrigated areas: a study case. Irrig. Sci. 35(4), 327–345.

Zapata, N., Playán, E., Martínez-Cob, A., Sánchez, I., Faci, J.M., Lecina, S., 2007. From on-farm solid-set sprinkler irrigation design to collective irrigation network design in windy areas. Agric. Water Manage. 87, 187–199.

Objetivos

Objetivo general:

Analizar la viabilidad de los sistemas de riego por aspersión a baja presión en cobertura total y en máquinas de riego tipo pivote, atendiendo a la calidad del riego y a la producción de un cultivo.

Objetivos específicos:

1. Evaluación en campo de las diferencias entre la presión estándar (300 kPa) y la baja presión (200 kPa) en la calidad del riego y en la producción de un cultivo de maíz bajo un sistema de riego de cobertura total dando seguimiento a un ensayo experimental a lo largo de dos campañas de riego.

2. Evaluar las diferencias en la calidad del riego evaluada sobre y bajo la cubierta vegetal de un cultivo de maíz en cobertura total usando tratamientos de riego con presión estándar en boquilla y otro con baja presión en una temporada de cultivo.

3. Modificar, calibrar y validar un modelo balístico de riego por aspersión en cobertura total, con especial énfasis en el riego por aspersión de baja presión incorporando una base de datos de ensayos experimentales y un módulo de autocalibración que permita la incorporación de nuevos experimentos.

4. Modificar, calibrar y validar un modelo balístico de riego por aspersión para simular el reparto de agua de aspersores de pivote central que operan a bajas presiones (<103 kPa) utilizando diferentes tamaños de boquillas.

El desarrollo de los objetivos específicos de esta tesis doctoral se encuentra dentro de los capítulos 2, 3, 4 y 5, respectivamente.

CHAPTER II. ASSESSING LOW-PRESSURE SOLID-SET SPRINKLER IRRIGATION IN MAIZE

ASSESSING LOW-PRESSURE SOLID-SET SPRINKLER IRRIGATION IN MAIZE[1]

Resumen

El agua y la energía son recursos limitados y costosos. La conservación de agua y energía es un requisito para asegurar la viabilidad de los modernos sistemas de riego presurizado. El objetivo de este trabajo fue analizar las posibilidades de reducir la presión de operación en la boquilla de aspersores en sistemas de cobertura total desde 300 kPa (presión estándar) a 200 kPa (baja presión) sin reducir el espaciamiento y manteniendo el rendimiento del cultivo. Se diseñaron tres tratamientos combinando diferentes tipos de aspersores y presiones de operación: 1) aspersor de impacto convencional a 300 kPa (CIS300), 2) aspersor de impacto convencional a 200 kPa (CIS200), y 3) aspersor de impacto modificado con placa deflectora con presión de operación de 200 kPa (DPIS200). Se aplicó un diseño experimental aleatorio de los tratamientos a un cultivo de maíz en dos temporadas (2015 y 2016). El riego fue medido utilizando una malla de pluviómetros en una réplica de cada tratamiento. Se realizaron mediciones durante el crecimiento del maíz, en la cosecha y en sus componentes. Se realizó un análisis estadístico usando ANOVA para el contenido de agua en el suelo, el crecimiento del maíz y las variables de la cosecha entre tratamientos. La uniformidad de riego estacional evaluada por encima del dosel de la planta resultó mayor para el tratamiento de presión estándar (93%) en comparación que los tratamientos de baja presión (82% y 84% para los tratamientos DPIS200 y CIS200, respectivamente). El promedio de las pérdidas por evaporación y arrastre en la temporada 2016, fueron mayores para el tratamiento CIS300 (17%) que para los tratamientos de baja presión DPIS (15%) y CIS200 (13%). Los tratamientos de baja presión no redujeron la cosecha de grano en comparación con los tratamientos de presión estándar. Las diferencias en el riego efectuado y en la cosecha de maíz entre los tratamientos de baja presión, DPIS200 kPa y CIS200, no fueron estadísticamente significativas. La reducción de energía por la disminución en la presión de operación de 300 kPa a 200 kPa permitió incrementar los beneficios netos en la etapa de manejo y particularmente en la fase de diseño sistemas de riego individuales y colectivos.

Palabras clave: cobertura total, riego por aspersión, eficiencia energética, aspersores de baja presión, rendimiento de maíz.

[1] Robles, O., Cavero, J., Playán, E., Zapata, N., 2017. Assessing low-pressure solid-set sprinkler irrigation in maize. Agric. Water Manag. 191: 37–49. (*published*)

Abstract

Water and energy are limited and expensive resources. Conserving water and energy is a requirement to ensure the viability of modern pressurized irrigation systems. The objective of this research was to analyze the possibilities of reducing the nozzle operating pressure of impact sprinklers from 300 kPa (standard pressure) to 200 kPa (low pressure) in solid-set irrigation systems without reducing the sprinkler spacing and maintaining crop yield. Three treatments resulting from combinations of sprinkler type, and working pressure were analyzed: 1) conventional impact sprinkler operating at 300 kPa (CIS300); 2) conventional impact sprinkler operating at 200 kPa (CIS200); and 3) modified deflecting plate impact sprinkler operating at 200 kPa (DPIS200). A randomized experimental design was applied to a maize crop during two seasons (2015 and 2016). Irrigation performance was measured by catch-can monitoring at one replicate of each treatment. Maize growth, yield and its components were measured. Differences between treatments on soil water content, maize growth and yield variables were analyzed using ANOVA. Seasonal irrigation uniformity evaluated at the top of the canopy resulted larger for the standard pressure treatment (93%) than for the low pressure treatments (82% and 84% for DPIS200 and CIS200, respectively). The average WDEL for the 2016 irrigation season resulted higher for the CIS300 treatment (17%) than for the low pressure treatments, DPIS200 (15%) and CIS200 (13%). Low pressure treatments did not reduce grain yield compared with the standard pressure treatment. Differences in irrigation performance and maize yield between the low pressure treatments, DPIS200 and CIS200, were not statistically significant. The reduction of energy by reducing the operating pressure from 300 kPa to 200 kPa could to increase net farming benefits at the management phase and particularly at the design phase of individual and collective systems.

Keywords: Solid-set, sprinkler irrigation, energy efficiency, low pressure sprinklers, maize yield.

Introduction

A number of countries have devoted intense efforts in the last years to modernize their irrigation systems. Among them, Spain, where new collective pressurized irrigation networks and on-farm irrigation systems have been designed to operate at the highest water management standards. Designs paid attention to energy dependence and to the resulting costs for the farmers. However, modernization projects did not foresee the sudden rise in agricultural electricity prices in 2008, resulting from the discontinuation of the specific electricity tariff for agricultural irrigation (Rocamora et al., 2013; Tarjuelo et al., 2015). This new situation forced Water Users Associations operating pressurized networks with pumping stations to optimize irrigation management and to apply water in the daily or weekly periods of relatively low tariffs (Moreno et al., 2010). In our days, being efficient in the use of water (applying irrigation when needed and in the amount that the crops need) is not sufficient when water is applied through energy-dependent pressurized irrigation systems. In these cases, farmers also need to be efficient in the use of energy: reducing the energy used per unit volume of water and scheduling irrigation when energy cost is low. Taking these challenges into consideration, many recent research works have focused on improving the energy efficiency of irrigation facilities, optimizing pumping stations and irrigation network designs (Rodríguez-Díaz et al., 2009; Moreno et al., 2010; Fernández-García et al., 2013). However, it is necessary to move forward in energy optimization, paying attention to irrigation in its agricultural context: the plot, the crop, its yield and the resulting economic profit.

Traditional solid-set irrigation designs usually aim at ensuring a minimum of 300 kPa at the nozzle of the impact sprinklers. As energy costs increase, there is a need to find ways to operate sprinkler systems at reduced pressure without reducing the sprinkler spacing and maintaining high irrigation uniformity (Kincaid, 1991). Farmers would find it difficult to accept narrower sprinkler spacings because this would increase the cost of the installation and make mechanization more difficult. Additionally, Playán et al. (2006) reported very small differences in uniformity in the range of sprinkler layouts commonly used for field crops (from 21 x 18 m to 18 x 15 m, triangular and rectangular).

With standard pressure, 300 kPa, the jet breaks up sufficiently to produce an adequate conical water distribution pattern. As pressure is reduced the pattern becomes annular or doughnut shape, reducing the uniformity of the overlapped configuration. Recently, new impact sprinklers have been commercialized which are specially designed to operate at reduced pressure. These new sprinklers are based on developments by Kincaid (1991) who proposed a modification of the impact-type sprinkler adding a deflector attached to the drive arm. The device diffuses the jet of a standard circular-orifice nozzle, maintaining the radius range and potentially improving the distribution pattern. Kincaid (1991) proposed an intermittent deflection of the jet to fill in the intermediate and lower irrigated portion of the annular pattern (the proximal region).

Reductions in the energy requirements of center pivot and lateral move irrigation machines have been successfully achieved by replacing the traditional impact sprinklers by spray sprinklers. These spray sprinklers operate at reduced pressure without affecting irrigation performance (Omary & Sumner, 2001). Kincaid (1982) analyzed the possibilities of reducing energy requirements of a sprinkler stationary system, the sideroll wheel line lateral. His results indicated that for 12.2 m to 15.2 m lateral move distances, pressures of 206 kPa produced irrigation uniformities nearly equivalent to the 379 kPa pressure. For longer lateral move distances, the low pressure configuration significantly reduced uniformity.

Encouraging results were presented by Playán et al. (2006) in solid-set sprinkler irrigation systems when reducing the nozzle pressure from 300 kPa to 200 kPa in two conventional impact-type sprinklers. Differences were analyzed in a solid-set sprinkler layout of 18 x 15 m with a 2 m sprinkler riser height. The radial application patterns were very similar, and Distribution Uniformity was slightly higher (< 5%) for the highest pressure. Paniagua (2015) analyzed the effect of reducing the pressure at the nozzle from 300 kPa to 200 kPa in modified impact sprinklers with a deflecting plate in the drive arm. The comparison was performed in two solid set sprinkler layouts commonly used to irrigate field crops (18 x 18 m and 18 x 15 m). The author concluded that for the experimental conditions, modified impact sprinklers operating at 200 kPa performed adequately and could substitute the traditional impact sprinklers operating at 300 kPa in solid-set layouts. Sahoo et al. (2008), working in solid-set spacings smaller than the previous authors (12 x 12 m or 6 x 12 m) and at pressures ranging from 100 kPa to 250 kPa, concluded that the nozzle pressure of 200 kPa performed better than the rest of nozzle pressures analyzed, using small and medium sized nozzles. For larger nozzles, the pressure of 200 kPa performed better than lower pressures and equal than the nozzle pressure of 250 kPa. These authors recommended selecting relatively large size nozzles for operating low pressure sprinklers in windy conditions.

Several variables affect the water distribution pattern of a solid-set sprinkler irrigation system: the spacing among sprinklers and laterals, wind speed and direction, sprinkler type, working pressure, nozzle size and sprinkler riser height (Tarjuelo et al. 1999; Playán et al. 2005). While the effect of reducing sprinkler nozzle pressure on irrigation performance of individual irrigation events has been analyzed in the literature (Kincaid, 1991; Playán et al., 2006; Sahoo et al., 2008; Paniagua, 2015), the seasonal effect on crop yield has not been assessed.

This research was set out to analyze the possibilities of reducing energy requirements of solid-set sprinkler irrigation systems by reducing the pressure at the sprinkler nozzle from 300 kPa to 200 kPa, without reducing the sprinkler spacing and maintaining maize yield. A field experiment was designed to compare the irrigation performance and the crop yield of three different sprinkler configurations (conventional

impact sprinkler and modified impact sprinkler) and operating pressures (300 kPa and 200 kPa).

Materials and Methods

Experimental site and design

The experiment was conducted in a 2.0 ha solid-set facility located at the experimental farm of the Aula Dei Agricultural Research Centre in Montañana (Zaragoza, NE Spain). Geographical coordinates are 41°43' N latitude and 0°49' W longitude, and elevation is 225 m above mean sea level. The sprinkler layout of the irrigation system was square, with a spacing of 18 m between sprinkler lines and 18 m between sprinklers of the same line. Riser pipes were used to locate the sprinkler nozzle at an elevation of 2.5 m above the ground level. The irrigation system was composed by 14 irrigation blocks. Two linear blocks irrigated the borders of the experiment, while twelve square blocks corresponded to the experimental plots. Each experimental plot was composed by four impact sprinklers (324 m^2) and was controlled by a hydraulic valve equipped with a pressure regulator. Blocks were named after the number of the valve irrigating them: from V1 to V14.

Three treatments were designed for this research, each of them with four replicates randomly distributed in the twelve experimental plots (Fig. 1). Two types of impact sprinklers were tested. The first one was a standard brass impact sprinkler, Costa RC-130 (CIS, Conventional Impact Sprinkler). The second one was a plastic impact sprinkler (NaanDanJain 5035) resulting from the application of the developments by Kincaid (1991). This modified impact sprinkler adds a deflecting plate to the drive arm (DPIS, Deflecting Plate Impact Sprinkler). Two nozzle pressures were evaluated: the standard 300 kPa and the low 200 kPa.

The three treatments were: 1) the standard brass impact sprinkler equipped with double brass nozzle (4.4 mm and 2.4 mm) operating at a pressure of 300 kPa (CIS300); 2) the standard brass impact sprinkler equipped with double plastic nozzle (5.16 mm and 2.5 mm) operating at a pressure of 200 kPa (CIS200); and 3) the modified plastic impact sprinkler equipped with double plastic nozzle (5.16 mm and 2.5 mm) operating at a pressure of 200 kPa (DPIS200). The treatments with low working pressure implemented larger nozzles than the treatment with standard pressure to obtain a similar gross irrigation application rate, 5.2 mm h^{-1}.

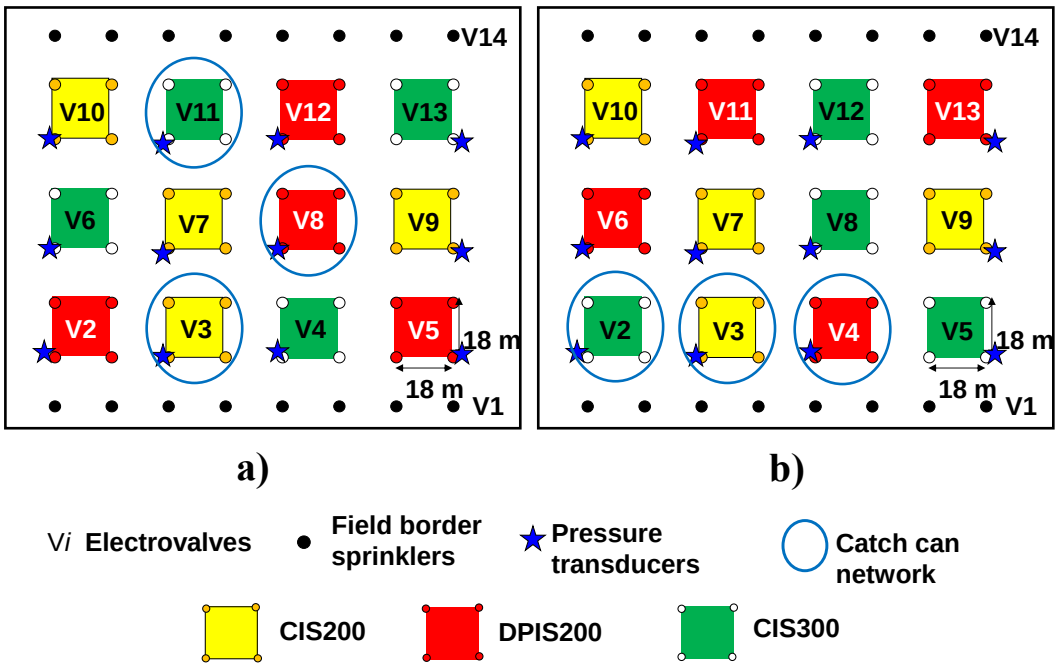

Figure 1. *Experimental design configuration, location of the three treatments and four replicates in 2015 season (Fig. 1a) and in 2016 season (Fig. 1b). Treatments were: CIS300, standard pressure treatment; CIS200, low pressure treatment; and DPIS200, low pressure treatments with modified sprinkler. Location of the pressure transducer in each experimental plot and the experimental plots selected for catch-cans evaluation in each season are also shown.*

The 14 irrigation blocks (including the 12 experimental plots) were irrigated from the same hydrant. Irrigation blocks of the field border, V1 and V14 (Fig. 1), were irrigated independently from the experimental plots. The 12 experimental plots were always irrigated at the same time. The collective irrigation network provided a quasi-constant pressure of 420-440 kPa upstream from the hydrant. The pressure at each experimental plot was manually adjusted using the pressure regulator of its hydraulic valve. Pressure was set according to the plot treatment (200 kPa or 300 kPa). A manometer was installed at each hydraulic valve to measure and verify pressure at each irrigation event. Additionally, a pressure transducer (Dickson, PR150) and a manometer were installed in one of the sprinkler risers of each irrigation block (Fig. 1). Pressure transducers were connected to a data logger recording measurements every five minutes.

Soil characterization

Soil samples were taken before sowing at each experimental plot in 2015 to determine field capacity (FC, %), wilting point (WP, %), soil water holding capacity (WHC, mm m^{-1}) and initial gravimetric soil water content (ISWC, %). ISWC was also determined in 2016 before sowing. Soil samples were also taken after harvesting in both crop seasons to determine the final gravimetric soil water content (FSWC, %). Two measurement points were selected at each plot for FC, WP, ISWC and FSWC (Fig. 2a). At

each measurement point samples were collected every 0.3 m, to a depth of 1.2 m with a 5 cm diameter hand auger (Eijkelkamp Agriresearch Equipment BV, The Netherlands). Gravimetrical soil water content was determined for the samples. Soil fertility, including nitrogen (N), phosphorus (P) and potassium (K) were determined after harvest in 2015. Two soil cores were taken from each experimental plot with the 5 cm diameter hand auger to a depth of 1.2 m for N determination and to a depth of 0.3 m for P and K determination. The two samples were combined and fresh-sieved to pass a 2 mm sieve, and 10 g were extracted with 30 mL of KCl 2 N solution for colorimetric determination of $N\text{-}NO_3^-$ concentration with a continuous flow analyzer (AA3, Bran+Luebbe, Norderstedt, Germany). Soil available phosphorus (Olsen method) and potassium (extraction in ammonium acetate and atomic absorption) concentrations were determined by an external laboratory. Differences between treatments in the measured soil variables were established using analysis of variance.

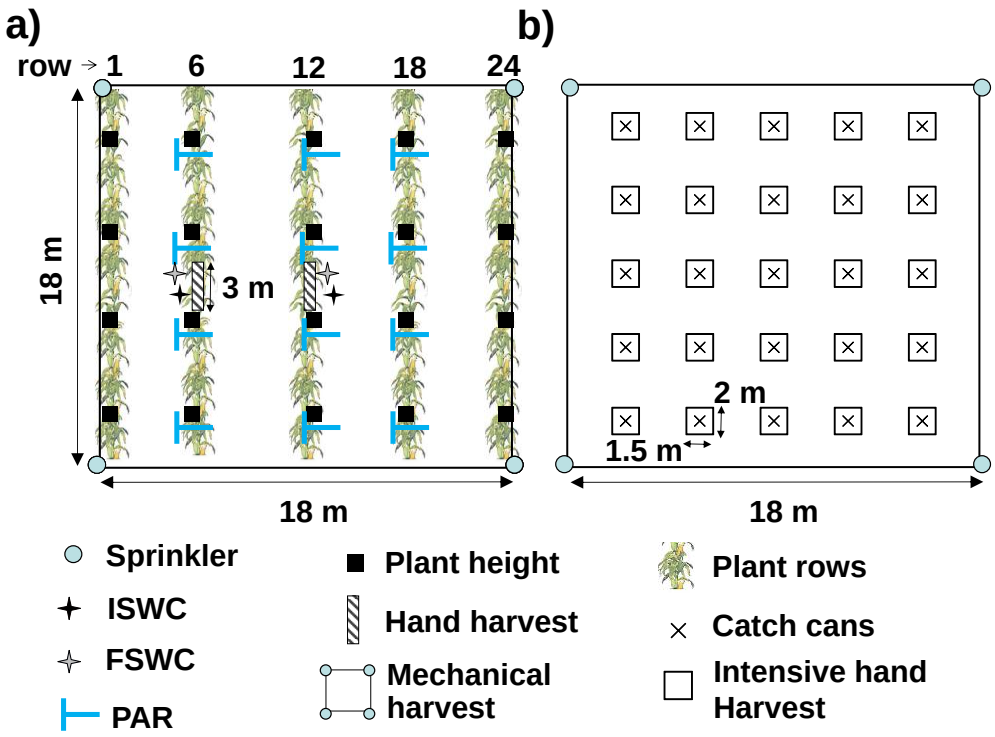

Figure 2. *Location of the measurement points for plant height, photosynthetically active radiation intercepted by the crop (PAR) and hand harvest for biomass and yield components determination at each experimental plot (Fig. 2a). Arrangement of the 25 catch-cans network and intensive hand harvest area at the three experimental plots were irrigation uniformity and yield variability was measured, was also presented (Fig. 2b).*

Crop variety and fertilization

The experiment was performed in a maize crop during two crop seasons, 2015 and 2016. Maize (Pioneer P1758) was sown in April 14, 2015 and April 13, 2016, in rows separated 0.75 m and with a density of 89500 seeds ha^{-1}. In 2015, the fertilization consisted in 64 kg ha^{-1} of N, 120 kg ha^{-1} of P_2O_5 and 120 kg ha^{-1} of K_2O applied before the planting date, and 100 kg ha^{-1} of N as ammonium-urea-nitrate solution (32% N) applied with the irrigation water at the V9 growth stage. Alfalfa had been sowed in the field during the previous three years. In 2016, the same fertilization was applied before planting, but two applications of 100 kg ha^{-1} of N as ammonium-urea-nitrate solution (32% N) were done at V6 and V12 growth stages. Weeds and pests were controlled according to the best management practices in the area during both experimental years.

Irrigation requirements

Maize evapotranspiration (ET_c) for 2015 and 2016 was computed from reference evapotranspiration (ET_0) data and crop coefficients (Allen et al., 1998). ET_0 data were obtained from the Montañana station, the nearest agrometeorological station of the SIAR agrometeorological network (www.magrama.gob.es/siar/informacion.asp). This station is located at a distance of 1.2 km from the experimental site. Maize crop coefficients were derived from the model of relative cumulative degree-days proposed by Martínez-Cob (2008) in the experimental area. Maize irrigation requirements (CIR) were weekly obtained as a balance between ET_c, effective precipitation (considered 75% of weekly precipitation), soil water availability and net irrigation application. An irrigation efficiency of 85% was assumed in this work, in agreement with efficiency estimates reported in the literature for solid-set sprinkler irrigation systems (Clemmens and Dedrick, 1994). The three treatments were irrigated at the same time to ensure equal meteorological conditions. Since the irrigation application rate was constant among treatments, the seasonal irrigation volume was the same for the three treatments.

Irrigation performance

Short irrigation events (lasting for one hour) were applied at the beginning of the crop season to facilitate crop emergence. Once emergence was completed, irrigation events were scheduled to last for 2, 3 or 4 hours.

The water distribution pattern was evaluated by a 25 catch-can network (Fig. 2b) installed in one of the replicates of each irrigation treatment. The experimental plots monitored with catch-cans were not the same in 2015 and 2016 (Fig. 1). Catch-cans had a total height of 0.37 m and a diameter of the upper part of 0.016 m. Catch-cans were marked in mm for direct readout up to 0.045 m. The mouth of the catch-cans was installed at 1.0 m above ground level at the beginning of each season. During the 2016 irrigation season catch-cans were elevated as maize grew to be always above the crop canopy, until a

maximum height of 2.3 m. Only six irrigation events were evaluated in 2015, while most of the irrigation events were evaluated in 2016. The Christiansen Uniformity Coefficient (CUC, %) (Christiansen, 1942) was determined for each evaluated irrigation event in 2015 and 2016. Seasonal CUC ($CUC_{seasonal}$) was also determined in 2016 by applying the CUC equation to the cumulative seasonal irrigation in each catch-can. Wind drift and evaporation losses (WDEL) were estimated as the difference between applied irrigation depth and collected irrigation depth at the catch-can network (Playán et al., 2005), expressed as percentage of the applied irrigation depth. WDEL were determined for each evaluated irrigation event in 2015 and 2016, and seasonally in 2016.

Maize growth and yield variables

Plant height was measured after tasseling (30 July in 2015 and 28 July in 2016), using a ruler with centimetric accuracy. Twenty measurement points were homogeneously distributed at each experimental plot (Fig. 2a). The height of two plants was measured at each point. Plant height at an experimental plot was determined as the average of all measurements.

The photosynthetically active radiation (PAR, %) intercepted by the crop was measured at each experimental plot in both seasons. PAR intercepted by the crop was measured at R5 growth stage (17 August in 2015 and 18 July in 2016) with a 1-m-long ceptometer using 64 photodiodes (Sunscan, Delta-T, Cambridge, UK) and a PAR sensor (BF3 Sunshine sensor, Delta-T, Cambridge, UK). The PAR sensor continuously measured radiation above the crop canopy. Radiation at the soil surface was measured at each experimental plot by taking 12 readings with the ceptometer placed perpendicular to the plant rows and moving it across the rows of the plot, covering consecutive sections 1 m in length (Fig. 2a). Measurements were taken around 12:00 GMT. The fraction of PAR intercepted by the crop was computed as the percentage of the difference between the BF3 readings and the ceptometer readings, to the BF3 readings. The PAR intercepted by the plants at each plot was determined as the average of the 12 measurements.

On 28 September (in both seasons) hand harvest was performed at each experimental plot to determine aerial biomass. The maize plants located in a 3-m-long section of two different rows (rows 6 and 12), a total of 4.5 m^2 in each experimental plot (Fig. 2a), were hand harvested by cutting them at the soil surface level. The grain was separated from the cob and both parts were dried at 60ºC. The final number of plants, number of ears, total biomass, kernel mass and harvest index (HI) were determined for each plot and treatment.

On 29 September 2016 an intensive hand harvest was performed at three experimental plots to determine the intra-plot spatial variability of grain yield. The three experimental plots, one replicate per treatment, were coincident with those of pluviometry measurements in 2016. The maize grain was manually harvested at 25 points in each

experimental plot (Fig. 2b). The maize ears located in a 2-m-long section of two different rows (one at each side of the pluviometer) were hand harvested in each point. The grain was separated from the cob and dried to 60ºC. Grain yield was adjusted to standard 140 g kg^{-1} moisture content. The spatial variability of grain yield was established for the measured plot. Comparisons were performed between treatments and with the spatial variability of seasonal irrigation collected at the catch-can network for every treatment.

The experimental plots (18 × 18 m) were machine harvested on 30 September in 2015 and on 5 October in 2016 using a combine. Grain was weighed with a 1-kg-precision scale. A grain subsample was collected to measure grain moisture. Another subsample of the combine-harvested grain from each experimental plot was dried at 60°C to measure kernel mass. The number of grains per unit area was calculated from kernel mass and grain yield.

Economic issues

The effect of the irrigation pressure treatments (300 kPa and 200 kPa) on electricity cost depends on network topology. In this research, the tool presented by Zapata et al. (2015) was used to illustrate the economic implication of reducing irrigation pressure in a simulation phase. With this tool, the effect of reducing the operating pressure at the sprinkler nozzle form 300 kPa to 200 kPa was analyzed on a collective pressurized sprinkler irrigation network. The topology of the studied collective network is considered representative of the conditions in the Ebro Valley.

Data analysis

The relationships between wind speed and irrigation uniformity and between wind speed and WDEL were analyzed for the three treatments using regression. Spatial variability in water distribution patterns and hand harvested grain yield was assessed using contour line maps produced with the SURFER software (copyright Golden Software Inc.). Differences between treatments in measured water application, maize growth variables, yield and its components were analyzed using ANOVA. Means were separated using Fisher's Protected LSD at $P = 0.05$.

Results and Discussion

Soil characterization

The soil of the experimental farm was classified as a Typic Xerofluvent. The initial soil water content of the treatments was very similar between seasons, ranging from 23.9% to 26.7%. The final soil water content (after harvest) was higher in 2015 than in 2016. This can be explained by a more adjusted irrigation schedule to crop water requirements in 2016 (Fig. 3). Within each experimental season, significant differences were not found between treatments for WHC, ISWC or FSWC.

In 2015, the values of soil nitrogen, phosphorus and potassium were within normal bounds, and did not show fertility problems at the experimental plots. Statistically significant differences between the soils assigned to the different treatments were not found for phosphorus soil content and potassium soil content. Soil nitrogen of treatment CIS200 was significantly lower than for the soils of the other two treatments.

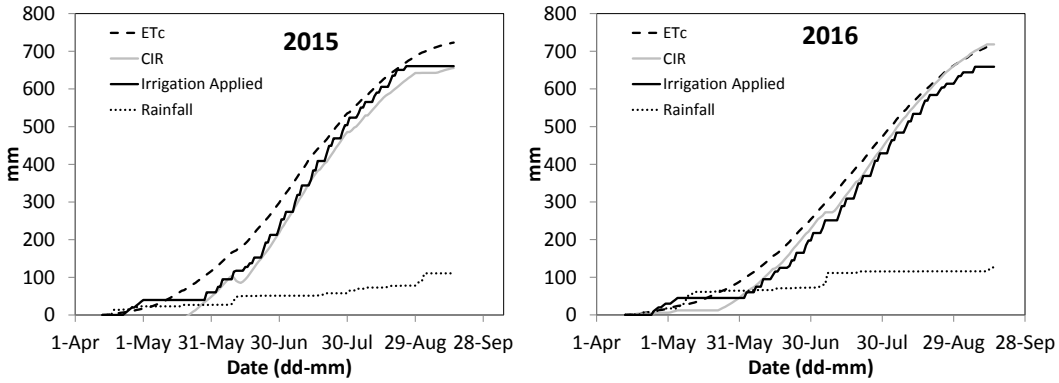

Figure 3. *Cumulative calculated crop evapotranspiration (ETc), rainfall, crop irrigation requirement (CIR) and irrigation applied water as a function of time during the season 2015 and 2016.*

Characterization of meteorology

The meteorological characteristics of the experimental seasons, 2015 and 2016 (considered from April to September), were compared with the available semi-hourly meteorological data set in the area (ranging from 1995 to 2016). Both experimental seasons can be classified as average in terms of reference evapotranspiration, since the seasonal values (952 mm and 924 mm, for 2015 and 2016, respectively) were similar to the average season (927 mm). Both seasons were drier (116 mm and 130 mm of precipitation in 2015 and 2016 seasons, respectively) than the average season (170 mm). The inter-seasonal variability of precipitation is high in the area. Regarding the average daily wind speed, the values of both seasons (2.2 m s^{-1} and 2.3 m s^{-1}, for 2015 and 2016, respectively) were slightly lower than the value of the average season (2.4 m s^{-1}).

Irrigation requirements and irrigation application

The average soil available water at planting was 50 mm in 2015 and 40 mm in 2016. The rainfall from seeding date (April 13) to senescence (September 15) was 78 mm in 2015 and 126 mm in 2016. Fig. 3 presents the cumulative ET_c, rainfall, crop irrigation requirements (CIR) and irrigation application as a function of time. In general, irrigation application was close to CIR (Fig. 3). Some differences can be observed during the seasons, mostly due to rainfall. In 2016, irrigation application was slightly below crop irrigation requirements, leading to a reduction of the soil water content at the end of the cropping season. The total volume of irrigation applied was similar in both seasons, 661

mm in 2015 and 659 mm in 2016. The total irrigation time (132.0 h and 131.5 h, in 2015 and 2016, respectively) was arranged in 43 irrigation events in 2015 and in 47 events in 2016 (Table 1). In both seasons 12% of the irrigation time suffered wind speeds larger than or equal to 4 m s^{-1}. A 33% and a 21% of the irrigation time in 2015 and 2016, respectively, was performed under wind speeds between 2 m s^{-1} and 4 m s^{-1}. Finally, 55% and 67% of the irrigation time in 2015 and 2016, respectively, was performed under wind speeds lower than 2 m s^{-1}. In general, irrigations in 2015 were applied under higher wind speeds than irrigations in 2016.

Table 1. *Date, catch-can elevation, irrigation time, wind speed, temperature, relative humidity, irrigation uniformity and wind drift and evaporation losses measured in each experimental treatment for each of the 36 evaluated irrigation events in 2016.*

Date	Catchcan height (m)	Irrig. time (h)	WS (m s^{-1})	Temp (ºC)	RH (%)	CUC (%)			WDEL (%)		
						DPIS200	CIS200	CIS300	DPIS200	CIS200	CIS300
6/7/2016	1.0	3.0	1.2	22	66	88	85	91	25	13	17
6/10/2016	1.0	4.0	1.0	20	72	86	84	91	20	7	13
6/14/2016	1.0	2.0	4.5	19	53	67	73	72	30	21	23
6/15/2016	1.0	2.0	1.6	18	61	86	82	88	22	21	20
6/17/2016	1.0	2.0	1.1	16	69	85	78	87	26	23	23
6/24/2016	2.0	4.0	0.8	19	68	78	80	94	14	11	17
6/28/2016	2.0	4.0	0.6	17	75	75	75	89	14	13	16
6/29/2016	2.0	2.5	1.9	20	70	78	80	87	13	18	18
7/1/2016	2.0	4.0	1.1	20	76	79	76	79	10	11	21
7/5/2016	2.0	2.7	2.3	21	85	81	82	84	20	23	25
7/6/2016	2.0	4.0	2.6	20	78	74	76	78	10	13	14
7/12/2016	2.0	3.5	3.0	20	66	69	66	70	18	26	21
7/13/2016	2.0	4.0	4.5	17	58	62	63	65	17	16	22
7/15/2016	2.0	4.0	1.1	14	71	77	81	86	11	5	21
7/19/2016	2.0	4.0	1.1	19	63	77	80	84	13	15	19
7/20/2016	2.0	4.0	1.0	21	70	80	79	86	14	14	18
7/22/2016	2.0	4.0	2.7	20	70	68	64	77	8	16	9
7/26/2016	2.0	4.0	1.3	20	75	77	75	87	14	16	12
7/27/2016	2.3	4.0	2.4	21	69	77	75	83	12	16	16
7/29/2016	2.3	4.0	0.4	19	75	72	72	88	12	12	13
8/2/2016	2.3	4.0	0.6	18	72	71	72	92	17	13	14
8/3/2016	2.3	3.0	0.5	21	70	71	73	89	13	12	10
8/5/2016	2.3	4.0	4.7	20	59	53	55	54	19	19	21
8/9/2016	2.3	3.0	2.4	20	69	73	70	77	13	14	16
8/10/2016	2.3	3.0	4.0	17	58	59	62	66	19	17	20
8/12/2016	2.3	4.0	0.8	13	79	68	72	88	14	10	12
8/16/2016	2.3	4.0	1.0	19	82	74	76	91	13	8	14
8/17/2016	2.3	3.0	0.8	20	81	73	76	90	13	9	16
8/19/2016	2.3	3.0	0.8	21	80	71	72	90	15	16	15
8/23/2016	2.3	2.0	0.6	22	75	70	75	90	14	4	17
8/24/2016	2.3	2.0	0.8	21	70	71	74	87	13	7	17
8/26/2016	2.3	2.0	0.9	20	63	69	74	89	18	8	17
8/30/2016	2.3	2.0	1.4	17	70	78	80	91	10	6	17
8/31/2016	2.3	2.0	1.2	20	78	80	77	86	8	9	17
9/2/2016	2.3	2.0	1.2	20	78	79	73	86	8	7	16
9/7/2016	2.3	3.0	0.6	18	81	78	74	87	7	9	14

Irrigation performance

The average and standard deviation of the nozzle pressure measured with pressure transducers are presented in Fig. 4. The seasonal average and the standard deviation are presented for each treatment and both seasons. Pressures were slightly higher in 2015 than in 2016. The inter-seasonal variation in pressure was also larger for the first season (larger error bars) than for the second. The control of the nozzle pressure by pressure regulation pilots at the hydraulic valves proved effective to maintain the required pressure of the different experimental plots and treatments and irrigation events (Table 2).

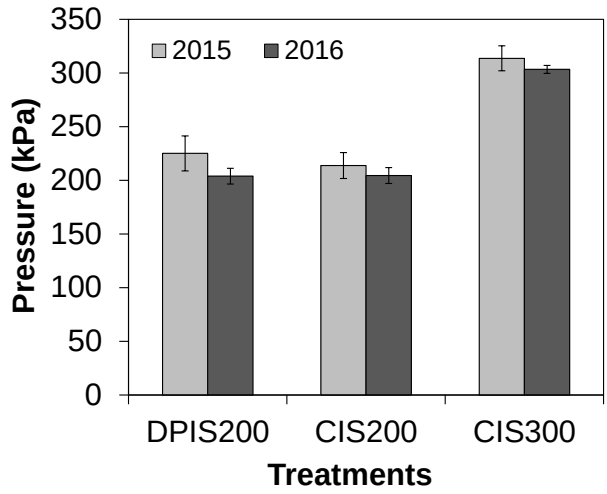

Figure 4. *Seasonal average of the water pressure measured with the pressure transducer at the sprinkler riser for each treatment during the 2015 and 2016 irrigation seasons. Error bars represent one standard deviation.*

Table 2. *Main characteristics of the irrigations applied, the irrigation evaluated and the wind during irrigation in each experimental season. Variables include the number of irrigation events, the number of evaluated irrigation events, the seasonal irrigation time, the average wind speed during irrigation, and the percentage of irrigation time in three wind speed classes.*

Season	Irrigation				Irrigation time (%)		
	No (-)	Evaluated (-)	Time (h)	Avg. Wind Speed ($m\ s^{-1}$)	$< 2\ m\ s^{-1}$	$2 \leq WS < 4$	$\geq 4\ m\ s^{-1}$
2015	43	6	133	2.2	55	33	12
2016	47	36	130	1.8	67	21	12

Irrigation uniformity

Table 3 presents average and seasonal catch-can elevation, wind speed, temperature, relative humidity, irrigation uniformity and wind drift and evaporation losses for each treatment. Data for the 36 irrigation events evaluated in 2016 (Table 1). The relationship between wind speed and irrigation uniformity for all evaluated irrigation

events was stronger for the treatment with standard pressure (CIS300, correlation coefficient of 0.92) than for the low pressure treatments (correlation coefficients of 0.75 for DPIS200 and 0.72 for CIS200). This data set was plotted for each treatment and catch-can elevation (Figs. 5a, 5b and 5c). Differences in CUC between treatments increased as catch-can elevation increased. This was particularly evident for the irrigations performed under low wind speeds. At 1 m catch-can elevation, differences in CUC between treatments were not relevant. CIS300 treatments had slightly higher CUC (88%) than the low pressure treatments (85% and 87%, for CIS200 and DPIS200, respectively) for wind speeds lower than 2 m s^{-1}. These results are in agreement with the findings of Paniagua (2015) when comparing CUC of a DPIS operating at 300 and at 210 kPa over bare soil with catch-cans installed at 0.45 m above ground level. As catch-can elevation increases differences in CUC between treatments of standard pressure (CIS300) and low pressure (CIS200 and DPIS200) accentuate, particularly for low wind speeds (Figs. 5b and 5c). Under low wind speeds, the CUC of CIS300 did not change with catch-can elevation (87% and 89% for 2 m and 2.3 m catch-can elevation, respectively), but the CUC of low pressure treatments sharply decreased with increasing catch-can elevation (78% for both low pressure treatments at 2 m catch-can elevation and 74% and 73% for CIS200 and DPIS200, respectively at 2.3 m catch-can elevation).

Table 3. *Average and seasonal catch-can elevation, wind speed, temperature, relative humidity, irrigation uniformity and wind drift and evaporation losses measured in each experimental treatment for the irrigation applied in 2016.*

	Catch-can height (m)	WS (m s^{-1})	Tª (ºC)	RH (%)	CUC (%)			WDEL (%)		
					DPIS200	CIS200	CIS300	DPIS200	CIS200	CIS300
Average	1	1.9	18.9	64.2	82	80	86	25	17	19
	2	1.8	18.9	71.0	75	75	82	13	15	18
	2.3	1.4	19.1	72.6	72	72	85	13	11	16
	All	1.6	19.0	70.9	74	74	84	15	13	17
Seasonal	All	1.6	19.0	70.9	82	84	93	15	13	17

When analyzing all the irrigations evaluated in 2016, $CUC_{seasonal}$ was higher in CIS300 than in CIS200 and DPIS200 (93%, 84% and 82%, respectively). The large number of irrigations evaluated under high catch-can elevation determined the differences in $CUC_{seasonal}$. Sánchez et al. (2010b) reported that the vertical distance between the sprinkler nozzle and the opening of the catch-cans affects the estimation of both CUC and WDEL, particularly under high wind speed conditions. Dogan et al. (2008) stated that the accuracy of the water depth estimation increased with the vertical distance between the sprinkler nozzle and the collector. In fact, ISO standard 15886-3 states that the vertical elevation difference between sprinkler nozzle and collector should be larger than 300 mm. Sánchez et al. (2010b) reported that as the water interception plane raises, the sprinkler overlap worsens. In the present experimental conditions, this effect was noticeably larger for the low pressure treatments than for the standard pressure treatment, presumably owing to differences in jet trajectory.

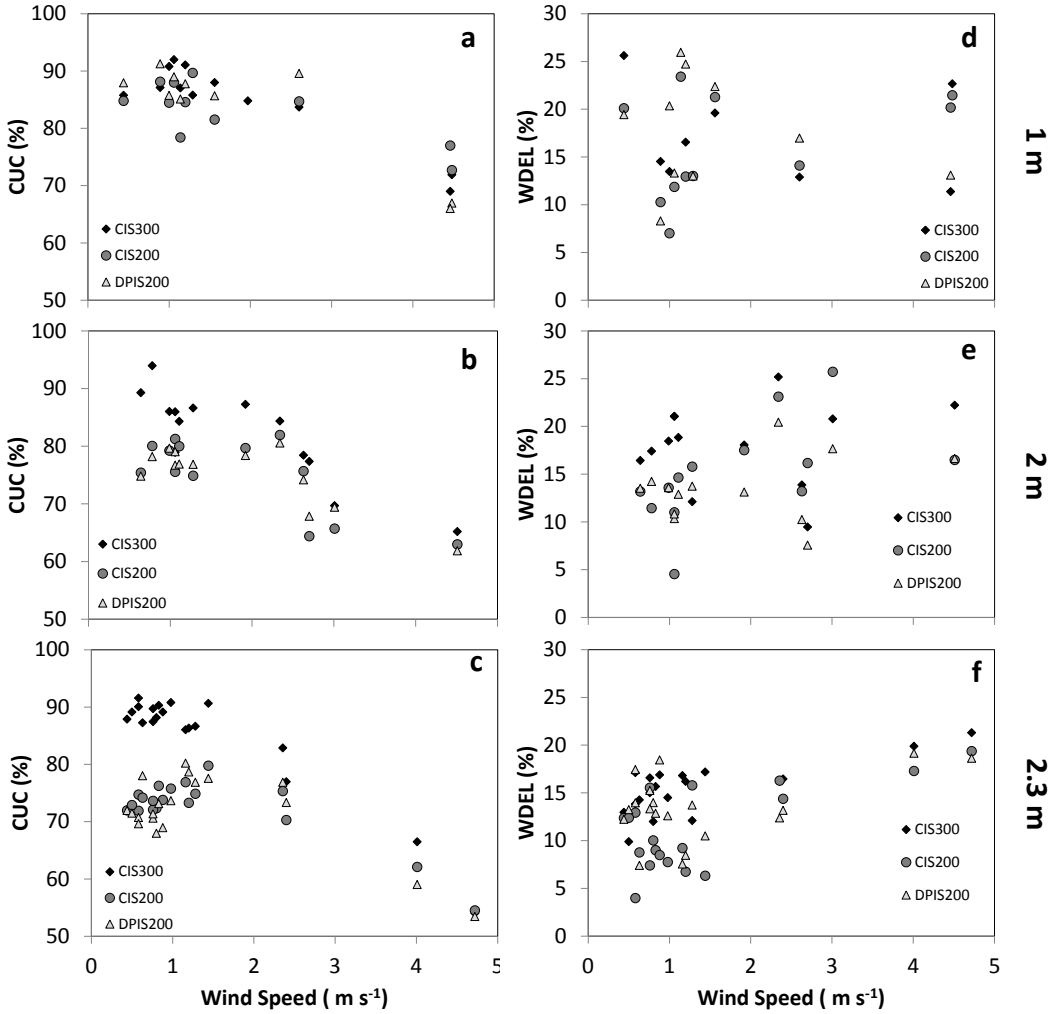

Figure 5. *Relationships between wind speed and uniformity coefficient, CUC, (a, b and c) and between wind speed and wind drift and evaporation losses, WDEL, (d, e and f) for each treatment and catch-cans elevation (1 m, 2 m and 2.3 m). Data presented for 1 m catch-cans elevation correspond to irrigations evaluated in 2015 and 2016 (a and d). Data for the other catch-cans elevations correspond only for irrigations evaluated in 2016.*

Summarizing, at low catch-can elevation results are in agreement with the literature, and the uniformity of the three treatments shows small differences: the treatments can be ranked as CIS300, DPIS200 and CIS200, with respective CUC of 86, 82 and 80% (Table 3). As catch-cans are raised, the difference between CIS300 and the low pressure treatments is magnified. It is to be assessed whether these differences in measured irrigation uniformity translate to differences in crop growth and yield.

Fig. 6 shows the intra-plot water distribution pattern of two irrigation events performed under low wind speed (1 m s^{-1}) and high wind speed (4.5 m s^{-1}) for the three treatments in 2015 (catch-can elevation of 1 m). Higher CUC was observed for CIS300

(92%) than for DPIS200 and CIS200 (89 and 88%, respectively) under low wind speed conditions. Lower CUC was observed under high wind (Fig. 6), but the differences between treatments followed a different pattern than those for low wind speed conditions. The uniformity of CIS300 (72%) was similar to CIS200 (73%), and both were higher than DPIS200 (67%). These results are in agreement with Fig. 5a.

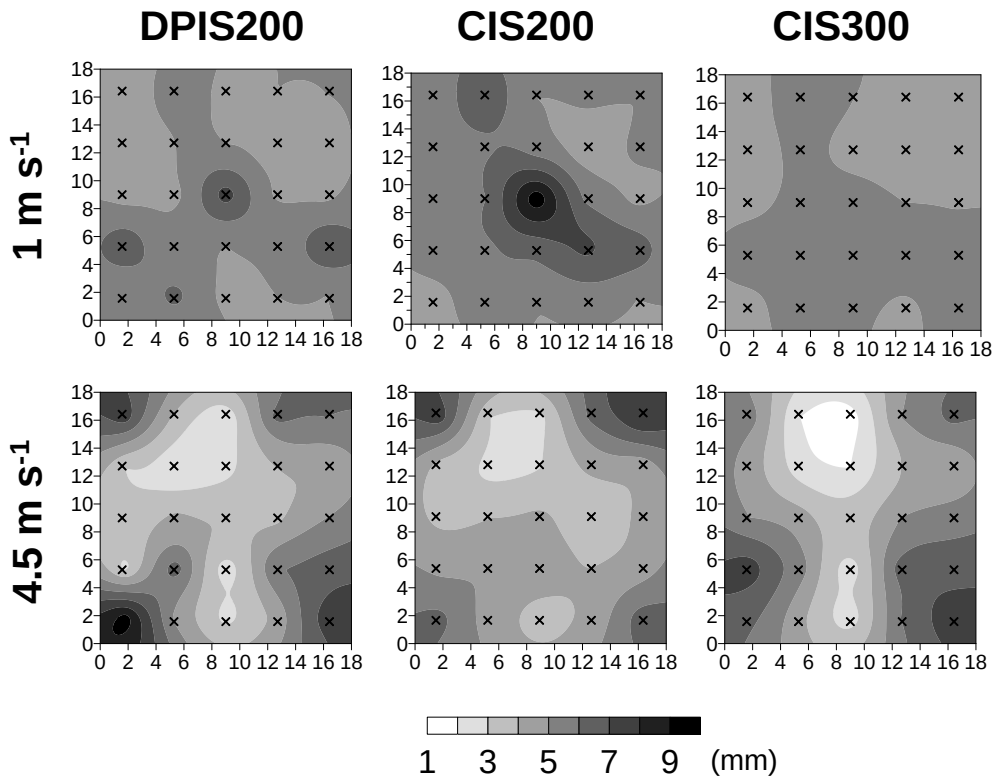

Figure 6. *Water distribution patterns of two individual irrigation events, one under low wind speed (upper figures) and the other under high wind speed conditions (lower figures), for the three treatments.*

Fig. 7 presents contour maps of the seasonal water distribution pattern corresponding to each treatment (adding the observations of the 36 evaluated irrigation events in 2016). DPIS200 (Fig. 7a) and CIS200 (Fig. 7b) showed common traits, with under irrigation near the center and over irrigation near the sprinkler. The correlation coefficient between both seasonal water distribution patterns was 0.55. CIS300 (Fig. 7c) showed a homogeneous water distribution pattern, and no correlation with the distribution patterns of the low pressure treatments.

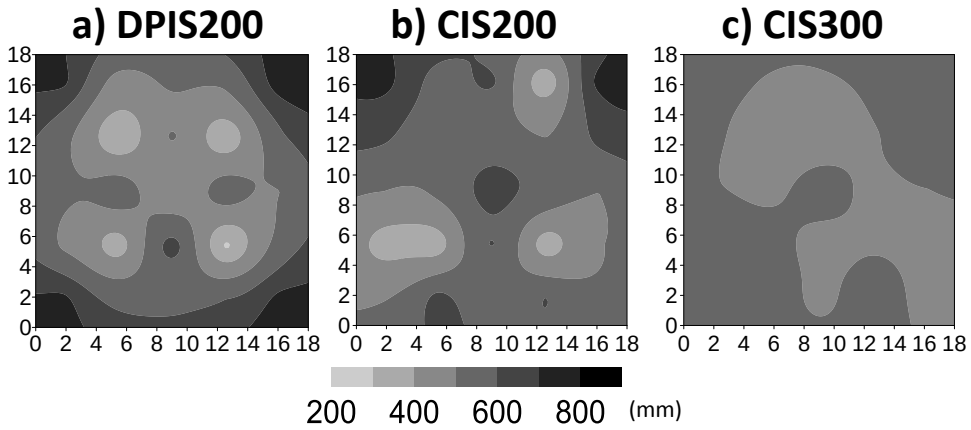

Figure 7. *Water distribution pattern of the accumulated irrigation applied in 2016 to one replicate of each treatment: DPIS200 (a), CIS200 (b) and CIS300 (c).*

Wind drift and evaporation losses

Figures 5d, 5e and 5f present the relationship between wind speed and WDEL for the three treatments and the different catch-can elevations. As in the case of CUC, the differences in WDEL between pressure treatments change with catch-can elevations. For catch-cans installed at the lowest elevation (1 m, Fig. 5d), treatment DPIS200 resulted in WDEL (25%) noticeably larger than the other two treatments (19% and 17% for CIS300 and CIS200, respectively). As catch-can elevation increases WDEL decreases for all the treatments (Table 3), but particularly for low pressure treatments. Sánchez et al (2010b) measured WDEL at 1 m and 2 m catch can elevations at the same time over an alfalfa crop, and reported that under wind speeds higher than 2 m s^{-1}, measurements at 2 m catch-can elevation overestimated WDEL. For wind speeds lower than or equal to 2 m s^{-1}, these authors reported a slight decrease in WDEL with increasing catch-can elevation; similar to what was observed for the CIS300 treatment. For wind speeds lower than 2 m s^{-1}, as catch-can elevation increases the WDEL of CIS300 slightly varied (18%, 18% and 15% for 1 m, 2 m and 2.3 m catch-can elevation, respectively), while the WDEL of CIS200 (16%, 13% and 10% for 1 m, 2 m and 2.3 m catch-can elevation, respectively) and particularly DPIS200 (23%, 13% and 13% for 1 m, 2 m and 2.3 m catch-can elevation, respectively) showed relevant decreases (Fig. 5d, 5e and 5f).

Differences in WDEL were observed between the two low pressure treatments. Treatment CIS200 presented the lowest WDEL for the lowest and the highest catch can elevations. Treatment DPIS200 presented the largest WDEL for the lowest catch-can elevation, and showed a sharp WDEL decrease as catch-can elevation increased from 1 m to 2 m.

The average WDEL for the 2016 irrigation season was higher for the CIS300 treatment (17%) than for the low pressure treatments, DPIS200 (15%) and CIS200 (13%).

The large number of irrigations evaluated under high catch-can elevation determined the seasonal differences in WDEL. As nozzle diameter decreases and pressure increases, the number of drops with small diameter increases and the number of drops with large diameter decreases (Kincaid et al., 1996). The increase in drop surface area per unit volume of water delivered with the smaller droplets increases evaporation. At the same time, small drops are more likely to be drifted by wind (Kincaid and Longley, 1986; Kincaid, 1996). The deflecting plate of the DPIS sprinkler diffuses the jet, reducing drop size. This contributed to explain the differences in WDEL between both low pressure treatments, particularly for the 1 m catch-can elevation.

Literature can explain the seasonal differences in WDEL between treatments obtained in this research as previously discussed. It can also explain the reduction in WDEL as catch-can elevation increases (smaller distance for the drops to be evaporated and drifted). However, it is difficult to explain why the reduction in WDEL and CUC with increasing catch-can elevation was mainly observed for low pressure treatments. These results suggest that the use of catch-can networks over the crop canopy of tall crops (such as maize) to estimate sprinkler irrigation performance (CUC and WDEL) could introduce noise as the elevation of the catch-cans approximates the sprinkler nozzle height. This seems particularly relevant when the sprinkler operating pressure is lower than 300 kPa.

Crop height and PAR interception

A remarkable delay in maize emergence was observed in plots V13 and V11 in 2015, compared to the other plots. This delay affected crop development variables and yield components in these plots. Measurements of soil water content and soil fertility could not explain the different behavior of experimental plots V13 and V11 compared to the rest. In 2015 both plots were excluded for the ANOVA analysis. In 2016, no emergence problems were observed, and all the plots were included in the ANOVA analysis. Table 4 presents the average and standard deviation of crop height and PAR interception, per treatment and season. Differences in crop height were observed between seasons: in 2016 maize height (2.15 m) was higher than in 2015 (1.96 m). In 2015 the irrigation treatment did not affect crop height. In 2016, the crop height of DPIS200 was significantly lower than for the other two treatments.

Table 4. *Average and standard deviation values of measured plant height and photosynthetically active radiation intercepted by the crop (PAR) for each treatment and crop season. Average values are also presented for all treatments.*

Treatment	2015				2016			
	Plant Height (m)		PAR (%)		Plant Height (m)		PAR (%)	
	Avg.	SD	Avg.	SD	Avg.	SD	Avg.	SD
DPIS200	2.00[a]	0.05	90.8[a]	1.85	2.08[a]	0.06	96.2[a]	0.87
CIS200	1.94[a]	0.06	94.1[a]	0.63	2.20[b]	0.04	97.1[a]	0.21
CIS300	1.95[a]	0.00	92.8[a]	2.31	2.20[b]	0.02	96.1[a]	0.51
All	1.96	0.05	92.6	2.10	2.15	0.07	96.5	0.71

The experimental season had a significant effect on PAR interception, with values in 2016 (96.5%) being higher than those in 2015 (92.6%) (Table 4). The irrigation treatment did not affect the intercepted PAR in any of the seasons.

Crop yield and components

Grain yield and biomass per experimental plot are presented in Table 5 per treatment and season. Maize grain yield presented differences between seasons, with 2016 being more productive than 2015 (17.4 *vs.* 15.2 Mg ha^{-1}). The effect of the irrigation treatment on grain yield was not statistically significant in 2015 neither in 2016 (Table 5). Low pressure treatments did not reduce yield, neither in 2015 nor in 2016.

Table 5. *Average grain yield and biomass for each treatment and crop season. Average values are also presented for all treatments.*

Treatment	2015		2016	
	Yield (Mg ha^{-1})	Biomass (Mg ha^{-1})	Yield (Mg ha^{-1})	Biomass (Mg ha^{-1})
DPIS200	15.7[a]	25.8[a]	16.9[a]	24.1[a]
CIS200	15.0[a]	26.4[a]	17.6[a]	28.1[b]
CIS300	14.6[a]	25.5[a]	17.6[a]	25.8[a]
Average	15.2	26.0	17.4	26.0

Aerial biomass did not show differences between seasons. The irrigation treatments did not affect maize biomass in 2015, but did so in 2016 (Table 5). The statistically significant biomass differences in 2016 between CIS200 and the other two treatments were not associated to differences in maize grain yield.

Yield components: plant density, number of grains per square meter, kernel mass (KM) and harvest index (HI) for each treatment and season are presented in Table 6. Differences in grain yield between seasons (Table 5) were due to differences in kernel mass, since the number of grains per square meter and plant density were not significantly different between seasons. Differences in HI between seasons could be explained by differences in grain yield, since aerial biomass was not significantly different.

The irrigation treatment had no effect on plant density, kernel mass and harvest index in 2015 and 2016 (Table 6). The irrigation treatment did not affect the number of grains per square meter in 2016, but did so in 2015. The number of grains per square meter of the CIS300 treatment resulted significantly lower than the number of grains of the treatment DPIS200 in 2015 (Table 6).

Table 6. *Plant density, number of grains, kernel mass (KM) and harvest index (HI) for the three treatments and the two irrigation seasons (2015 and 2016). Average seasonal values are also presented.*

Treatment	Plant density (plants ha^{-1})		No. of grains (grains m^{-2})		KM (mg kernel^{-1})		HI (-)	
	2015	2016	2015	2016	2015	2016	2015	2016
DPIS200	83889^{a}	86667^{a}	3699^{a}	3695^{a}	364^{a}	393^{a}	0.48^{a}	0.57^{a}
CIS200	85556^{a}	86667^{a}	3625^{ab}	3918^{a}	357^{a}	387^{a}	0.49^{a}	0.53^{a}
CIS300	86667^{a}	90000^{a}	3462^{b}	3909^{a}	363^{a}	387^{a}	0.49^{a}	0.56^{a}
Average	85371	87778	3621	3841	361	389	0.49	0.55

The results of the intensive hand harvest performed in one of the replicates of each treatment to analyze intra-plot yield variability are presented in Fig. 8. The grain yield variability of low pressure treatments (Fig. 8a and b) was slightly higher than that of the standard pressure treatment (Fig. 8c). However, the Christiansen coefficients of uniformity of grain yield were very high, and similar for the three experimental plots (94.0%, 94.5% and 95.0%, for DPIS200, CIS200 and CIS300, respectively).

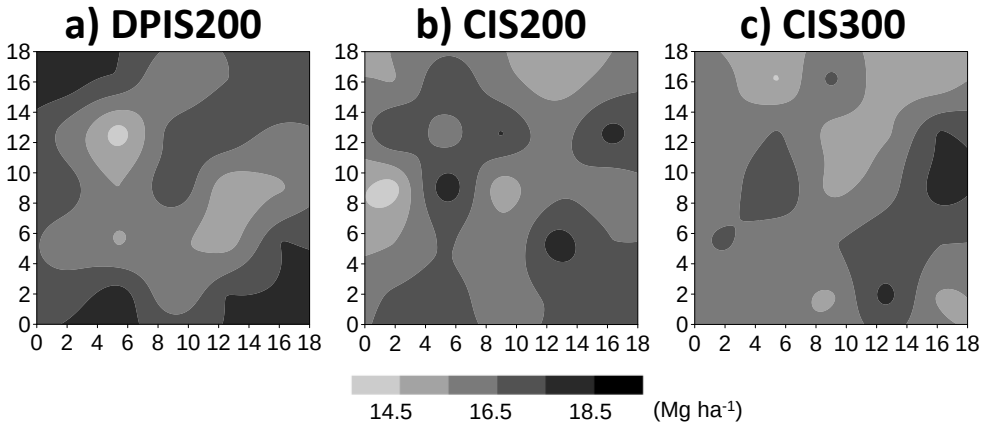

Figure 8. *Spatial variability of grain yield obtained by the intensive hand harvest performed in one replicate of each treatment: DPIS200 (a), CIS200 (b) and CIS300 (c), in 2016 crop season.*

Seasonal irrigation and crop yield

When comparing maize plot yield maps (Fig. 8) with seasonal water distribution maps (Fig. 7), no clear associations could be observed, except for the DPIS200 treatment. This treatment had the lowest $CUC_{seasonal}$ (82%) also the correlation performed between the measured seasonal irrigation depth and the hand harvested grain yield was significant (0.42). The DPIS200 and CIS300 treatments, showed no intra-plot correlation between measured seasonal irrigation depth and measured hand harvest grain yield.

Following the discussion on Tables 5 and 6, low pressure treatments did not reduce maize grain yield respect to the standard pressure treatment. However, seasonal irrigation uniformity was about ten points higher in the standard pressure treatment than the low pressure treatments. This important difference in $CUC_{seasonal}$ was expected to have an effect on maize grain yield.

Many studies have been published about the impact of irrigation non-uniformity on crop yield. Some of these studies have reported low impacts (Mateos, 1997; Allaire-Leung et al., 2001; Li and Rao, 2003), but others have found crop yield to be notably influenced by the decrease of irrigation uniformity (Stern and Bresler, 1983; Mantovani et al., 1995; Cavero et al., 2001; Dechmi et al., 2003; Salmerón et al., 2012; Urrego-Pereira et al., 2013). The conclusions of these studies seem to be affected by the amount of irrigation applied to the crop and by the crop sensitivity to water stress. If the irrigation applied to the crop is lower than its water requirements, irrigation uniformity will influence crop yield (Mantovani et al., 1995; Dechmi et al., 2003; Montazar and Sadeghi, 2008; Urrego-Pereira et al., 2013). If the crop is over irrigated non-uniformity may not show its effect on crop yield (Sánchez et al., 2010a, 2010b). These authors concluded that the effect of irrigation performance on maize growth and yield depends on irrigation depth, uniformity and irrigation scheduling. The influence of irrigation uniformity on maize yield increases with water stress, and it is particularly significant during the earliest growth period and during the tasseling stage (Dechmi et al., 2003). Sprinkler irrigation water is partitioned by the crop canopy in three components: stemflow, throughfall and interception storage (Lamm and Manges, 2000). The crop canopy redistributes the irrigation water (Steiner et al., 1983; Paltineanu and Starr, 2000; DeBoer et al., 2001) and reduces the effect of non-uniformity on crop yield.

Low pressure treatments showed lower seasonal WDEL than the standard pressure treatment (15%, 13% and 17% for DPIS200, CIS200 and CIS300, respectively). The differences between DPIS200 and CIS300 are mostly based on data measured with catch-can installed at tall elevation (2 m and 2.3 m), since differences based on 1 m catch-can elevations are different (25%, and 19% for DPIS200, and CIS300, respectively). WDEL of CIS200 treatment was the lowest for all the evaluated conditions.

Maize was selected for this experiment because it is the main crop irrigated by solid-set sprinkler systems in the central Ebro river basin and because of its sensitivity to water stress. The irrigation depth and scheduling were adjusted to gross crop water requirements in both experimental seasons. The methodology used to estimate irrigation CUC using catch-cans installed over the crop canopy has been shown to reduce its accuracy as the distance between the sprinkler nozzle and the catch-can reduces, particularly for low operating pressures (200 kPa). Taking into account the quantitative importance of stemflow and interception storage, keeping the catch-cans below the crop canopy would result in even more methodological problems. Due the difficulty in obtaining adequate estimates of the spatial variability of irrigation depth in maize, grain

yield variability or even soil water variability stand as interesting alternatives to indirectly assess irrigation performance.

Integrating low pressure solid-set sprinkler irrigation in commercial farming

Net economic benefits are the major criteria for determining acceptability of changes in design and operation of irrigation systems for energy use reduction (Allen et al., 1984). In this research we proved the feasibility of reducing energy requirements by reducing the sprinkler operating pressure from 300 kPa to 200 kPa without affecting crop yield. Anticipating the application of low-pressure irrigation, Zapata et al. (2015) presented a simulation study analyzing the economic implications of reducing the pressure at the sprinkler nozzle from 300 kPa to 200 kPa in a collective pressurized sprinkler irrigation network. The study area had an irrigation electricity cost of 200 € ha^{-1} yr^{-1} for maize operating at 300 kPa. This cost was reduced by 21% (42 € ha^{-1} yr^{-1}) when pressure was reduced to 200 kPa. Further cost reductions could have been obtained through the consideration of related infrastructure, such as the pumping station.

The issue is how to implement low pressure sprinkler irrigation in the commercial solid-sets of the central Ebro valley and beyond, ensuring an increase in farmers' net benefit. Most of these irrigation systems are connected to collective pressurized networks and large pumping stations belonging to Water Users Associations (WUA). Two different situations arise in this discussion: irrigation management and irrigation design.

In the management area, existing solid-sets can be converted into low pressure irrigation by reducing the target pressure downstream from the pumping station. In order to be able to apply crop water requirements at the farm level, the sprinkler nozzles may need to be enlarged to maintain the irrigation application rate. If the change of nozzles is needed, this can be paid for in a crop season, capitalizing the savings of about 42 € ha^{-1} yr^{-1} in the electricity bill. No further changes will be required at the farm level or at the collective network.

In the design area, the potential of low pressure irrigation is much more important, particularly when designing the modernization of WUAs and their collective networks. Low on-farm pressure requirements represent an increase of the area that can be irrigated by natural pressure (the areas of the WUA with low elevation respect to the water source). In these areas, the full cost of the electricity bill can be saved. In other cases, the pressure requirements of a few elevated farms dictate the target pumping pressure of a WUA network. Reducing the operating pressure of these few elevated farms will extend the energy savings to the whole WUA. Finally, any reduction in the target pressure or area of the collective pressurized network will imply a reduction in the cost of the pumping station.

Conclusions

For catch-cans installed at an elevation of 1.0 m, under low wind speed conditions the standard pressure treatments had slightly higher CUC than the low pressure treatments. Under high wind speed conditions differences in irrigation uniformity between low and standard pressure treatments were not clear. At this catch-can elevation, differences in irrigation uniformity of individual events between the two sprinkler models operating at 200 kPa (CIS and DPIS) were not clear. In 2016 the seasonal irrigation uniformity ($CUC_{seasonal}$) for the treatment with standard pressure was higher than for the low pressure treatments, with differences between 9-11%.

Differences in CUC between treatments increased with the elevation of the catch-cans, apparently penalizing the uniformity of low pressure treatments as the distance between sprinkler nozzle and catch-can was reduced. These differences could have led to unrealistic estimates of CUC for individual irrigation and for complete seasons. Similar results were found in the estimation of WDEL in individual irrigations. The methodology used to determine irrigation performance indexes, CUC and WDEL, using catch-cans installed above the crop canopy and at elevations near the sprinkler nozzles, should be specifically assessed for reliability.

Low pressure treatments, using conventional brass impact sprinklers or modified plastic impact sprinklers, did not reduce maize grain yield compared to a standard pressure (300 kPa) treatment using conventional brass impact sprinklers. Differences in maize grain yield could not be established between the two low pressure treatments, CIS200 and DPIS200.

In order to evaluate seasonal irrigation performance of sprinklers operating at low pressure and irrigating tall crop canopies, agronomic determinations, such as maize grain yield and its variability, were more adequate than uniformity estimates. Detailed soil water analyses could have supported the information obtained from grain yield.

It is possible to save energy on-farm by reducing the sprinkler operating pressure from 300 to 200 kPa in maize and in the experimental conditions, without reducing the sprinkler spacing and maintaining crop yield.

The present research leads to improved net economic benefits in commercial maize farms. Benefits will be much more important when considering low pressure irrigation at the time of designing collective pressurized networks for water users associations.

Acknowledgments

This paper applies the “first-last-author-emphasis” approach for the sequence of authors. This research was funded by MICINN of the Government of Spain through grant

AGL2013-48728-C2-1-R.Octavio Robles has a scholarship funded by the Minister of Economy and Competitiveness of the Spanish Government. The authors would like to thank the CSIC/CITA field staff and technicians: Eva Medina, Pilar Paniagua, Miguel Izquierdo, Miguel Á. Millán, Vicente Villarroya, César Romano, Pablo García and Laura Pérez for their technical support.

References

Allaire-Leung, S.E., Wu, L., Mitchell, J.P., Sanden, B.L., 2001. Nitrate leaching and soil nitrate content as affected by irrigation uniformity in a carrot field. Agric. Water Manage. 48 (1), 37–50.

Allen, R.G., Brockway, C.E., 1984. Concepts for energy-efficient irrigation system design. J. Irrig. Drain. Eng. 110 (2), 99–106.

Allen, R.G., Pereira, L.S., Raes, D., Smith, M., 1998. Crop evapotranspiration: guidelines for computing crop water requirements. (FAO irrigation and drainage paper 56) FAO, Rome.

Cavero, J., Playán, E., Zapata, N., Faci, J.M., 2001. Simulation of maize grain yield variability within a surface-irrigated field. Agronomy Journal 93, 773–782.

Christiansen, J.E., 1942. Irrigation by sprinkling. Agric. Exp. Stn. Bull. 670. Univ. of California, Berkeley.

Clemmens, A.J., Dedrick, A.R., 1994. Irrigation techniques and evaluations. Advanced series in agricultural sciences. K.K. Tanji and B.Yaron, eds., Springer, Berlin. pp. 64–103.

DeBoer, D.W., Stange, K.A., Beck, D.L., 2001. Sprinkler and corn canopy effects on water application characteristics. J. Irrig. Drain. Eng. 127 (5), 272–276.

Dechmi, F., Playán, E., Cavero, J., Faci, J.M., Martínez-Cob, A., 2003. Wind effects on solid set sprinkler irrigation depth and yield of maize (Zea mays). Irrig. Sci. 22, 67–77.

Dogan, E., Kirnak, H., Doyan, Z., 2008. Effect of varying the distance of collectors below a sprinkler head and travel speed on measurements of mean water depth and uniformity for a linear move irrigation sprinkler system. Biosyst. Eng. 99 (2), 190–195.

Fernández García, I., Rodríguez Díaz, J.A., Camacho Poyato, E., Montesinos, P., 2013. Optimal operation of pressurized irrigation networks with several supply sources. Water Resour. Manag. 27, 2855–2869.

ISO-15886-3., 2004. Agricultural irrigation equipment, Sprinklers. Part 3: Characterization of distribution and test methods.

Kincaid, D.C., 1982. Reducing Energy requirements for sprinkler systems. Proceeding of the Irrigation Association Technical Conference, Portlan, Oregon, 35 p.

Kincaid, D.C., 1991. Impact sprinkler pattern modification. Trans. ASAE. 34 (6), 2397–2403.

Kincaid, D.C., 1996. Spray drop kinetic energy from irrigation sprinklers. Trans. ASAE 39 (3), 847–853.

Kincaid, D.C., Longley, T.S., 1986. A water droplet evaporation and temperature model. Trans. ASAE. 32 (2), 457–462.

Kincaid, D.C., Solomon, K.H., Oliphant, J.C., 1996. Drop size distributions for irrigation sprinklers. Trans. ASAE. 39(3), 839–845.

Lamm, F.R., Manges, H.L., 2000. Partitioning of sprinkler irrigation water by a corn canopy. Trans ASAE. 43 (4): 909–918.

Li, J., Rao, M., 2003. Field evaluation of crop yield as affected by nonuniformity of sprinkler-applied water and fertilizers. Agric. Water Manage. 59 (1): 1–13.

Mantovani, E.C., Villalobos, F.J., Orgaz, F., Fereres, E., 1995. Modelling the effects of sprinkler irrigation uniformity on crop yield. Agric. Water Manage. 27, 243–257.

Martínez-Cob, A., 2008. Use of thermal units to estimate corn crop coefficients under semiarid climatic conditions. Irrig. Sci. 26, 335–345. Doi: 10.1007/s00271-007-0097-5.

Mateos, L., 1997. Cotton response to non-uniformity of conventional sprinkler irrigation. Irrig. Sci. 17, 47–52.

Montazar, A., Sadeghi, M., 2008. Effects of applied water and sprinkler irrigation uniformity on alfalfa growth and hay yield. Agric. Water Manage. 95 (11),1279–1287.

Moreno, M.A., Ortega, J.F., Córcoles, J.I., Martínez, A., Tarjuelo, J.M., 2010. Energy analysis of irrigation delivery systems: monitoring and evaluation of proposed measures for improving energy efficiency. Irrig. Sci. 28, 445–460.

Omary, M., Sumner, H., 2001. Modeling water distribution for irrigation machine with small spray nozzles. J. Irrig. Drain. Engi, ASCE. 127(3), 156–160.

Paltineanu, I.C., Starr, J.L., 2000. Preferential water flow through corn canopy and soil water dynamics across rows. Soil Sci. Soc. Am. J. 64, 44–54.

Paniagua, M.P., 2015. Mejora del riego por aspersión en parcela. PhD Dissertation. Universidad de Zaragoza, 261 p (*in Spanish*).

Playán, E., Salvador, R., Faci, J.M., Zapata, N., Martínez-Cob, A., Sánchez, I., 2005. Day and night wind drift and evaporation losses in sprinkler solid-sets and moving laterals. Agric. Water Manage. 76 (3), 139–159.

Playán, E., Zapata, N., Faci, J.M., Tolosa, D., Pelegrín, J., Salvador, R., Lafita, A, Sánchez, I., 2006. Assessing sprinkler irrigation uniformity using a ballistic simulation model. Agric. Water Manage. 84 (1-2), 89–100.

Rocamora, C., Vera, J., Abadía, R., 2013. Strategy for efficient energy management to solve energy problems in modernized irrigation: analysis of the Spanish case. Irrig. Sci. 31(5), 1139–1158.

Rodríguez Díaz, J.A., López Luque, R., Carrillo Cobo, M.T., Montesinos, P., Camacho Poyato, E., 2009. Exploring energy saving scenarios for on demand pressurized irrigation networks. Biosyst. Eng. 104, 552–561.

Sahoo, N., Pradhan, P.L., Anumala, N.K., Ghosal, M.K., 2008. Uniform water distribution from low pressure rotating sprinklers. Agricultural Engineering International: the CIGRE journal. Manuscript LW 08 014. Vol. X. October, 2008.

Salmerón, M., Urrego, Y.F., Isla, R., Cavero, J., 2012. Effect of non-uniform sprinkler irrigation and plant density on simulated maize yield. Agric. Water Manage. 113, 1–9.

Sánchez, I., Zapata, N., Faci, J.M., 2010a. Combined effect of technical, meteorological and agronomical factors on solid-set sprinkler irrigation. I. Irrigation performance and soil water recharge in alfalfa and maize. Agric. Water Manage. 97(10), 1571–1581.

Sánchez, I., Zapata, N., Faci, J.M., 2010b. Combined effect of technical, meteorological and agronomical factors on solid-set sprinkler irrigation. II. Modifications of the wind velocity and of the drops interception plane by the crop canopy. Agric. Water. Manage. 97(10), 1591–1601.

Steiner, J.L., Kanemasu, E.T., Clark, R.N., 1983. Spray losses and partitioning of water under a centre pivot sprinkler system. Trans. ASAE. 26 (4), 1128–1134.

Stern, J., Bresler, E., 1983. Nonuniform sprinkler irrigation and crop yield. Irrig. Sci. 4 (1), 17–29.

Tarjuelo, J.M., Montero, J., Honrubia, F.T., Ortiz, J.J., Ortega, J.F., 1999. Analysis of uniformity of sprinkle irrigation in a semiarid area. Agric. Water Manage. 40, 315–331.

Tarjuelo, J.M., Rodríguez-Díaz, J.A., Abadía, R., Camacho, E., Rocamora, C., Moreno, M.A., 2015. Efficient water and energy use in irrigation modernization: Lessons from Spanish case studies. Agric. Water Manage. 162, 67–77.

Urrego-Pereira, Y., Martínez-Cob, A., Cavero, J., 2013. Relevance of sprinkler irrigation time and water losses on maize yield. Agron. J. 105, 845–853.

Zapata, N., Latorre, B., Citoler, F.J., Gallinat, J., Bescós, M., Castillo, R., Mantero, N., Burguete, J., Playán, E., 2015. Collective irrigation network design and management for energy optimization: the "CINTEGRAL" tool. ICID 26th Euro Mediterranean Regional Conference and ICID 56th International Executive Council. Montpellier, France. 11–16 October 2015.

CHAPTER III. LOW-PRESSURE SPRINKLER IRRIGATION IN MAIZE: DIFFERENCES IN WATER DISTRIBUTION ABOVE AND BELOW THE CROP CANOPY

LOW-PRESSURE SPRINKLER IRRIGATION IN MAIZE: DIFFERENCES IN WATER DISTRIBUTION ABOVE AND BELOW THE CROP CANOPY[2]

Resumen

La reducción de la presión de operación en la boquilla de los aspersores de impacto es una de las alternativas para reducir los requerimientos de energía en los sistemas de riego de cobertura total. Estudios anteriores reportan aproximadamente un 10% menos del coeficiente de uniformidad de Christiansen (CUC) para los tratamientos de baja presión respecto a los de presión convencional, pero sin diferencias en la cosecha de maíz. Este trabajo analiza el efecto del dosel de maíz en los índices de evaluación del riego por aspersión (CUC, y las pérdidas por evaporación y arrastre–WDEL–). Se consideraron tres tratamientos de riego, basados en la presión de operación: 1) un aspersor de impacto de latón con presión de operación de 300 kPa (CIS300); 2) un aspersor de impacto de latón a una presión de 200 kPa (CIS200); y 3) un aspersor de impacto de plástico modificado (con una placa deflectora unida al brazo difusor) con presión de operación de 200 kPa (DPIS200). Se evaluaron los eventos de riego usando una malla de pluviómetros instalados por encima del dosel del maíz (CUC_{ac}, $WDEL_{ac}$) en toda la temporada de cultivo, además, se evaluaron en ocho riegos la precipitación por el tallo y por las hojas del maíz (CUC_{bc}, $WDEL_{bc}$) en ocho riegos. Se midió la altura del maíz, la cosecha y sus componentes. El CUC_{bc} resultó mayor que CUC_{ac} para los tratamientos de baja presión en condiciones de viento bajo y en total desarrollo del dosel vegetal (situación común en riego de maíz), explicando por qué no hay diferencias de cosecha de grano entre ellos. Se debe tener precaución al medir los índices de calidad del riego por encima de doseles altos, pues la altura de los pluviómetros y la división del dosel del cultivo afectan a estas estimaciones.

Palabras clave: pluviómetros, flujo del tallo, flujo a través las hojas, uniformidad de riego, baja presión, pérdidas por evaporación y arrastre.

[2] Zapata, N., Robles, O., Playán, E., Paniagua, P., Romano, C., Salvador, R., Montoya, F., 2018. Low-pressure sprinkler irrigation in maize: Differences in water distribution above and below the crop canopy. Agric. Water Manag. 203: 353–365. (*published*)

Abstract

Reducing the working pressure at the sprinkler nozzles is one of the alternatives to reduce energy requirements in solid-set sprinkler irrigation systems. Previous studies reported ≈10% lower seasonal Christiansen uniformity coefficient (CUC) for low-pressure treatments than for standard treatments, but no differences in maize yield. This research analyses the effect of maize canopy partitioning in irrigation performance indexes (CUC and wind drift and evaporation losses, WDEL). Three irrigation treatments were considered, based on the working pressure: 1) a standard brass impact sprinkler operating at a pressure of 300 kPa (CIS300); 2) a standard brass impact sprinkler operating at a pressure of 200 kPa (CIS200); and 3) a modified plastic impact sprinkler (with a deflecting plate attached to the drive arm) operating at a pressure of 200 kPa (DPIS200). Irrigation performance was measured using a catch-can network located above the maize canopy (CUC_{ac}, $WDEL_{ac}$) along the whole crop season, and stemflow and throughfall devices below the maize canopy (CUC_{bc}, $WDEL_{bc}$) in eight irrigation events. Maize growth, yield and its components were measured. Under low wind and fully developed canopy conditions (a frequent situation for maize irrigation), CUC_{bc} resulted higher than CUC_{ac} for the low-pressure treatments, while the opposite was observed for the standard pressure treatment. Maize canopy partitioning reduces the differences in irrigation performance indexes between pressure treatments, explaining why there are no differences in grain yield between them. Caution should be used when measuring sprinkler irrigation performance above tall canopies, since the elevation of the catch-cans and the crop canopy partitioning affect performance estimations.

Keywords: catch-cans, stemflow, throughfall, irrigation uniformity, low-pressure, wind drift and evaporation losses.

Introduction

Reducing the energy requirements of pressurized irrigation systems is one of the key objectives of farmers and Water Users Associations (WUA). The optimization of irrigation facilities (pumping stations and collective pressurized networks) has proven useful and cost effective (Rodríguez Díaz et al., 2009; Moreno et al., 2010; Fernández García et al., 2013). Additional solutions are currently being analyzed at the WUAs. Among them, the reduction of energy requirements at the farm level by reducing the working pressure at the sprinkler nozzles (Robles et al., 2017). Reducing pressure at the nozzles will result in lower pumping requirements and therefore in a reduction of the energy bill. Further, when low-pressure is considered at the design phase of the collective network, the area of a WUA requiring pumping can be reduced.

Coefficient of Uniformity (CUC) (Christiansen, 1942) measurement above the crop canopy is the standard method used to analyze the variability in sprinkler irrigation water application for irrigation design and management purposes. Such measurements intend to characterize variability at the horizontal plane where sprinkler irrigation water is intercepted by the crop. For solid-set sprinkler systems, Keller and Bliesner (1991) classified irrigation uniformity as ‘‘low’’ when the CUC is below 84%. Irrigation design is a compromise between investment cost, system performance and net income. For high-value crops, the chances of investing in high-uniform irrigation systems are higher than for low value crops (Seginer, 1978).

Uniformity is a key performance indicator for irrigation design purposes. Environmental factors - such as wind speed and direction - change during the crop season, affecting uniformity in each irrigation event. Over-irrigation, a common practice of farmers in windy areas, reduces the effect of low irrigation uniformity on crop yield (Sánchez et al., 2010). Measuring uniformity on tall crop canopies (such as fully developed maize) constitutes an experimental challenge. Additionally, the distribution of water measured above a developed crop canopy may differ from the distribution measured below the canopy or in the soil.

The effect of sprinkler irrigation CUC (measured above the crop canopy) on crop yield has been analyzed in a number of papers. Rezende et al. (2000) reported than the yield of grain bean changed between uniformity treatments, although the highest uniformity did not lead to the highest yield. Li and Rao (2003) analyzed irrigation events differing in uniformity and did not observe any effect on wheat yield. It is important to note that only half of the wheat water requirements were applied by irrigation, while the rest come from precipitation and soil water. Mateos et al. (1997) reported that for crops with curvilinear crop production function (such as cotton) low irrigation uniformity did not reduce yield. However, it induced variations in vegetative growth and in the time blooming, hindering mechanical harvest. Montazar and Sadeghi (2008) reported that sprinkler uniformity had a direct effect on alfalfa growth and hay yield. Brennan (2008)

found important economic incentives for adopting more uniform sprinkler irrigation systems in lettuce production. Jiménez et al. (2010) reported a strong effect of sprinkler CUC on onion yield. The experimental research found in the literature on sprinkler irrigated maize (Stern and Bersler, 1983; Dechmi et al., 2003; Cavero et al., 2008; Sánchez et al., 2010; Urrego-Pereira et al., 2013) agreed that when irrigation was applied according to crop water requirements, grain yield and its variability were affected by irrigation uniformity.

Several research works have focused on soil water redistribution in sprinkler irrigated crops (van Wesenbeeck and Kachanoski, 1988; van Wesenbeeck et al., 1988; Li and Kawano, 1996; Paltineanu and Starr, 2000; Sánchez et al., 2010; Martello et al., 2015). In particular, Paltineanu and Starr (2000) and Sánchez et al. (2010), measured soil water dynamics at row and interrow maize positions using capacitance probes. They reported on the importance of canopy-induced water redistribution, which affected the spatial variability of soil water.

Irrigation precipitation reaching the soil surface after its passage through a developed crop canopy can have a different spatial variability than the precipitation collected above the canopy. In fact, the canopy architecture distributes the incident precipitation into three processes: stemflow, throughfall and interception storage (Bui and Box, 1992). Stemflow is the portion of water that is intercepted and collected by leaves and branches, and flows down the stem to the soil surrounding the plant. Throughfall is the water that falls on the soil surface directly or indirectly through the leaves. Interception storage is the amount of water that temporally remains on the plant after irrigation and that evaporates directly from the leaves and stems. Several authors (van Wesenbeeck and Kachanoski, 1988; van Wesenbeeck et al., 1988; Lamm and Manges, 2000; Li and Rao, 2000; Paltineanu and Starr, 2000; Canone et al., 2017; Sun et al., 2017) reported that crop canopy architecture plays a major role on the spatial distribution of rainfall and sprinkler irrigation water.

Measuring the sprinkler water distribution above the crop canopy is a well-defined task, regulated by standards (ISO, 1990; ASAE, 1994; ISO, 1995). However, the measurement of sprinkler water distribution below the crop canopy is not standardized, and remains within the research domain. Several authors have reported the interaction between sprinkler or rainfall water and crop canopies (van Wesenbeeck and Kachanoski, 1988; van Wesenbeeck et al., 1988; Lamm and Manges, 2000; Li and Rao, 2000; Paltineanu and Starr, 2000). These works presented different measurement methodologies, often focusing on stemflow determination. Van Wesenbeeck and Kachanoski (1988) and van Wesenbeeck et al. (1988) did not measure stemflow directly, but measured soil water content with Time Domain Reflectometry (TDR) at maize rows and interrows. These authors reported on the importance of water partitioning induced by the crop canopy when it comes to determining the spatial pattern of soil water. Li and Rao (2000) measured soil water distribution above and below a wheat canopy by using the same catch-can devices. The catch-cans installed

below the wheat canopy did not separate stemflow and throughfall. These authors reported that wheat irrigation uniformity was higher below the canopy than above the canopy. Lamm and Manges (2000) directly measured stemflow and throughfall in 18 individual plants within a center-pivot irrigated maize field. The stemflow measurement device was a plastic pipe tube with a diameter of 0.05 m and a full length slot cut fitted around the plant stem. These authors found that stemflow decreased linearly with plant spacing and increased linearly with irrigation depth, whereas throughfall increased linearly with both plant spacing and irrigation depth. Hupet and Vanclooster (2005) estimated stemflow as the difference between measured incident rainfall, measured throughfall and estimated crop interception. These authors reported that rainfall reaching the ground below the maize canopy was very spatially variable, with coefficients of variation ranging between 78% and 189%. Martello et al. (2015) measured maize water partitioning (stemflow and throughfall) in twelve plants positioned in pairs across a plot irrigated by a travelling big-gun sprinkler. The devices used for stemflow measurement were similar to those used by Lamm and Manges (2000). Martello et al. (2015) concluded that the stemflow / throughfall ratio logarithmically decreased with the increase in precipitation, suggesting that under water stress conditions maize can effectively confine precipitation water close to the roots. Liu et al. (2015) used high water adsorption sheets wrapped around each maize stem to measure water stemflow. Twenty plants were selected for stemflow measurements in a total experimental area of 6 m^2. These authors concluded that stemflow increased with increasing precipitation and leaf area index, but decreased with increasing precipitation intensity.

In a clear precedent to this research, Robles et al. (2017) (Chapter II) performed two years of experimental field work to measure differences in maize yield and irrigation performance (CUC and WDEL) resulting from three irrigation treatments. These included two nozzle pressures (standard of 300 kPa and low-pressure of 200 kPa) and, in the case of low-pressure, two sprinkler models (conventional brass impact sprinkler CIS and plastic impact sprinkler with deflecting plate in the drive arm DPIS). These authors did not find statistical differences in maize yield between the three irrigation treatments guided by crop water requirements. However, the CUC measured above maize canopy was 10% higher for the standard pressure treatment (93%) than for the low-pressure treatments (averaging 83%).

The objective of this research was to analyze why a considerable (10%) and consistent (two crop seasons) difference in CUC measured above the maize canopy between two pressure irrigation treatments (200 kPa and 300 kPa) had no effect on maize yield. The experimental design reported by (2017) was repeated for one additional year, implementing its three treatments CIS300, CIS200 and DPIS200. Treatments had the same application rate and irrigation scheduling. To accomplish this objective, differences in drop size distribution, radial distribution curves, soil water distribution and maize canopy water partitioning were experimentally measured for the three irrigation treatments. The effect of

irrigation water distribution (above and below the maize canopy) on grain yield was statistically analyzed for all irrigation treatments.

Materials and Methods

Technical characterization of the sprinklers

Three impact sprinklers were used in the field experiment: 1) a standard brass impact sprinkler (RC FARM 130, Riegos Costa, Lleida, Spain) equipped with double brass nozzle (4.4 mm and 2.4 mm) operating at a pressure of 300 kPa (CIS300); 2) a standard brass impact sprinkler (RC FARM 130, Riegos Costa, Lleida, Spain) equipped with double plastic nozzle (5.16 mm and 2.5 mm) operating at a pressure of 200 kPa (CIS200); and 3) a modified plastic impact sprinkler with a deflecting plate attached to the drive arm (5035, NaanDanJain, Naan, Israel) equipped with double plastic nozzle (5.16 mm and 2.5 mm) operating at a pressure of 200 kPa (DPIS200). Commercial sprinklers and nozzles were used in all cases. The average flow of the three sprinklers was 1680 L h^{-1}, with differences between pressure treatments lower than 4%.

The DPIS is a new impact sprinkler commercialized to operate at low pressures. It is based on developments by Kincaid (1991), who proposed a modification of the impact-type sprinkler by adding a deflector attached to the drive arm. The modification results in a larger intermittent deflection of the jet that adds precipitation to the proximal region, which is typically infra irrigated in low-pressure conditions.

The radial water distributions of the three isolated sprinkler types were characterized at an outdoor research facility. Each sprinkler was installed at the top of a riser pipe at 2.30 m above ground level (a.g.l.). The precipitation created by the sprinkler was collected in four catch-can radii at distances from the sprinkler ranging from 0.50 m to 16.0 m, with a catch-can spacing of 0.50 m. Each radius had a different catch-can elevation. The mouth of the catch-can was located at 0.50 m, 1.00 m, 1.50 m and 2.00 m a.g.l., for the first, second, third and fourth radii, respectively. Experiments were always performed under low-wind conditions (< 1.0 m s^{-1}).

Drop diameter distribution was measured for the three sprinkler types using an optical disdrometer. Drop diameters were measured at: 1) horizontal distances from the sprinkler ranging from 1.00 m to 13.00 m, with a 1.00 m step, using a disdrometer elevation of 1.00 m a.g.l.; and 2) horizontal distances from the sprinkler ranging from 3.00 m to 14.00 m, with a 1.00 m step, using a disdrometer elevation of 2.00 m a.g.l. A particle size and velocity disdrometer (PARSIVEL, OTT Messtechnik GmbH & Co. KG, Kempten, Germany) was used to measure sprinkler drop size distribution. This is a laser-optical disdrometer that can independently measure the size and the fall velocity of hydrometeors falling through a laser sheet. The laser sheet is approximately 180 mm long, 30 mm wide (5400 mm^2), and 1 mm high. The size of the hydrometeor is estimated from

the maximum attenuation of the signal. The duration of the hydrometeor within the laser beam provides the fall speed (Tokay et al., 2014).

Adaptations reported by Paniagua (2015) to improve disdrometer data retrieval and processing for sprinkler irrigation applications were used in this study. Sprinkler water drops do not fall horizontally. In fact, Paniagua (2015) reported that the fall angle changes with the horizontal and vertical distance to the sprinkler. In order to render disdrometer measurements comparable, the cross-sectional area of the laser beam exposed to falling drops should be the same. Paniagua (2015) developed a disdrometer pedestal that allows tilting the laser sensor to make it perpendicular to the average drop fall angle. The pedestal was used in all experiments reported in this paper.

The low-speed (1/100 s) photography method proposed by Salvador et al. (2009) was applied at each horizontal distance from the sprinkler and disdrometer elevation to determine the most frequent drop angle. Drops photographed in good quality were selected for angle measurement. At each location, the falling drop angle was obtained as an average of the most frequent drop angles obtained from each picture. Further, the disdrometer was installed at each location with a tilt angle equal to the falling drop angle. This ensured perpendicularity between the laser beam and the drops.

Comparisons were established at the different horizontal distances from the sprinkler between drop diameter frequencies, sprinkler types and disdrometer elevations. The estimated irrigation volumes at each measurement point were also compared.

Description of experimental site and agronomic management

The agronomic experiment was conducted in a 2.0 ha solid-set facility located at the experimental farm of the Aula Dei Agricultural Research Centre in Montañana (Zaragoza, NE Spain). The sprinkler layout was square, with a spacing of 18 m between sprinkler lines and 18 m between sprinklers of the same line. The irrigation system was composed by 14 irrigation blocks. Two linear blocks irrigated the borders of the experiment, while twelve square blocks corresponded to the experimental plots. Each experimental plot was composed by four impact sprinklers (324 m^2) and was controlled by a hydraulic valve equipped with a pressure regulator.

Three irrigation treatments were analyzed: CIS300, CIS200 and DPIS200. The treatments with low working pressure implemented larger nozzles than the treatment with standard pressure. The goal was to obtain in all treatments a similar gross irrigation application rate of 5.2 mm h^{-1}. Each treatment had four replicates, randomly distributed in the twelve experimental plots (Fig. 9a). The experimental details of the three treatments could be found in the Chapter II, with the exception of the sprinkler riser height, which in this case was set at 2.30 m a.g.l.

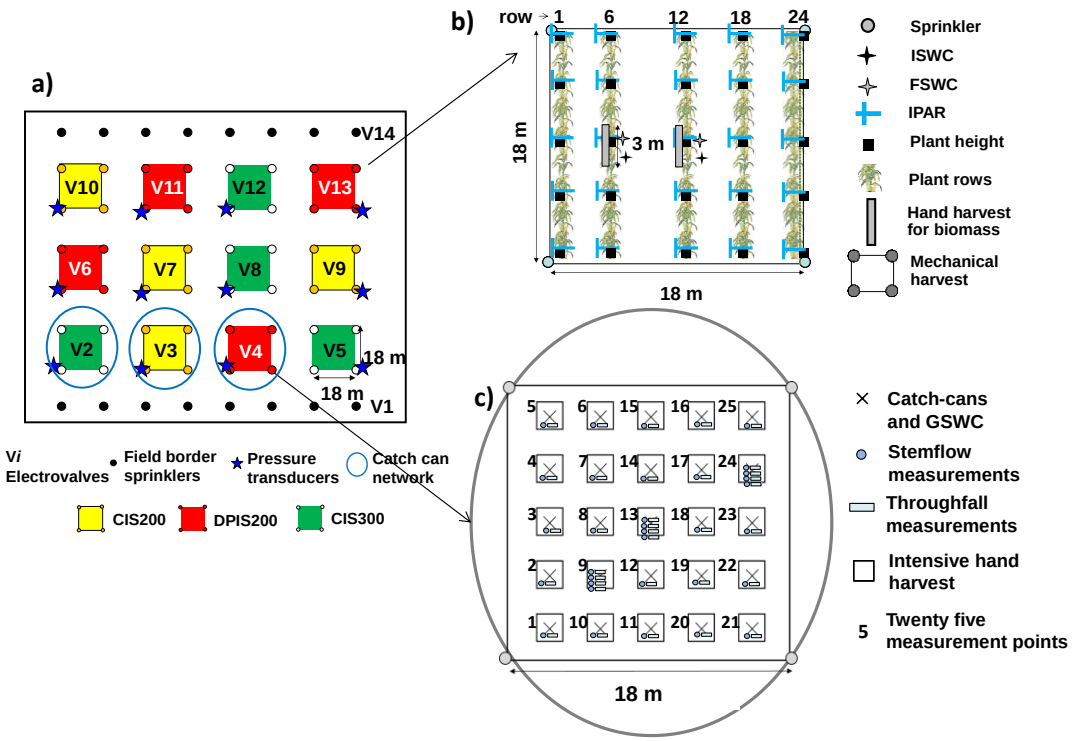

Figure 9. *a) experimental design, detailing the location of the three treatments and four replicates. b) measurement points for variables monitored at all the experimental plots: plant height, photosynthetically active radiation (PAR) and hand harvest for biomass, initial and final soil water content (ISWC and FSWC). c) measurement points for variables monitored at one replicate of each treatment: catch-can network, stemflow and throughfall network, soil water content (SWC) and intensive hand harvest area.*

The experiment was performed on a maize crop during the 2017 crop season. Maize (Pioneer P1758) was sown in April 4 in rows separated 0.75 m and with a density of 89500 seeds ha^{-1}. Fertilization consisted in 64 kg ha^{-1} of N, 120 kg ha^{-1} of P_2O_5 and 120 kg ha^{-1} of K_2O applied before the planting date. Two applications of 100 kg ha^{-1} of N as ammonium-urea-nitrate solution (32% N) were performed at V6 and V12 growth stages. Weeds and pests were controlled according to best management practices in the area.

Irrigation requirements

Maize evapotranspiration (ET_c) was computed from reference evapotranspiration (ET_0) and crop coefficients (Allen et al. 1998). ET_0 was obtained from the Montañana station, the nearest station of the SIAR agrometeorological network (www.magrama.gob.es/siar/informacion.asp). This station is located at a distance of 1.2 km from the experimental site. Maize crop coefficients were derived from the model of relative cumulative degree-days proposed by Martínez-Cob (2008) in the experimental area. Maize irrigation requirements were weekly determined as a balance between ET_c, effective precipitation (considered 75% of weekly precipitation), soil water availability and

net irrigation application. An irrigation efficiency of 85% was assumed in this work, in agreement with efficiency estimates reported in the literature for solid-set sprinkler irrigation systems (Clemmens and Dedrick, 1994). The three treatments were simultaneously irrigated to ensure equal meteorological conditions. Since the irrigation application rate was constant among treatments, the seasonal irrigation volume was the same for the three treatments.

Soil water measurements

Initial and final soil water content (ISWC and FSWC, %) were gravimetrically determined before sowing and after harvesting, respectively. Two measurement points were selected at each plot for soil water sampling (Fig. 9b). The intra-plot spatial variability of gravimetric soil water content (SWC) was determined before and after two irrigation events. Soil samples were manually collected with a 0.05 m diameter hand auger (Eijkelkamp Agrisearch Equipment BV, The Netherlands) every 0.30 m, to a depth of 0.90 m. Twenty-five measurement points (Fig. 9c) were sampled at one replicate plot of each irrigation treatment.

Irrigation water distribution measurements above the crop canopy

The irrigation water distribution pattern above the maize canopy was evaluated by a double network of 25 catch-cans at the beginning of the crop season. The catch-can mouths were located at respective elevations of 1.00 and 2.00 m a.g.l. (Fig. 9c). Catch-can networks were installed in one replicate of each irrigation treatment (Fig. 9a), the same one where SWC was monitored. Each catch-can was conical in shape, 0.40 m high and had a circular mouth with a diameter of 0.16 m (catchment area of 0.020 m^2). Catch-cans were marked at 1 mm precipitation intervals.

When the crop reached 1.00 m height, the catch-can network located at 1.00 m a.g.l. was removed. The second network was maintained until the maize canopy reached 2.00 m. Then the network was raised to remain always above the crop canopy. At the end of the growing season, the catch-can mouth was set at an elevation of 2.65 m a.g.l. Uniformity was determined for each evaluated irrigation event above the crop canopy (CUC_{ac}, %). Seasonal CUC ($CUC_{ac\_seasonal}$) was determined by applying the CUC equation to the cumulative above-canopy seasonal irrigation depth collected in each set of catch-cans. Wind drift and evaporation losses above the crop canopy ($WDEL_{ac}$) were estimated as the difference between applied irrigation depth and collected irrigation depth at the catch-can network (Playán et al., 2005), expressed as percentage of the applied irrigation depth. $WDEL_{ac}$ were determined for each evaluated irrigation event and seasonally ($WDEL_{ac\_seasonal}$).

The irrigation events evaluated with the double catch-can network were compared in terms of collected irrigation depth, CUC (CUC_{1m} and CUC_{2m}) and WDEL ($WDEL_{1m}$ and $WDEL_{2m}$).

Irrigation water distribution measurements below the crop canopy

Stemflow and throughfall were measured from July 18th to July 28th to evaluate irrigation water partitioning by the maize canopy. These variables were separately measured in 25 plants of each irrigation treatment (one replicate per treatment). The selected plants were located near each catch-can (Fig. 9c). From July 24th to July 28th three selected measurement points of each treatment were reinforced by measuring four plants per catch-can. These points were 1, 13 and 24 in CIS300, 9, 18 and 24 in CIS200 and 9, 13 and 24 in DPIS200 (Fig. 9c).

A stemflow collector and a throughfall collector were installed at each measurement point. Stemflow water was captured by a plastic device fixed to the plant stem (Fig. 10a). The plastic device corresponded to the inverted upper part of a polypropylene water bottle with its cap. A vertical v-shaped cut was performed on one side of the bottle part to hug the stem. American waterproof tape was used to attach the collector device to the stem. The stemflow collector was installed just below the insertion of the last active leaf (Fig. 10a). The attachment was reinforced with paperclips. A small plastic hose, glued into a hole of the bottle cap, led stemflow water to a container (Fig. 10a). Throughfall water was caught in a rectangular plastic rain gauge with an opening area of 0.120 m x 0.385 m (0.0462 m^2, Fig. 10b). Stemflow and throughfall were volumetrically measured. The collected volume at the stemflow measurement devices was converted to depth (mm) by assigning an area of 0.116 m^2 to one maize plant (0.155 m x 0.75 m, distance between plants and distance between plant lines, respectively). The volume collected at the throughfall devices was converted to depth (mm) dividing by the opening area of these devices (0.0462 m^2). Precipitation below the maize canopy (mm) at each measurement point was obtained by adding stemflow and throughfall.

Uniformity was determined for each irrigation evaluated for water partitioning: stemflow water ($CUC_{Stemflow}$), throughfall water ($CUC_{Throughfall}$) and the addition of both (below-canopy, CUC_{bc}). Wind drift and evaporation losses below-canopy ($WDEL_{bc}$) were estimated as the difference between applied irrigation depth and collected irrigation depth with stemflow and throughfall measurement devices, expressed as percentage of the applied irrigation depth. Please note that this estimate of $WDEL_{bc}$ is affected by the interaction of the irrigation water with the crop canopy. This interaction results in interception storage and evaporation from maize stems and leaves. Martínez-Cob et al. (2008) presented a detailed analysis of these processes in fully developed maize canopies.

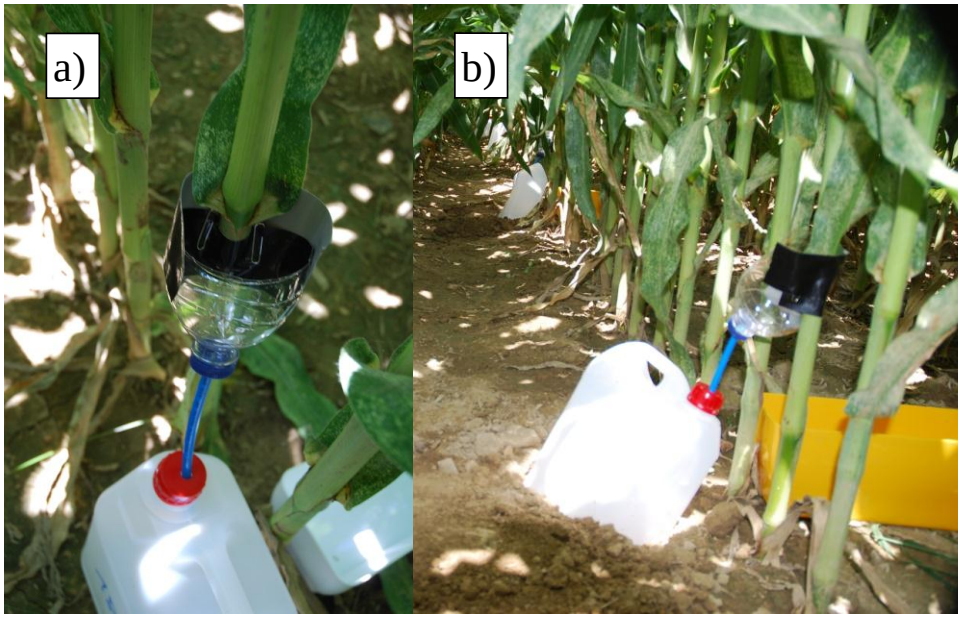

Figure 10. *a) Stemflow measurement device. b) Stemflow and throughfall collectors at a measured plant.*

Maize growth and yield variables

Plant height was measured after tasseling (27-28 June), using a ruler with centimetric accuracy. Twenty-five measurement points were homogenously distributed at each experimental plot (Fig. 9b). Plant height at an experimental plot was determined as the average of all measurements.

The photosynthetically active radiation (PAR, %) intercepted by the crop was measured at each experimental plot at R5 growth stage (31 July) with a 1-m-long ceptometer using 64 photodiodes (Sunscan, Delta-T, Cambridge, UK) and a PAR sensor (BF3 Sunshine sensor, Delta-T, Cambridge, UK). The PAR sensor continuously measured radiation above the crop canopy. Radiation at the soil surface was measured at each experimental plot by taking 25 readings (Fig. 9b) with the ceptometer placed perpendicular to the plant rows and moving it across the rows of the plot, covering consecutive sections 1 m in length. Measurements were taken around 12:00 GMT. The fraction of PAR intercepted by the crop was computed as the percentage of the difference between the BF3 readings and the ceptometer readings, to the BF3 readings. The PAR intercepted by the plants at each plot was determined as the average of the 25 measurements.

Hand harvest was performed on September 25 at each experimental plot to determine aerial biomass. The maize plants located in a 3-m-long section of two different rows (rows 6 and 12), a total of 4.5 m^2 in each experimental plot (Fig. 9b), were hand harvested by cutting them at the soil surface level. The grain was separated from the cob and both parts were dried at 60ºC. Grain yield was adjusted to standard 140 g kg^{-1} moisture

content. The final number of plants, number of ears, total biomass and harvest index (HI) were determined for each plot and treatment.

An intensive hand harvest was performed on the same day at three experimental plots to determine the intra-plot spatial variability of grain yield. The three experimental plots, one replicate per treatment, were coincident with those used for intensive precipitation measurements. Maize grain was manually harvested at 25 points in each experimental plot (Fig. 9c). The maize ears located in a 2-m-long section of two different rows (one at each side of the pluviometer) were hand harvested at each point. The grain was separated from the cob and dried at 60ºC. Grain yield was adjusted to standard 140 g kg^{-1} moisture content. Comparisons were established between treatments and with the spatial variability of seasonal irrigation for every treatment.

The twelve experimental plots (18 × 18 m) were independently harvested on September 28 using a combine. Grain was weighed with a 1-kg-precision scale. A grain subsample was collected to measure grain moisture and then used to determine plot yield at 140 g kg^{-1} moisture content.

Data analysis

The relationships between water measured at two catch-can elevations, between wind speed and irrigation uniformity, between wind speed and WDEL and between water measured above and below maize canopy were analyzed for the three treatments using statistical regression. Contour line maps produced with the SURFER software (© Golden Software Inc.) were used to represent drop spatial distribution at the irrigation treatments, irrigation water distribution and hand harvested grain yield. Differences between treatments in maize growth variables yield and its components were analyzed using ANOVA. Means were separated using Fisher's Protected LSD at $P = 0.05$.

Results

Technical characterization of the sprinklers

Figure 11 presents the radial water distribution curves of the three sprinklers types at four catch-can elevations. The largest effect of catch-can elevation was observed near the sprinkler. The water volume collected in the first meters was higher for the 2 m elevation radius than for the rest of radii. The difference was larger for the low-pressure irrigation treatments (CIS200 and DPIS200) than for the standard pressure treatment (CIS300). This was particularly important for DPIS200, where the difference remained relevant until a distance of 5 m from the sprinkler.

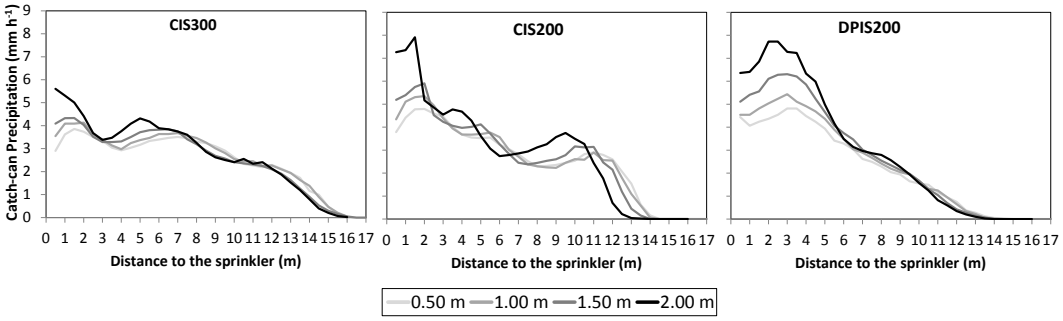

Figure 11. *Radial water application pattern for the CIS300, CIS200 and DPIS200 sprinkler. Precipitation was measured at 0.50, 1.00, 1.50 and 2.00 m above ground level.*

The simulated overlapping of the radial curves in a rectangular sprinkler arrangement of 18 m by 18 m revealed that the effect of catch-can elevation on CUC was large for the low-pressure treatments and irrelevant for the standard pressure treatment. Differences in CUC between the lowest and highest catch-can elevations (0.5 and 2.0 m, respectively) were of 24%, 13% and 3%, for the CIS200, DPIS200 and CIS300 treatments, respectively.

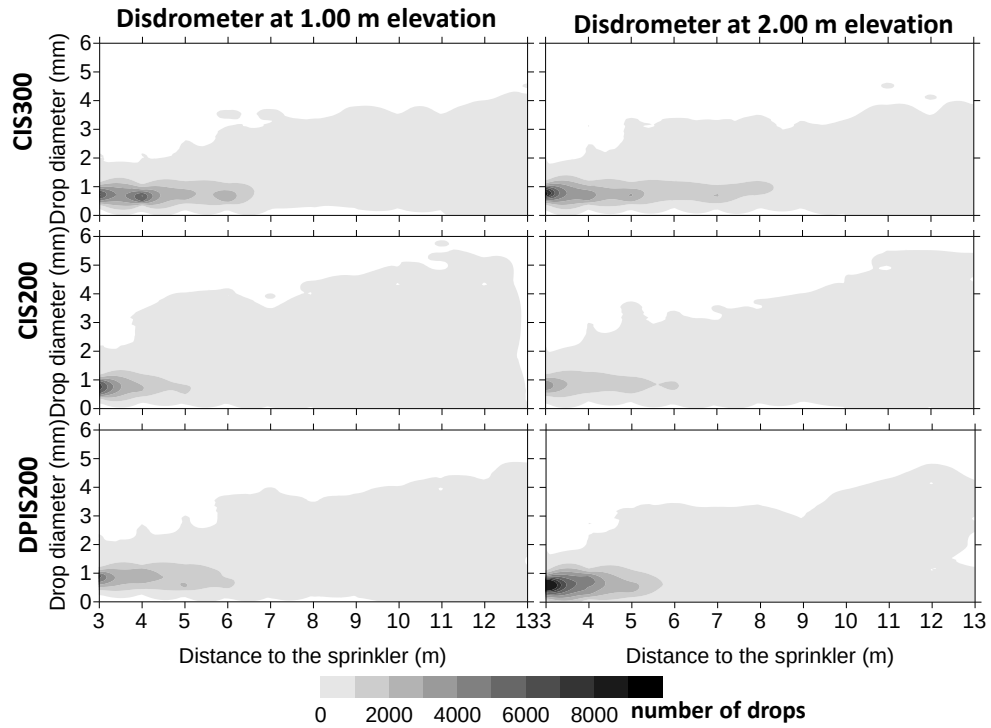

Figure 12. *Number of drops of different diameters at different distances from the treatment sprinklers and at two disdrometer elevations (1.00 and 2.00 m).*

Drop diameter distributions are presented for the three irrigation treatments at different distances from the sprinkler and at two measurement elevations (Fig. 12). In general, treatments CIS300 and DPIS200 showed smaller drops than CIS200. As the distance to the sprinkler increased the variability in drop diameter increased. Drops smaller than 1 mm represented the largest part of the total volume at the first meters from the sprinkler. Small drops prevailed at large distances from the sprinkler for the high measurement elevation, particularly for CIS300. For CIS300 and DPIS200, and to a distance of 8 m, drops collected at 2.00 m represented more water volume than those collected at 1.00 m. Opposite results were found for CIS200 (Fig. 13).

Differences between measurement elevations in total collected water volume till a distance of 5 m were particularly relevant (double) for DPIS200. The lowest differences in total collected volume between measurement elevations were obtained for CIS200.

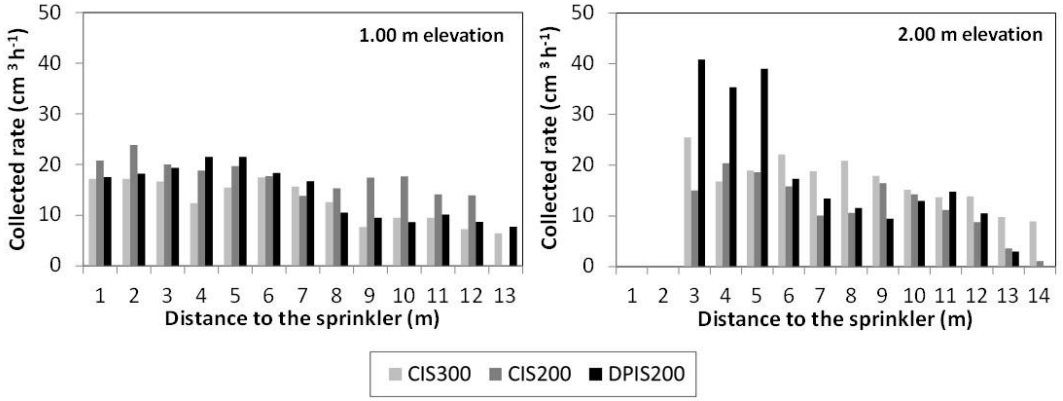

Figure 13. *Rate of disdrometer collected water (cm^3 h^{-1}) at two measurement elevations (1.00 m and 2.00 m) and at different distances from the sprinkler. Results are presented for the sprinklers of the three treatments.*

Soil water

The initial and the final soil water were not statistically different between treatments. Average ISWC was 19%, while average FSWC was 15%, resulting in net soil water extraction by the crop.

The spatial variability of SWC was assessed the day before and the day after the irrigation events applied on 4 July and 31 July. Linear regressions between catch-can irrigation water and: a) SWC after an irrigation event and; b) soil water recharge (difference between SWC after and before the irrigation event) were not statistically significant for both irrigation events and for the three treatments. Fig. 14 presents measured SWC before and after the irrigation applied on 4 July for the first 30 cm of soil and catch-can precipitation measurements for this irrigation event. The contour maps do not permit to identify areas of agreement between these variables. Similar results were obtained for the irrigation performed on July 31 (results not presented).

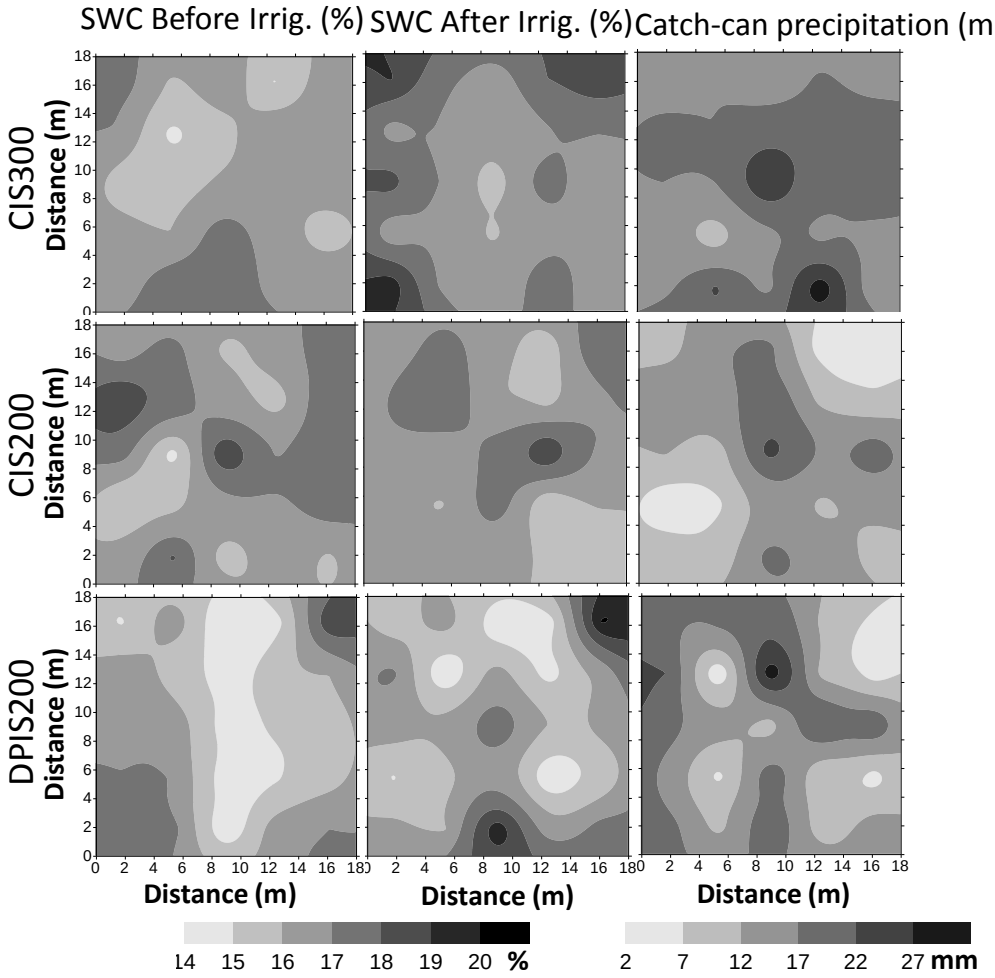

Figure 14. *Spatial variability of gravimetrical soil water content (SWC, %) at the first 0.30 m of the soil before and after the irrigation applied on 4 July. Spatial variability of irrigation precipitation (mm) measured with the catch-can network. Results are presented for each irrigation treatment.*

Irrigation scheduling

The cumulative ET_c of the experimental maize was 719 mm, rainfall was 135 mm, crop irrigation requirements were 680 mm and the irrigation was 623 mm. The difference between crop irrigation requirements and irrigation application was compensated by soil water depletion. Irrigation was applied in 45 events lasting for a total of 119.6 h. The first six irrigations, each of them lasting for two hours, were applied to promote crop emergence. The average wind speed during irrigation was 1.8 m s^{-1}. During 70% of the irrigation time wind speed was lower than 2 m s^{-1} (low wind conditions); during 24% of the irrigation time wind speed was between 2 m s^{-1} and 4 m s^{-1} (moderate wind conditions), and only during 6% of the irrigation time wind speed exceeded 4 m s^{-1} (high wind conditions).

Irrigation performance measured above the crop canopy

The first five irrigations applied to the crop after emergence were evaluated with both catch-can networks (at elevations of 1.00 and 2.00 m a.g.l.). Five, nine and nineteen irrigation events were evaluated with one catch-can network located at 2.00 m, 2.30 m and 2.65 m a.g.l., respectively. In total, the spatial distribution of irrigation water and CUC_{ac} was evaluated in 38 irrigation events.

The five irrigations evaluated with two catch-can networks were performed under low wind conditions (averaging 1.0 m s^{-1}). The average collected irrigation depths were similar between catch-can elevations for the three treatments (Fig. 15a). Fig. 15b presents the relationship between CUC_{ac} measured at 1.00 vs. 2.00 m catch-can elevations (CUC_{1m} and CUC_{2m}). A similar plot is presented for $WDEL_{ac}$ in Fig. 15c. Under the experimental low wind conditions, CUC_{1m} was higher than CUC_{2m} in all treatments. In general, differences in CUC_{ac} between catch-can elevations resulted larger for the low-pressure treatments than for the standard pressure treatment. In the experimental conditions, differences in $WDEL_{ac}$ between catch-can elevations resulted small, with slightly higher average values for the 2.00 m catch-can elevation.

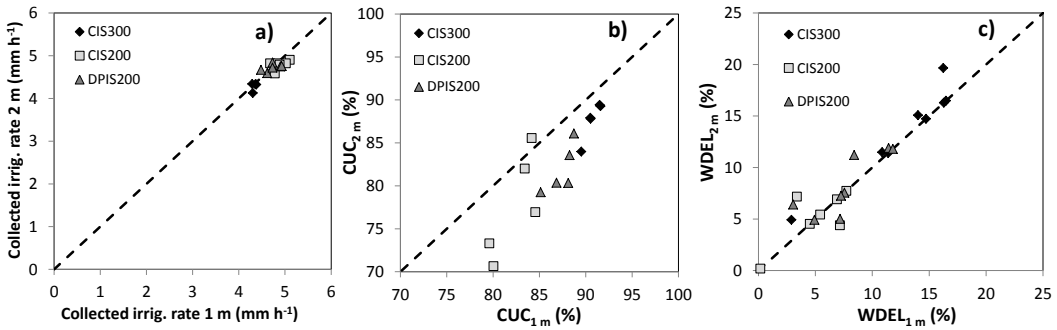

Figure 15. *Relationship between collected irrigation rate (mm h^{-1}) at the catch-can networks located at 1.00 and 2.00 m elevation (Fig. 15a). Relationship between CUC and WDEL measured at two catch-can elevations, 1.00 and 2.00 m a.g.l. (Figs. 15b and 15c, respectively). Different symbols are used for the three irrigation treatments. The dashed line represents the 1:1 line.*

The evolution of CUC_{ac} along the maize season showed similar trends in all irrigation treatments, but with different magnitude. The CUC_{ac} of the standard treatment was always higher than those of the low-pressure treatments (Table 7). CUC_{ac} of CIS300 moderately decreased with crop height, while the CUC_{ac} of low-pressure treatments decreased more drastically. The decrease in CUC_{ac} for DPIS200 was particularly important: from 87.4% at 1.00 m to 59.6% at 2.65 m (Table 7). From the beginning of the crop season to the end of June (maize height of 2 m), differences in CUC_{ac} between the standard and low-pressure treatments were lower than 8%. For catch-can elevations higher than 2 m, the difference in CUC_{ac} between low and standard pressure increased (average of 16% for CIS200 and 18% for DPIS200). The $CUC_{ac\_seasonal}$ of the standard pressure

treatment was about 13% higher than for the low-pressure treatments. In agreement with these results, in the Chapter II is reported that as catch-cans elevation increased, differences in CUC_{ac} between similar treatments of standard and low-pressure were accentuated, particularly for low wind speeds.

Table 7. *Summary of the irrigation events evaluated with catch-can networks located above the crop canopy. Catch-can elevation, number of irrigations, average wind speed, average CUC_{ac} (%), average WDEL (%) and seasonal CUC for each catch-can elevation and treatment.*

Catch-can elevation (m)	Irrigation events (#)	Averaged Wind speed ($m\ s^{-1}$)	Average CUC_{ac} (%)			Average $WDEL_{ac}$ (%)			$CUC_{ac\_seasonal}$ (%)		
			CIS300	CIS200	DPIS200	CIS300	CIS200	DPIS200	CIS300	CIS200	DPIS200
1	5	1.0	90.7	82.4	87.4	11.2	5.8	7.5			
2	5	1.8	83.9	76.8	80.4	15.7	6.5	12.5			
2.3	9	1.8	82.6	66.0	65.2	18.1	17.4	20.7	93.1	81.1	79.1
2.65	19	1.8	78.8	62.8	59.6	13.9	15.1	30.4			
Total	38	1.7	84.0	72.0	73.2	14.7	11.2	17.8			

The differences in $WDEL_{ac}$ between pressure treatments changed with catch-can elevations. For irrigations with catch-can elevation lower than or equal to 2.00 m, $WDEL_{ac}$ at standard pressure was always higher than $WDEL_{ac}$ at low-pressure (Table 7). However, for irrigations evaluated with catch-can elevation higher than 2.00 m an opposite trend was observed. The largest increment in $WDEL_{ac}$ was observed for the DPIS200 treatment when raising the catch-cans from 2.30 m (20.7%) to 2.65 m (30.4%).

The CUC_{ac} and $WDEL_{ac}$ of the low-pressure treatments showed the largest change with catch-can elevation. These results are in agreement with the differences observed in the collected volume between both catch-can elevations using the radial water distribution curves (Fig. 11) and the disdrometer (Fig. 13).

The relationship between wind speed and CUC_{ac} was strong and significant for all treatments until a catch-can elevation of 2.00 m (Fig. 16a). For elevations higher than 2.00 m, wind speed showed strong correlation with CIS300 CUC_{ac} (correlation coefficient of 0.91), but no relationship with the CUC_{ac} of the low-pressure treatments (Fig. 16b).

The relationship between wind speed and $WDEL_{ac}$ varied between catch-can elevations lower than or equal to 2 m (Fig. 16c) and higher than 2 m (Fig. 16d) for the low-pressure treatments. For low catch-can elevations, the $WDEL_{ac}$ of the standard pressure treatment were larger than those of the low-pressure treatments, with CIS200 showing the lowest $WDEL_{ac}$.

When analyzing all the evaluated irrigations, $CUC_{ac\text{-}seasonal}$ was higher in CIS300 than in CIS200 and DPIS200 (93.1, 81.1 and 79.1%, respectively) (Table 7). In the Chapter II (Robles et al., 2017), is reported that seasonal CUC for standard pressure

(CIS300) was higher than for low-pressure (CIS200 and DPIS200) by about 10%. Slightly higher values were measured in this research (about 13%).

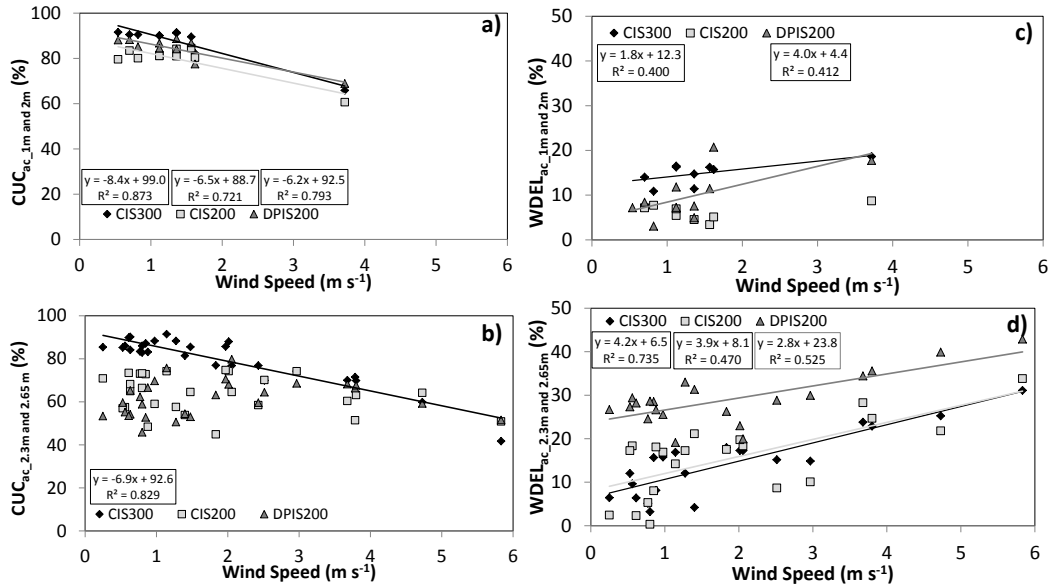

Figure 16. *Regression analysis between wind speed and irrigation uniformity above crop canopy for irrigations applied with catch-can elevations between 1.00 and 2.00 m (Fig. 16a) and between 2.30 and 2.65 m (Fig. 16b). Regression analysis between wind speed and wind drift and evaporation losses (WDEL) measured above the crop canopy for irrigations applied with catch-can elevations between 1.00 and 2.00 m (Fig. 16c) and between 2.30 m and 2.65 m (Fig. 16d).*

Figure 17 presents the spatial variability of seasonal water application (adding the above-canopy measurements of the 38 evaluated irrigation events) for the three irrigation treatments. In agreement with the results for $CUC_{ac\_seasonal}$, the largest variability was observed in the low-pressure treatments.

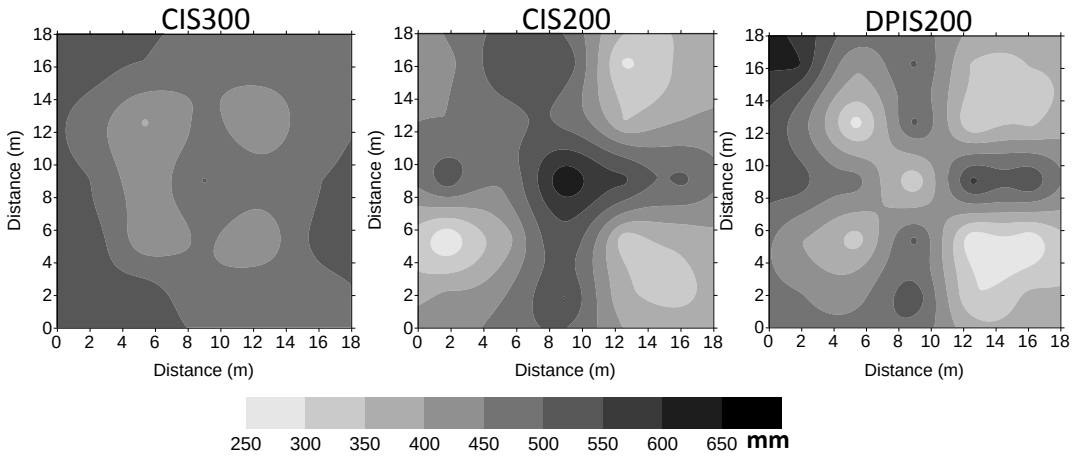

Figure 17. *Seasonal water application pattern in one replicate of each irrigation treatment.*

Irrigation performance measured below the crop canopy

The methodology used in this research permits to assess below-canopy irrigation performance in standard and low-pressure conditions, and to compare with the performance above canopy. Below-canopy irrigation performance is determined from water measurements performed near the soil surface. Therefore, these conditions are assumed to characterize crop response more accurately than above-canopy measurements.

Table 8 presents the date, the irrigation time and the meteorological conditions of the eight irrigation events in which irrigation performance was assessed above and below the crop canopy. Precipitation collected by the throughfall devices represents 18%, 17% and 24% of total precipitation collected below the maize canopy for the CIS300, CIS200 and DPIS200 treatments, respectively. Differences among treatments seem to be largely related to the characteristics of the crop canopy in the experimental plots.

The variability of stemflow and throughfall measurements between plants located near the same location within the plot was established with the measurements performed in four plants and three locations of one replicate of each treatment (Fig. 9c). The coefficient of variation (CV, %) of the throughfall measurements (CV= 57%) was larger than for the stemflow measurements (CV= 36%). The CV of precipitation measured below the maize canopy averaged 34%, 25% and 36% for CIS300, CIS200 and DPIS200, respectively. Variability was found to be relevant, but it affects all treatments and measurement locations with comparable intensity.

Fig. 18a presents the relationship between the average precipitation above and below the maize canopy for the eight evaluated irrigation events and for the three treatments. CIS300 precipitation above the maize canopy was slightly higher than below the maize canopy. Precipitation above and below the maize canopy for the low-pressure treatments was more similar. Differences can be largely attributed to crop intercepted water.

Figure 18b presents the relationship between the Christiansen uniformity coefficient of the measurements above and below the maize canopy (CUC_{ac} and CUC_{bc}, respectively) for the eight intensively evaluated irrigation events and for the three treatments. The standard pressure treatment, CIS300, systematically showed higher values for CUC_{ac} than for CUC_{bc} (the average difference was 10%). However, the CUC_{ac} of the low-pressure treatments, was lower than the corresponding CUC_{bc}, (average differences of 9% and 5% for CIS200 and DPIS200, respectively), with the exception of the irrigations performed under windy conditions. Differences in the directional impact of the water drops on the maize canopy and on drop sizes between pressure treatments could partially explain these differences.

Table 8. *Summary of the irrigation events evaluated above and below the maize canopy: irrigation date, irrigation time (h), temperature (T, °C), relative humidity (RH, %), wind speed (m s^{-1}) and average collected precipitation (mm) above the maize canopy (catch-cans) and below the maize canopy (stemflow and throughfall), for the three treatments.*

Date	Irrig. Time (h)	Temp (ºC)	RH (%)	Wind Speed (m s^{-1})	Average collected precipitation (mm)											
					Catch-cans			Stemflow			Throughfall			Stemflow +Throughfall		
					CIS300	CIS200	DPIS200	CIS300	CIS200	DPIS200	CIS300	CIS200	DPIS200	CIS300	CIS200	DPIS200
18-Jul-17	2	19.1	88.4	0.6	9.2	7.9	7.2	6.6	6.1	5.2	1.5	1.7	1.8	8.1	7.8	7.0
19-Jul-17	2	21.9	84.1	0.6	11.3	9.8	9.0	8.2	7.8	6.8	1.6	1.5	1.9	9.7	9.3	8.7
20-Jul-17	3	18.6	80.1	1.4	13.7	11.5	10.1	10.3	11.3	8.1	1.7	1.8	2.2	11.9	13.1	10.3
21-Jul-17	3	18.3	70.9	1.3	13.8	11.6	9.9	9.9	10.8	8.4	2.3	1.8	2.4	12.3	12.6	10.8
25-Jul-17	3	19.0	57.6	5.8	10.6	9.0	8.7	7.7	7.9	6.3	1.6	1.4	1.5	9.3	9.3	7.8
26-Jul-17	3	18.0	62.7	3.7	11.9	10.4	10.0	7.5	9.4	6.5	1.8	1.9	2.1	9.3	11.4	8.6
27-Jul-17	3	19.8	68.1	1.0	13.0	11.8	12.0	8.8	9.2	8.5	2.3	2.4	2.9	11.1	11.6	11.4
28-Jul-17	3	18.8	82.7	0.5	13.6	11.6	11.5	9.0	9.5	8.1	2.3	2.1	3.0	11.3	11.6	11.1
Average	2.8	19.2	74.3	1.9	12.2	10.5	9.8	8.5	9.0	7.2	1.9	1.8	2.2	10.4	10.8	9.5

The wind speed of irrigations performed on July 25 and 26 was 5.8 m s^{-1} and 3.7 m s^{-1}, respectively. In these events, CUC_{ac} was larger than CUC_{bc} in all treatments (Fig. 18b). Since 70% of the seasonal irrigation time was performed under wind speeds lower than 2 m s^{-1} and 47% of the seasonal irrigation time was applied to the fully developed maize canopy, seasonal CUC_{ac} underestimated the performance of the low-pressure treatments and overestimated the performance of the standard pressure treatment. Differences in the average CUC_{ac} between the treatments of standard and low-pressure averaged 20% for the eight evaluated irrigation events. However, differences in the average CUC_{bc} between CIS300 and CIS200, and between CIS300 and DPIS200 averaged 2% and 5%, respectively (Table 9).

The comparison between WDEL measured above and below the maize canopy is presented in Figure 18c. In the standard pressure treatment, $WDEL_{bc}$ (average 24.7%) was higher than $WDEL_{ac}$ (average 13.5%). However, in the low-pressure treatments $WDEL_{bc}$ was very similar to $WDEL_{ac}$, with respective values of 16% and 18.5% for CIS200, and 31.5% and 30.5%, for DPIS200. Above-canopy measurements underestimated WDEL in CIS300 respect to measurements below the crop canopy. Interception losses alone cannot explain the large differences observed in CIS300. The largest WDEL were found for DPIS200 and the lowest for CIS200. Although low-pressure treatments produce larger drops than the standard pressure treatment, the deflecting plate of the DPIS200 sprinkler breaks down the water jet (Fig. 12), potentially contributing to increase WDEL.

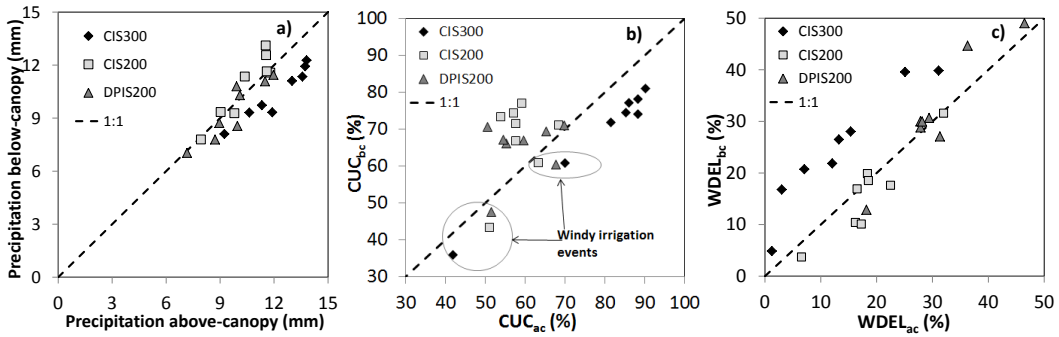

Figure 18. *Relationship between collected precipitation (mm) above and below the maize canopy (Fig. 18a). Relationship between Christiansen uniformity coefficient above the maize canopy (CUC_{ac}) and below the maize canopy (CUC_{bc}) (Fig. 18b). Relationship between wind drift and evaporation losses above the maize canopy ($WDEL_{ac}$) and below the maize canopy ($WDEL_{bc}$) (Fig. 18c). Comparisons are presented for the three irrigation treatments. The dashed line represents the 1:1 line.*

Table 9. *Irrigation date, Christiansen Uniformity Coefficient of the catch-can measurements above the maize canopy (CUC_{ac}, %), of the stemflow measurements ($CUC_{stemflow}$, %), of the throughfall measurements ($CUC_{throughfall}$, %) and of the sum of stemflow and throughfall measurements (CUC_{bc}, %). Results are presented for the three irrigation treatments.*

Date	CUC_{ac} (%)			$CUC_{Stemflow}$ (%)			$CUC_{Throughfall}$ (%)			CUC_{bc} (%)		
	CIS300	CIS200	DPIS200	CIS300	CIS200	DPIS200	CIS300	CIS200	DPIS200	CIS300	CIS200	DPIS200
18-jul-17	86.0	57.5	55.2	79.0	55.0	60.1	46.0	63.4	50.0	76.9	67.4	66.2
19-jul-17	90.2	68.2	65.3	80.7	67.3	69.4	47.6	59.2	35.0	81.0	71.2	69.4
20-jul-17	81.5	53.9	54.5	76.7	69.1	58.7	52.7	40.9	20.2	70.7	69.9	59.0
21-jul-17	88.3	57.6	50.6	79.7	67.2	66.3	44.7	54.9	26.8	78.0	71.1	71.9
25-jul-17	41.7	50.9	51.6	33.6	43.2	43.2	27.2	29.1	22.3	35.7	43.5	47.5
26-jul-17	69.9	63.2	67.7	59.7	59.4	63.1	38.0	52.6	29.7	60.9	61.0	60.5
27-jul-17	88.3	59.1	69.7	73.6	71.9	73.9	47.0	49.5	28.9	74.1	77.1	71.2
28-jul-17	85.2	57.0	59.7	73.7	72.2	66.1	48.9	50.1	43.4	74.5	74.4	67.0
Average	78.9	58.4	59.3	69.6	63.2	62.6	44.0	50.0	32.0	69.0	67.0	64.1

The correlation between wind speed and irrigation uniformity measured above maize canopy for the eight evaluated irrigation events (Fig. 19a), resulted similar to that presented for all the irrigation events evaluated with the catch-can located at an elevation higher than 2 m a.g.l. (CUC_{ac} 2.3 m and to 2.65 m, Fig. 16b). CUC_{ac} of low-pressure treatments did not show significant correlation with wind speed, but CUC_{ac} of the standard pressure treatment showed a strong and significant correlation with wind speed (Fig. 19a). However, the correlation between wind speed and CUC_{bc} resulted strong and significant for the three irrigation treatments (Fig. 19b). The relationship between wind speed and CUC_{bc} resulted similar to that presented between wind speed and CUC_{ac} to 1m and to 2 m (Fig 16a). These results confirm that when measuring uniformity above a fully developed corn canopy, the CUC of the low-pressure treatments was more biased than that of the standard pressure treatment.

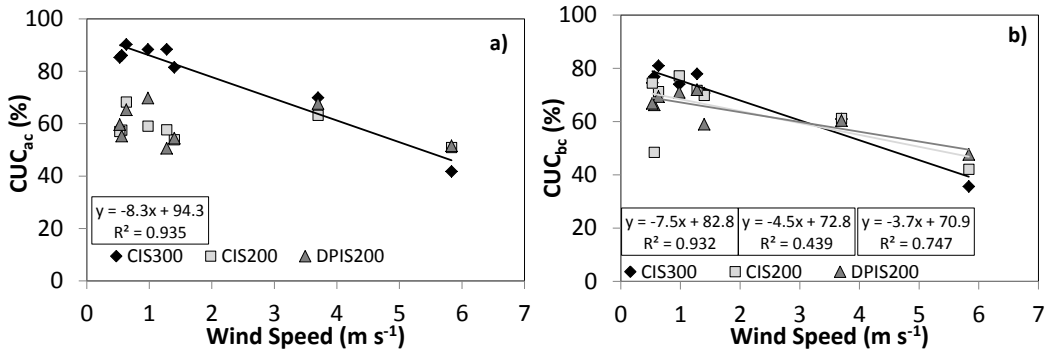

Figure 19. *Regression analysis between wind speed and Christiansen uniformity coefficient above the maize canopy (CUC_{ac}, Fig. 19a) and below the maize canopy (CUC_{bc}, Fig. 19b), for the eight evaluated irrigation events. Results are presented for the three irrigation treatments.*

A correlation analysis was performed between the twenty-five points of water measurement above and below maize canopy for each of the eight irrigation events. No correlation was found between both variables, except for the two irrigations performed under windy conditions (days 25th July and 26th July). In these two irrigation events moderate correlations (r^2) with respect the wind velocity were found (0.8, 0.7 and 0.7 for CIS300, CIS200 and DPIS200, respectively, on July 25th and 0.6 for the three treatments on July 26th).

As previously stated, irrigation water distribution below the crop canopy should be more related to crop water uptake than water distribution above the canopy. Additionally, the area monitored with the above-canopy devices was smaller (0.02 m^2) than the area used in below-canopy measurements (0.112 m^2), increasing the reliability of below-canopy measurements. On the other hand, experimental errors could be relevant for below-canopy measurements, as denoted by its coefficients of variation.

Maize growth and yield variables

The intra-plot yield variability resulting from the intensive hand harvest performed in one of the replicates of each treatment is presented in Fig. 20. The grain yield variability of low-pressure treatments (CIS200 and DPIS200) was slightly higher than that of the standard pressure treatment (CIS300). However, the CUC of grain yield were very high, and quite similar for the three experimental plots (93%, 91% and 91%, for CIS300, CIS200 and DPIS200, respectively). CIS300 and CIS200 showed similar variability patterns in the center of the layout, where the highest grain yield was found. On the contrary, the central area of the DPIS200 layout was characterized by the lowest grain yield.

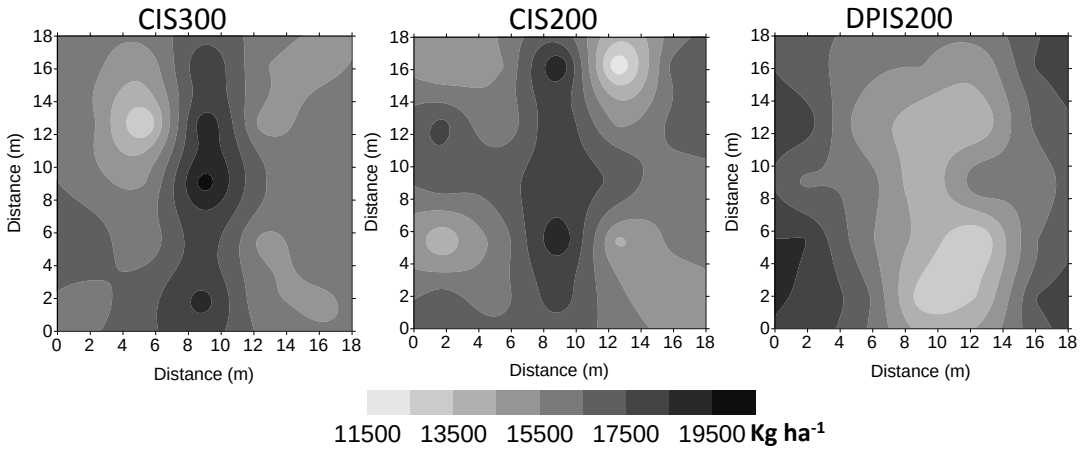

Figure 20. *Spatial variability of grain yield in one replicate of each irrigation treatment.*

A correlation analysis between seasonal water distribution measured above maize canopy and grain yield measured with the intensive hand harvest, showed relatively weak relationships for the CIS300 and DPIS200 treatments (0.34 and 0.23, respectively), and a moderate relationship (0.72) for the CIS200 treatment.

Table 10 presents the results of the ANOVA analysis for the agronomic measurements on the 12 plots, grouped by treatments. Total and treatment averages are presented for plant height, photosynthetically active radiation (PAR, %), plant density, grain yield, biomass and harvest index (HI, %). Results indicate that the irrigation treatment had no effect on any of these variables.

Table 10. *Average values of measured plant height, photosynthetically active radiation intercepted by the crop (PAR), plant density, grain yield, biomass and harvest index (HI) for each irrigation treatment. The average of the three treatments is also presented.*

Treatment	Plant height (m)	PAR (%)	Plant density (Plants ha^{-1})	Yield (Mg ha^{-1})	Biomass (Mg ha^{-1})	HI (-)
CIS300	2.39[a]	94.72[a]	86667[a]	17.69[a]	29.57[a]	0.52[a]
CIS200	2.41[a]	95.40[a]	86111[a]	17.80[a]	30.75[a]	0.50[a]
DPIS200	2.38[a]	95.69[a]	85556[a]	17.44[a]	29.20[a]	0.52[a]
Average	2.39	95.22	86111	17.64	29.84	0.51

The reduction of the working pressure at the sprinkler nozzle from 300 to 200 kPa had no effect on grain yield, neither for a standard brass impact sprinkler, nor for a plastic deflecting plate impact sprinkler. In the eight irrigation events where above and below water application is available, differences in irrigation uniformity between pressure treatments decreased from 20% to 2-5% when switching from above to below measurements. Results indicate that the canopy of tall crops (like maize) plays an important role in irrigation water partitioning (stemflow and throughfall). In the experimental conditions, maize canopy partitioning reduced the difference in seasonal uniformity between pressure treatments, providing an explanation for the three-year experimentation (including the preceding two years presented in the Chapter II (Robles et al., 2017) without differences in grain yield between treatments.

Discussion

Discrepancies in the characterization of sprinklers

The results obtained with the radial water distribution methodology did not show full correspondence with those obtained with the disdrometer. Both methodologies agree on: a) precipitation near the sprinkler is larger with measurements at 2.00 m than at 1.00 m, and b) the largest differences in precipitation between measurements elevations correspond to DPIS200. However, both methods disagree on the treatment least affected by the measurement elevation: CIS200 for the disdrometer vs. CIS300 for the radial catch-can experiment.

Differences in the monitored area could partially explain these discrepancies. In fact, the catch-can measurement area was about 3.7 times larger than that of the disdrometer. The small measurement area of the disdrometer made this methodology particularly sensitive to wind speed. In the catch-can methodology, measurements at different elevations were performed at the same time and therefore under the same meteorological conditions. However, this did not apply to the disdrometer method. Although all experiments were performed under low wind conditions (lower than 1.3 m s^{-1}), the meteorological conditions of the disdrometer experiments were not the same for the two measurement elevations.

Difficulties in characterizing soil water variability

In all treatments, gravimetric soil water before and after two irrigation events was not statistically related with the irrigation water above the maize crop canopy measured with catch-cans. The characterization of soil water after an irrigation resulted complex because of the small-scale variability induced by canopy partitioning of irrigation water (Paltineanu and Starr, 2000, Sánchez et al., 2010). Gravimetric measurements were performed in this research at between-row locations, with each measurement point representing only 0.0020 m^2. The low spatial representativeness of the soil samples did not permit to reveal the spatial variability of water available to the crop. More intense or more spatially relevant soil sampling would be required to overcome these problems, and to provide a soil water reference for irrigation uniformity in developed maize canopies.

Effect of catch-can elevation on irrigation performance

As catch-can elevation exceeded 2 m, a strong decrease of CUC_{ac} and a strong increment of $WDEL_{ac}$ were observed for the low-pressure treatments, particularly for DPIS200. Sánchez et al. (2010) and Stambouli et al. (2013), reported similar effects as catch-can elevation increased from 0.85 to 2.00 m. A similar tendency was found in the Chapter II until an elevation of 2.00 m, but a decrease in $WDEL_{ac}$ as elevation increased from 2.00 to 2.30 m, particularly for low-pressure treatments. Differences between the present experiment and the literature references in the highest catch-can elevation (0.35 m higher in this research) and in sprinkler nozzle elevation (0.20 m lower in this research) make comparisons difficult. Our results are in agreement with previous findings indicating that the use of catch-can networks above the crop canopy of tall crops (such as maize) to estimate sprinkler irrigation performance (CUC and WDEL) could introduce noise as the elevation of the catch-cans approximates the sprinkler nozzle height (Dogan et al., 2008; Sánchez et al., 2010; Robles et al., 2017). The accumulation of evidence requires caution when designing irrigation experiments.

A developed maize canopy modifies irrigation performance

The results reported in this paper indicate that throughfall conveyed 20% of the irrigation water reaching the canopy. These throughfall measurements showed more variability than stemflow measurements. Martello et al. (2015) reported an average of 78% of the rainfall below the maize canopy intercepted by the leaves and transferred along the stem (stemflow), while only 22% reached the ground directly (throughfall). Hupet and Vanclooster (2005) reported coefficients of variation larger than 75% for the throughfall measured below the maize canopy in rain events. Sun et al. (2017) also reported important variability of throughfall measures below maize canopy.

The interception storage of a corn canopy has been quantified between 0.4 mm and 2.7 mm (Norman and Campbell, 1983; Steiner et al., 1983; Martínez-Cob et al., 2008). According to our results, interception storage was more important in CIS300 than in the

low-pressure treatments, probably due to the reported differences in drop size distribution (Fig. 12). Dorr et al. (2016) concluded that the retention of sprays on plant leaves decreases with increasing droplet sizes. Additionally, differences in the area of the collectors used above (0.020 m^2) and below (0.116 m^2) the canopy may affect data reliability, with large collectors producing more reliable data than small collectors (Playán et al., 2005; Playán et al., 2006).

From a designer point of view, the low-pressure sprinkler irrigation treatments evaluated in this research, CIS200 and DPIS200, presented values of $CUC_{ac\_seasonal}$ (81% and 79%) that did not reach the minimum value of 84% proposed by Keller and Bliesner (1978). Additionally, the difference in CUC_{ac} favoring the high-pressure treatment (13% in 2017), permits to expect the highest yield for the most uniform treatment. In the Chapter II (Robles et al., 2017), similar findings were reported without a clear explanation of the effects of the CUC differences in maize yield.

In engineering practice, irrigation uniformity is assumed constant and characteristic of system operation. This research provides additional evidence indicating that standard, above-canopy uniformity estimates do not necessarily represent the variability perceived by the crop. In fact, several authors (van Wesenbeeck and Kachanoski, 1988; van Wesenbeeck et al., 1988; Lamm and Manges, 2000; Li and Rao, 2000; Paltineanu and Starr, 2000; Canone et al., 2017; Sun et al., 2017) have reported that crop canopy architecture plays a major role on the spatial distribution of rainfall and sprinkler irrigation water.

We have reported differences between treatments in maize canopy irrigation water partitioning. Paltineanu and Starr (2000) also found different water partitioning of maize canopy between sprinkler irrigation and rainfall for the same precipitation rate. Further, Lamm and Manges (2000) reported statistical differences in maize canopy water partitioning between two different sprinkler types and working pressures (310 kPa and 103 kPa). Differences in partitioning were attributed in these two research works to the water-canopy interception angle. In this Chapter, differences in the interception angle and in drop diameter distribution have been reported. Both differences can contribute to explain differences in maize canopy water partitioning.

The seasonal CUC_{ac} did not convey accurate information about the irrigation water distribution received by the experimental crop. Our results indicate that water partitioning improved the uniformity of the low-pressure treatments and slightly decreased that of the standard pressure treatment. Li and Rao (2000), experimenting on winter wheat, reported that when CUC_{ac} was lower than 80% (a common situation for the low-pressure treatments) CUC_{bc} were larger than CUC_{ac}. These authors also found that the differences between CUC_{ac} and CUC_{bc} decreased as the uniformity above the canopy increased (a common situation for the standard pressure treatment). The important differences between pressure treatments in CUC_{ac} (10% in 2016 and 13% in 2017) were strongly reduced (3-

5% for eight irrigation events) when uniformity was measured below the maize canopy. A similar trend was observed in WDEL: differences between treatments decreased when losses were estimated below the maize canopy. The increase in irrigation performance resulting from irrigation water passage through the maize canopy permits to explain the absence of differences in maize grain yield between treatments.

Conclusions

In general, treatments CIS300 and DPIS200 showed smaller drops than CIS200. Drop diameter distributions and collected water in radial curves were different between treatments and measurement elevations (1.00 *vs* 2.00 m).

Above canopy irrigation performance (CUC and WDEL) worsened with increasing catch-can elevation for all treatments. The effect was more important for the low-pressure treatments, and in particular for the DPIS200 treatment.

Under low-wind and fully developed canopy conditions (a frequent situation for maize irrigation), maize canopy partitioning reduced the observed differences in above canopy irrigation performance. Low differences in below canopy performance can explain why differences in grain yield were not observed.

When characterizing sprinkler irrigation performance the following points should be addressed: 1) a high catch-can elevation will result in CUC underestimation and WDEL overestimation; and 2) a tall maize canopy will modify irrigation performance, strongly reducing the differences between pressure treatments.

Three years of experimentation permit to conclude that low-pressure sprinkler irrigation conserves energy while maintaining water use and maize yield.

Acknowledgments

This paper applies the “first-last-author-emphasis” approach for the sequence of authors. This research was funded by the Minister of Economy, Industry and Competitiveness (MICINN) of the Government of Spain through grant AGL2013-48728-C2-1-R. Octavio Robles has a scholarship funded by the Minister of Economy and Competitiveness of the Spanish Government. The authors would like to thank the CSIC/CITA field staff and technicians: Eva Medina, Miguel Izquierdo, Miguel Á. Millán, Vicente Villarroya, Pablo García and Laura Pérez for their technical support.

References

Allen, R.G., Pereira, L.S., Raes, D., Smith, M., 1998. Crop evapotranspiration: guidelines for computing crop water requirements. (FAO irrigation and drainage Paper 56). FAO, Rome.

ASAE Standards, 1994. ASAE S330.1, 41st edn. Procedure for sprinkler distribution testing for research purposes. ASAE, St Joseph, Mich., pp. 600–690.

Brennan, D., 2008. Factors affecting the economic benefits of sprinkler uniformity and their implications for irrigation water use. Irrig. Sci. 26, 109–119.

Bui, E.N., Box, J.J.E., 1992. Stemflow, rain throughfall, and erosion under canopies of maize and sorghum. Soil Sci. Soc. Am. J. 56 (1), 242–247.

Canone, D., Previati, M., Ferraris, S., 2017. Evaluation of stemflow effects on the spatial distribution of soil moisture using TDR monitoring and an infiltration model. J. Irrig. Drain. Eng. 143(1), 04016075.

Cavero, J., Jiménez, L., Puig, M., Faci, J.M., Martínez-Cob, A., 2008. Maize growth and yield under daytime and nighttime solid-set sprinkler irrigation. Agron. J. 100, 1573–1579. doi:10.2134/agronj2008.0092.

Christiansen, J.E., 1942. Irrigation by sprinkling. Agric. Exp. Stn. Bull. 670. Univ. of California, Berkeley.

Clemmens, A.J., Dedrick, A.R., 1994. In: Tanji, K.K., Yaron, B. (Eds.), Irrigation techniques and evaluations. Advanced series in agricultural sciences. Springer, Berlin, pp. 64–103.

Dechmi, F., Playán, E., Cavero, J., Faci, J., Martínez-Cob, A., 2003. Wind effects on solid set sprinkler irrigation depth and corn yield. Irrig. Sci. 22, 67–77.

Dogan, E., Kirnak, H., Doyan, Z., 2008. Effect of varying the distance of collectors below a sprinkler head and travel speed on measurements of mean water depth and uniformity for a linear move irrigation sprinkler system. Biosyst. Eng. 99(2), 190–195.

Dorr, G.J., Forster W.A., Mayo, L.C., McCue, S.W., Kempthorne, D.M., Hanan, J., Turner, I.W., Belward, J.A., Young, J., Zabkiewicz, J.A., 2016. Spray retention on whole plants: modeling, simulations and experiments. Crop Protection. 88, 118–130.

Fernández García, I., Rodríguez Díaz, J.A., Camacho Poyato, E., Montesinos, P., 2013. Optimal operation of pressurized irrigation networks with several supply sources. Water Resour. Manage. 27, 2855–2869.

Hupet, F., Vanclooster, M., 2005. Micro-variability of hydrological processes at the maize row scale: implications for soil water content measurements and evapotranspiration estimates. Journal of Hydrology. 303, 247–270.

ISO- International Organization for Standardization, 1990. Agricultural irrigation equipment. Rotating sprinklers. Part 2. Uniformity of distribution and test methods. ISO Standard 7749/2. ISO, Geneva, Switzerland.

ISO- International Organization for Standardization, 1995. Agricultural irrigation equipment. Rotating sprinklers. Part 1. Design and operational requirements. ISO Standard 7749/1. ISO, Geneva, Switzerland.

Jiménez, M., De Juan, J., Tarjuelo, J., Ortega, J., 2010. Effect of irrigation uniformity on evapotranspiration and onion yield. The Journal of Agricultural Science. 148(2), 139–157.

Keller, J. Bliesner, R.D., 1991. Sprinkle and trickle irrigation. Van Nostrand Reinhold, New York.

Kincaid, D.C., 1991. Impact sprinkler pattern modification. Trans. ASAE. 34 (6), 2397–2403.

Lamm, F.R., Manges, H.L., 2000. Partitioning of sprinkler irrigation water by a maize canopy. Trans. ASAE. 43(4), 909–918.

Li, J., Kawano, H., 1996. The areal distribution of soil moisture under sprinkler irri-gation. Agric. Water Manage. 32, 29–36.

Li, J., Rao, M., 2000. Sprinkler water distributions as affected by winter wheat canopy. Irrig. Sci. 20(1), 29–35.

Liu, H., Zhang, R., Zhang, L., Wang, L., Li, Y., Huang, G., 2015. Stemflow of water on maize and its influencing factors. Agric. Water Manag. 158, 34–41.

Martello, M., Dal Ferro, N., Bortolini, L., Morari, F., 2015. Effect of incident rainfall redistribution by maize canopy on soil moisture at the crop row scale. Water (open access). 7, 2254–2271.

Mateos, L., Mantovani, E.C.; Villalobos, F.J., 1997. Cotton response to non-uniformity of conventional sprinkler irrigation. Irrig. Sci. 17, 47–52.

Martínez-Cob, A., 2008. Use of thermal units to estimate corn crop coefficients under semiarid climatic conditions. Irrig. Sci. 26, 335–345.

Martínez-Cob, A., Playán, E., Zapata, N., Cavero, J., Medina, E.T., Puig, M., 2008. Contribution of evapotranspiration reduction during sprinkler irrigation to application efficiency. J. Irrig. and Drain. Eng. ASCE. 134 (6), 745–756.

Montazar, A., Sadeghi, M., 2008. Effects of applied water and sprinkler irrigation uniformity on alfalfa growth and hay yield. Agric. Water Manag. 95(11), 1279–1287.

Moreno, M.A., Ortega, J.F., Córcoles, J.I., Martínez, A., Tarjuelo, J.M., 2010. Energy analysis of irrigation delivery systems: monitoring and evaluation of proposed measures for improving energy efficiency. Irrig. Sci. 28, 445–460.

Norman, J. M., Campbell, G., 1983. Application of a plant-environment model to problems in irrigation. Advances in irrigation, D. Hillel, ed., Vol. 2, Academic, New York. pp. 55–188.

Paltineanu, I.C., Starr, J.L., 2000. Preferential flow through maize canopy and soil water dynamics across rows. Soil Sci. Soc. Am. J. 64(1), 44–54.

Paniagua, M.P., 2015. Mejora del riego por aspersión en parcela. PhD Dissertation. Universidad de Zaragoza, 261 p (in Spanish).

Playán, E., Salvador, R., Faci, J.M., Zapata, N., Martínez-Cob, A., Sánchez, I., 2005. Day and night wind drift and evaporation losses in sprinkler solid-sets and moving laterals. Agric. Water Manage. 76 (3), 139–159.

Playán, E., Zapata, N., Faci, J.M., Tolosa, D., Lacueva, J.L., Pelegrín, J., Salvador, R., Sánchez, I., Lafita, A., 2006. Assessing sprinkler irrigation uniformity using a ballistic simulation model. Agric. Water Manage. 84(1-2), 89–100.

Rezende, R., Goncalves, A.C.A., Frizzone, J.A., Folegatti, M.V., Muniz, J.A., 2000. Non-uniformity conventional sprinkler irrigation effects on bean yield. Acta horticultura. 537, 853–865.

Robles, O., Playán, E., Cavero, J., Zapata, N., 2017. Assessing low-pressure solid-set sprinkler irrigation in maize. Agric. Water Manag. 191, 37–49.

Rodríguez Díaz, J.A., López Luque, R., Carrillo Cobo, M.T., Montesinos, P., Camacho Poyato, E., 2009. Exploring energy saving scenarios for on demand pressurized irrigation networks. Biosyst. Eng. 104, 552–561.

Salvador, R., Bautista, C., Burguete, J, Zapata, N., Serreta, A., Playán, E., 2009. A photographic method for drop characterization in agricultural sprinklers. Irrig. Sci. 27, 307–317.

Sánchez, I., Zapata, N., Faci, J.M., 2010. Combined effect of technical, meteorological and agronomical factors on solid-set sprinkler irrigation: I. Irrigation performance and soil water recharge in alfalfa and maize. Agric.Water Manag. 97(10), 1571–1581.

Seginer, I., 1978. Note on economic significance of uniform water application. Irrig. Sci., 1: 19–25.

Stambouli, T., Martínez-Cob, A., Faci, J.M., Howell, T.A., Zapata N., 2013. Sprinkler evaporation losses in alfalfa during solid-set sprinkler irrigation in semiarid areas. Irrig. Sci. 31(5), 1075–1089. DOI 10.1007/s00271-012-0389-2.

Steiner, J.L., Kanemasu, E.T., Clark, R.N., 1983. Spray losses and partitioning of water under a center pivot sprinkler system. Trans. ASAE. 26 (4), 1128–1134.

Stern, J., Bresler, E., 1983. Nonuniform sprinkler irrigation and crop yield. Irrig. Sci. 4 (1), 17–29.

Sun, Z., Li, Z., Li, B., Sun, T., Wang, H., 2017. Factors influencing corn canopy throughfall at the row scale in northeast China. Agron. J. 109, 1591–1601.

Tokay, A., Wolf, D.B., Petersen, W.A., 2014. Evaluation of the new version of the laser-optical disdrometer, OTT Parsivel (2). Journal of Atmospheric and Oceanic Technology. 31(6), 1276–1288.

Urrego-Pereira, Y.F., Martínez-Cob, A., Fernández, V., Cavero, J., 2013. Daytime sprinkler irrigation effects on net photosynthesis of maize and alfalfa. Agron. J. 105(6), 1515–1528.

van Wesenbeeck, I J., Kachanoski, R.J., 1988. Spatial and temporal distribution of soil water in the tilled layer under a maize crop. Soil Sci. Soc. Am. J. 52(2), 363–368.

van Wesenbeeck, I. J., Kachanoski, R. J., Rolston, D. E., 1988. Temporal persistence of spatial patterns of soil water content in the tilled layer under a maize crop. Soil Sci. Soc. Am. J. 52(4), 934–941.

CHAPTER IV. SELF-CALIBRATED BALLISTIC MODEL FOR SOLID-SET SPRINKLER IRRIGATION WITH A FIELD EXPERIMENTS DATA BASE

SELF-CALIBRATED BALLISTIC MODEL FOR SOLID-SET SPRINKLER IRRIGATION WITH A FIELD EXPERIMENTS DATA BASE[3]

Resumen

Los modelos de simulación de riego por aspersión son una herramienta valiosa para mejorar la gestión de agua de riego a escala parcelar. La teoría balística ha sido comúnmente usada para simular la dinámica de gotas en los modelos de riego por aspersión. Diversos experimentos en riego por aspersión realizados en estudios previos en el Valle del Ebro, España, fueron analizados e integrados en una base de datos. Las evaluaciones fueron realizadas en seis tipos de aspersores con diferentes tamaños de boquillas, presiones de operación bajo diferentes condiciones meteorológicas y espaciamientos. La base de datos incluye 40 ensayos en aspersor aislado y 167 en cobertura total que fueron procesados con un modelo auto-calibrado para calibrar y validar los parámetros balísticos. El modelo balístico usado en este trabajo fue mejorado respecto a uno previo, y además algunas novedades fueron agregadas. Estas modificaciones se hicieron en las fases: de solución numérica, un modelo de pérdidas por evaporación y arrastre, simulaciones considerando pendiente del terreno, generación de gotas (usando métodos regulares y aleatorios), el tamaño de celdas del terreno donde las gotas se simulan y la consideración de dos distribuciones de tamaños de gotas, lognormal con límite superior y Weibull. Los resultados indican diferencias mayores y significativas en el coeficiente de uniformidad de Christiansen medido y simulado cuando se considera un valor constante de la velocidad del viento (9%) con respecto aconsiderar la velocidad de viento con frecuencias de tiempo menores o iguales de 30 minutos (6%). Respecto el efecto de la pendiente en el terreno, se observaron diferencias relevantes (11%) para ambos coeficientes de uniformidad (medido y simulado) cuando la velocidad de viento es mayor a 4 m s^{-1}. Ambas distribuciones de tamaños de gotas fueron similares en precisión; sin embargo, la distribución de lognormal con límite superior resultó más adecuada para simular un aspersor espacialmente diseñado para operar a baja presión. La capacidad predictiva del modelo una vez calibrado y validado fue satisfactoria (99% y 75%, respectivamente). El nuevo modelo mejora la precisión respecto a los modelos anteriores y minimiza el tiempo de cálculo de los procesos de calibración y validación usando un clúster de computadoras.

Palabras clave: modelo auto-calibrado, modelo balístico mejorado, base de datos experimental, riego por aspersión.

[3] Robles, O., Borja, L., Zapata, N., Burguete, J., 201X. Self-calibrated ballistic model for sprinkler irrigation with a field experiments data base. Agric. Water Manag. Reference: AGWAT_2018_1185 (*submitted*)

Abstract

Simulation models of sprinkler irrigation are a valuable tool to improve the irrigation water management at plot scale. Ballistic theory has been commonly used to simulate drop dynamics in sprinkler irrigation models. A number of experiments on sprinkler irrigation performed in previous studies in the Ebro Valley Spain were analyzed and integrated in a data base. The evaluations were performed on six sprinkler types with different nozzle sizes, operating pressures under different meteorological conditions and spacing. The data base includes 40 isolated and 167 solid-set experiments that were processed with a self-calibrated model for calibrate and validate the ballistic parameters. The ballistic model used in this research was improved with respect to a previous model and moreover some novelties were added. These modifications were done in the phases of: the numerical solution, a wind drift and evaporation losses model, simulations considering slope in the terrain, drops generation (using regular and random methods), the size of the terrain cells where the drops are simulated and considering two drop size distributions, upper limit log-normal and Weibull. The results indicated larger and significant differences of Christiansen´s Uniformity Coefficient measured and simulated when considering a constant wind velocity (9%) and no differences when the wind velocity is defined for intervals equal or lower than 30 minutes (6%). Regarding the effect of the slope in the terrain, differences between both uniformity coefficients (measured *vs.* simulated) were relevant (11%) when the wind velocity is larger than 4 m s^{-1}. Both drop size distributions, were similar in accuracy, however the upper limit lognormal resulted more suitable to simulate a sprinkler especially designed to operate under low pressure. The predictive ability of the model once calibrated and validated was satisfactory (99% and 75%, respectively). The new model improves the accuracy with respect previous researches works and minimizes the computing time for the calibrations and validations processes using a computers cluster.

Keywords: self-calibrated model, ballistic model improved, experimental database, sprinkler irrigation.

Introduction

Simulation models of sprinkler irrigation are a valuable tool to improve the irrigation water management at plot scale. The simulation of the water distribution patterns of impact sprinkler has been performed through the study of the drops dynamics.

Ballistic theory has been commonly used to describe and simulate drop movements in sprinkler irrigation models. To simulate the dynamics of the droplets, first it is necessary to know where the drops are formed, its initial velocity and the volumetric drop size distribution.

The models have evolved along the time, improving the definition of the involved processes. A number of research works simulate drop dynamics assuming that all drops were formed at the nozzles (Fukui et al., 1980; Carrión et al., 2001; Playán et al., 2006; Zerihun et al., 2016). Vories et al. (1987) divided the main jet in two parts, the disturbed by the arm stream that is assumed to form individual drops immediately after the main nozzle and the undisturbed stream that assumes to travel one meter along the initial velocity vector before breaking into individual drops (von Bernuth and Gilley, 1984). In this research it is assumed that the jet of the main nozzle travels one meter without been affected by any drag force and then breaks into individual drops, while the drops formation of the secondary nozzle occurs at its exit.

A number of experimental techniques have been reported in the literature to measure drop sizes resulting from precipitation, sprinkler irrigation and atomization of liquids. The first intrusive methodologies (stain method, flour method, oil immersion method, momentum method) were replaced by non-intrusive optical methods (used in sprays or sprinkler irrigation) such as laser method (Montero et al., 2003; King et al., 2010), disdrometer method (Burguete et al., 2007), photographic method (Salvador et al., 2009) and particle tracking velocimetry (Bautista-Capetillo et al., 2014).

From the experimental data of the intrusive and non-intrusive methodologies, a number of volumetric drop size distributions have been proposed, some of them applied to sprays or impact sprinkler. Solomon et al. (1985) established the parameters of the Upper Limit Log Normal distribution (ULLN, Equation 1) presented by Mugele and Evans (1951) to adjust the volumetric drop size distribution of a spray sprinkler with different pressures and nozzle sizes. An exponential model based on Weibull distribution was later adapted to impact sprinklers by Li et al. (1994). The authors compared the ULLN and Weibull distributions using two impact sprinklers, concluding that both distributions are quite similar but Weibull (2 parameters) is much simpler than the ULLN distribution (3 parameters). Kincaid et al. (1996) used a modified distribution from Weibull (Equation 2) establishing as a constant one of the variables of the equation, lightening the calibration process. Different types of sprinklers were tested: impact sprinklers and spray sprinklers.

The authors conclude that the exponential distribution has a good fit except for drops smaller than 1 mm.

$$f(d) = \frac{\alpha \exp\left[-\frac{1}{2}\left(\frac{\beta - \mu}{\sigma}\right)^2\right]}{\sigma\, d\, (\alpha - d)\sqrt{2\pi}} \quad (1)$$

with β(d) = ln [d/(α-d)] and α the maximum drop diameter,

$$f(d) = 0.639\, n \frac{d^{n-1}}{d_{50}^n} \exp\left[-0.693\left(\frac{d}{d_{50}}\right)^n\right] \quad (2)$$

where *f(d)* is the volumetric probability density function of the total discharge from the sprinkler, d is the drop diameter, μ and σ are the mean and the standard deviation of β, respectively and d_{50} is the volume mean drop diameter. The ULLN distribution has three regression parameters α, μ and σ. The Weibull distribution has two regression parameters, d_{50} and n.

The expected value (*EV*), acting as the mean drop diameter for both volumetric drop size distributions, can be numerically approximated by:

$$EV = \frac{\sum_i f(d_i) \cdot d_i}{\sum_i f(d_i)} \quad (3)$$

were d_i are the numerical drop diameters tested from 0 mm to 7 mm with 0.1 mm intervals.

Recently, a new impact sprinkler has been commercialized specially designed to operate at low pressure (200 kPa) following the procedures of Kincaid (1991). The sprinkler has a flat plate attached to the arm that deflects the jet moreover breaking it with the arm. The device diffuses the jet filling the intermediate irrigated portion achieving a nearly triangular application pattern. Decreasing the pressure becomes the water application in an annular or toroidal shape. The previous suggest that a different drop size distribution has to be adapted to this patterns compared with standard pressures. The ULLN is a more flexible distribution that could allow adapting to these patterns.

The most common equation applied to sprinkler droplet dynamics is Newton´s second law of motion (Fukui et al., 1980; von Bernuth and Gilley, 1984; Vories et al., 1987; Seginer et al., 1991; Carrión et al., 2001; Playán et al., 2006). They involve a set of differential equations that can be solved by numerical methods to determine the landing point of a drop. Between the major aerodynamic forces acting on the droplet, the drag coefficient has been profusely studied. According to the literature, the drag coefficient could be established as a function of Reynolds number (Fukui et al., 1980) or as a function of the drops diameter (von Bernuth and Gilley, 1984; Hills and Gu, 1989) or as a function of pressure and diameter (Li and Kawano, 1995). Another advance in the definition of the

drag coefficient has been proposed by Seginer et al. (1991) and modified later by Tarjuelo et al. (1994). The authors introduced two factors, K_1 and K_2, describing the effect of the wind velocity and the direction of the drop movement:

$$C' = C(1 + K_1 \sin\theta - K_2 \cos\delta) \quad (4)$$

where *C'* is the drag coefficient of a drop in wind conditions, *C* is the Fukui et al. (1980) drag coefficient for a spherical drop in function of Reynolds number, θ is the angle formed by the drop velocity vector with respect to the air (**V**) and the drop velocity respect to the ground (**U**), and δ is the angle formed by the vectors **V** and the wind velocity (**W**), with **V**=**U**-**W**.

Among the numerical methods to solve droplet dynamics, the fourth order Runge-Kutta is the most used (Fukui et al., 1980; Vories et al., 1987; Carrión et al., 2001; Dechmi et al., 2003; Playán et al., 2006). Zapata et al. (2009) compared the fourth order Runge-Kutta with a second-third order Runge-Kutta pair concluding that the latter is more efficient, reducing the computational time on 90% from the original. Zerihun et al. (2016) used a fourth-fifth order Runge-Kutta pair in order to precise the drop dynamics but increasing the computational time.

Summarizing, the standard simulation model for sprinkler irrigation considers: a) a module to predict the volumetric drop size distribution, diameter ranges and model parameters (Li et al., 1994; Kincaid et al., 1996); b) the simulation of the trajectories of the individual droplets, accounting for the major forces acting on the droplet (including drag coefficient and wind distortion pattern), with a physically based droplet dynamics model (Fukui et al., 1980; von Bernuth and Gilley, 1984; Vories et al., 1987; Seginer et al., 1991; Carrión et al., 2001; Playán et al., 2006); and c) determination of irrigation precipitation patterns as a function of computed landing coordinates of the individual drops and the corresponding volumetric application rates, including water losses due to wind drift and evaporation (Carrión et al., 2001; Dechmi et al., 2004; Playán et al., 2005).

The objective of sprinkler droplet dynamics modeling is limited to compute the landing coordinates of the droplets on the field surface and does not include the determination of their volumetric application rates (Zerihun et al., 2016). Volumetric application rates and associated parameters are estimated using semi-empirical procedures (Fukui et al., 1980; von Bernuth and Gilley, 1984; Vories et al., 1987; Seginer et al., 1991; Montero et al., 2001; Playán et al., 2006; Zerihun and Sanchez, 2014). In order to overcome the empiricism that limits the predictive ability of the model, field experiments are required to calibrate and validate the model parameters. Authors such as Fukui et al. (1980), Vories et al. (1987) and Seginer et al. (1991), presented the parameter calibration for one type of sprinkler by single test under the same technical and meteorological conditions. Montero et al. (2001) reported the calibration of the parameters using SIRIAS model for different combinations of sprinkler types, riser heights, nozzle diameters,

pressure head and wind velocities and directions. Playán et al. (2006) presented the Ador-Sprinkler simulation model including a database for two sprinkler types commonly used in the Ebro Valley irrigation systems. The model parameters are presented as a function of sprinkler type, nozzle size (two combinations), nozzle pressure head (from 200 kPa to 400 kPa) and wind velocity (from 0 m s^{-1} to 8 m s^{-1}).

During the irrigation, a significant part of the water discharged by the sprinkler does not reach the soil surface due to evaporation and drift of the drops. These losses are known as Wind Drift and Evaporation Losses (*WDEL*) and depend mostly on meteorological conditions. Experimentally *WDEL* are measured as the percentage of the total water discharged by the sprinklers that is not collected inside the pluviometers (Playán et al., 2005). The sprinkler simulation models take these losses into account by: a) correcting the water distribution radial curve, b) subtracting it from the pluviometry accumulated in every cell of the simulated grid or c) by adjusting the volumetric drop size distribution curve (Carrión et al., 2001; Playán et al., 2006). SIRIAS (Carrión et al., 2001) implemented an experimentally based *WDEL* model on the findings of Montero et al. (1999), where the vapor pressure deficit of the air and the wind velocity are the main factors in the equation.

This research presents a new simulation model based on that reported in Playán et al. (2006) (Ador-Sprinkler). The new model includes improvements on the drops size distributions, drops generation, the ballistic model definition and on the calibration process. The new model incorporates a database of field experiments, 40 performed under isolated sprinkler and 167 under solid-set configuration (from which, 60 were performed under low operating pressures). The experiments include a wide variety of sprinkler types (including those with the modification of Kincaid et al. (1991)), nozzle sizes, pressure heads, sprinkler layouts and meteorological conditions (wind velocity and direction), that covers the features found in the sprinkler irrigated area of the Ebro Valley (Spain). In addition, a self-calibration module was developed to optimize model parameters based on the experimental database. The objective is to develop a simulation tool for sprinkler irrigation that adjusts the model parameters to the current experimental database or to an extended database including new experiments provided by the users. The specific objectives of this research are:

1. Compile a database of field-experiments considering a variety of sprinkler types, nozzle sizes, working pressures, solid-set configurations and meteorological conditions commonly used in the irrigation systems of the Ebro Valley.
2. Improve the ballistic simulation model.
3. Develop a self-calibration module to optimize the parameters of the model to reproduce adequately the field-experiment database.
4. Develop an on-farm sprinkler simulation model coupling the field-experiment database, the self-calibration module and the on-farm sprinkler simulation module.

Materials and Methods

The ballistic model

Numerical solution

Considering weight, buoyancy and drag forces, the ballistic dynamics of a spherical drop is given by:

$$\mathbf{A} = (1 - \rho_a/\rho_w)\,\mathbf{g} - \frac{3\,\rho_a\,C'|\mathbf{U}-\mathbf{W}|}{4\,\rho_w\,d}\,(\mathbf{U}-\mathbf{W}) \tag{5}$$

where **A** is the drop acceleration vector, **g** is the gravity vector ρ_a is the air density, ρ_w is the water density, **U** is the drop velocity vector with respect to the ground and **W** is the wind velocity vector.

The drops trajectory was solved by using the following third order Runge-Kutta (RK3):

$$\mathbf{R}_o = \mathbf{R}(t), \qquad \mathbf{U}_o = \mathbf{U}(t), \qquad \mathbf{A}_o = \mathbf{A}(\mathbf{U}_o)$$

$$\mathbf{R}_1 = \mathbf{R}_o + \mathbf{U}_o\Delta t, \qquad \mathbf{U}_1 = \mathbf{U}_0 + \mathbf{A}_o\Delta t, \qquad \mathbf{A}_1 = \mathbf{A}(\mathbf{U}_1)$$

$$\mathbf{R}_2 = \mathbf{R}_0 + \frac{\Delta t}{4}(\mathbf{U}_0 + \mathbf{U}_1), \qquad \mathbf{U}_2 = \mathbf{U}_0 + \frac{\Delta t}{4}(\mathbf{A}_0 + \mathbf{A}_1), \qquad \mathbf{A}_2 = \mathbf{A}(\mathbf{U}_2)$$

$$\mathbf{R}\,(t+\Delta t) = \mathbf{R}_0 + \frac{\Delta t}{6}(\mathbf{U}_0 + \mathbf{U}_1 + 4\mathbf{U}_2), \qquad \mathbf{U}\,(t+\Delta t) = \mathbf{U}_0 + \frac{\Delta t}{6}(\mathbf{A}_0 + \mathbf{A}_1 + 4\mathbf{A}_2) \tag{6}$$

where **R** is the position vector of the drop, Δt is the time (t) increase and the numbers 0, 1 and 2 are the step numbers.

A variable temporal increase has been used following Equation 7. The maximum error allowed for the drops trajectory was 10 cm.

$$\Delta t = k_t \left(\frac{4\,\rho_w\,d}{3\,\rho_a\,C'|\mathbf{U}-\mathbf{W}|}\right) \tag{7}$$

where k_t is a dimensionless stability factor ranged between 0 and 1.

An analysis of maximum efficiency has been performed between Runge-Kutta methods from first to fourth order and with different k_t (0.1, 0.2, 0.3 and 0.4). Comparisons were made based on the maximum error and computing time of the numerical solutions.

Meteorological simulation conditions

The simulation of a sprinkler irrigation event typically uses a mean of the meteorological variables during the total irrigation time. In this new approach, the measured variability of the meteorological data during the experiment was considered. The meteorological conditions of the experiments presented in Table 11 were obtained from an ad-hoc meteorological station that measured data every 5 or 10 seconds and record averages every 5 minutes. The meteorological variables were: air temperature, relative humidity, wind velocity, resultant of wind velocity and wind direction.

The experimental irrigation events lasted for two hours. The simulation of the irrigation events was performed with four different ways: considering only one average of the wind velocity data (120 min frequency), average of four wind velocity data (30 min frequency), with twelve wind velocity data (10 min frequency) and the average of twenty-four wind velocity data (5 min frequency). Differences on simulated Christiansen´s Uniformity Coefficient (*CUC* ─ Christiansen, (1942)) and the Root Mean Square Error (*RMSE*) between the four frequencies of wind data were analyzed. A common practice in sprinkler simulation modeling is to consider a constant wind velocity during the irrigation time that corresponds to the average value obtained from agrometeorological stations (the Spanish SIAR agrometeorological network provides data every 30 minutes). Field experiments presented in Table 11 have different availability of wind velocity data. Only some of them installed an *ad-hoc* meteorological station to record wind velocity data with a 5 minutes frequency. The experiments with high frequency wind velocity data were selected for this analysis.

Wind drift and evaporation losses model

A generalized equation for computing *WDEL* was obtained from a statistical analysis considering the whole solid-set experiments (167). The model was integrated in a multiple linear regression with the *WDEL* measured (dependent variable) and with five explicative variables (independent variables), three of them meteorological conditions (wind velocity, air temperature and relative humidity) and two more from sprinkler configuration and operation (nozzle diameter and operating pressure).

Throwing and landing point of the drops

The irrigated area was partitioned in square or rectangular cells to simulate its irrigation depth. In previous research works (Dechmi et al., 2004; Playán et al., 2006) the simulated area was considered flat and all the cells have the same elevation. In this research the topography of the terrain was incorporated in the model by introducing the elevation of several location points. The elevation of each cell was interpolated from three closest elevation points and its relative location. At each cell, two rainfalls were accumulated, the one that falls to the crop or the one that falls to the pluviometer at its corresponding height (if the cell as a pluviometer). The volume of a drop is associated to a

pluviometer if the cell has a pluviometer and if the drop falls downwards to the plane of the pluviometer. The trajectory of a simulated drop ends when the drop passes under the crop height.

The effect of the terrain topography (slope) on irrigation uniformity was studied. The whole sprinkler irrigation solid-set experiments of Table 11 were used for the analysis. Although all the field experiments of the database were performed under a flat terrain, slopes of 5% were also simulated. This is roughly the maximum slope in sprinkler irrigation that is observed in our study region. The simulated layouts had 16 sprinklers with different elevation describing the slope. The slope was rotated in the axis between the sprinkler lines from 0 to 360º with 45º intervals. Maximum and minimum differences on simulated *CUC* between considering a flat layout (CUC_{flat}) or a sloped layout (CUC_{slope}) were presented.

Generation of simulated drops

Ballistic models require the generation of a number of virtual drops to simulate their dynamics that matches the behavior of the real drops. The number of simulated drops does not need to be coincident with the number of real drops generated by the sprinkler. The large number of drops with similar characteristics landing in the area close to the sprinkler could be simulated by a low number of simulated drops with similar volume. The technique is especially important for the irrigated area far away from the sprinkler, where the number of landing drops is small. In this area, to simulate an adequate pluviometry it is needed a large number of simulated drops. The sampling error is the error due to the lack of representativeness of the virtual drops. In Monte-Carlo and regular sampling methods, this error is known to be inversely proportional to the root of the number of samples. Then, the sampling error in the simulated pluviometry is also inversely proportional to the root of the number of simulated drops landing on the terrain cell. Therefore, to minimize the sampling error and to maximize computing efficiency, the most convenient procedure is to have a uniform spatial density of simulated drops landing at the irrigated area. Also, a minimum number of simulated drops are required to land at each cell of the terrain to control the sampling error. It has to be noted that the number of simulated drops landing in an area is not proportional to the simulated pluviometry because depends on the drops associated volume.

In order to maintain the sampling error at low values (≈2%) around 2,000 drops were required to fall in each cell of the terrain, resulting in 7,200,000 total drops in isolated sprinklers and 800,000 for solid-set configuration.

Regular systematic sampling method (RSS)

In previous sprinkler simulation models (Fukui et al., 1980; Vories et al., 1987; Carrión et al., 2001; Dechmi et al., 2003; Playán et al., 2006) a set of regular horizontal angles from 0º to 360º and a set of regular drop diameters from 0.2 mm to 7 mm were

generated using a constant interval. The drop diameters and throw angles were generated following:

$$d_i = 0.2\text{ mm} + (7\text{ mm} - 0.2\text{ mm})\frac{D_i}{N_D},\ \varphi_i = 360°\frac{\psi_i}{N_\varphi} \quad (8)$$

where $D_i = 0,1,\dots,N_D$ and $\psi_i = 0,1,\dots,N_\psi$. with D_i and ψ_i as the sampled number of diameter and of throw angle, respectively. N_D and N_φ the total sampled number of drop diameter and of throw angle, respectively. And d_i and φ_i are the drop diameter (mm) and the horizontal throw angle of the *i*-th drop, respectively. The total number of virtual drops is given by: $(N_D + 1)\cdot(N_\varphi + 1)$.

In the RSS method, the number of virtual drops increases exponentially with the number of sampled variables. Therefore, the computational cost of this method can be too high at sampling three or more variables.

The density function of this sampling method is constant and can be defined by:

$$p(d,\varphi) = 1 \quad (9)$$

Uniform Monte-Carlo sampling method (UMCS)

In this research, the meteorological conditions were also sampled in the virtual drops. This additional variable increases the number of virtual drops of the RSS method. Random based methods, as UMCS, have been proved more efficient than regular systematic methods when sampling multiple variables (Bergstra and Bengio, 2012).

The UMCS method generates the drops according to:

$$d_i = 0.2\text{ mm} + (7\text{ mm} - 0.2\text{ mm})\,r_1,\quad \varphi_i = 360°\,r_2,\quad t_i = T\,r_3 \quad (10)$$

with t_i the meteorological conditions sampling time, T the total time simulated and r_1, r_2, y r_3 random numbers between 0 and 1. The total number of virtual drops is fixed, no depending on the number of sampled variables. Therefore, UMCS method is usually more efficient sampling three or more variables.

The sampling density function is constant and can be defined as:

$$p(d,\varphi,t) = 1 \quad (11)$$

Bimodal Monte-Carlo sampling method (BMCS)

In order to improve the computational efficiency and the sampling errors with respect to the UMCS method, a new Monte-Carlo method (BMCS) with a variable density function was analyzed. The BMCS method has a sampling density function depending on the drop diameter in a bimodal way:

$$p(d, \varphi, t) = d^{a-1} \exp(-b\, d^a) \tag{12}$$

with a and b two parameters to calibrate. This method generates t_i and φ_i in the same way as the UMCS method but the drop diameter as:

$$d_i = \left[0.2^a - \frac{1}{b} \ln(1 - \{1 - \exp[-b\,(7^a - 0.2^a)]\}\, r_1)\right]^{1/a}, \qquad \varphi_i = 360°\, r_2,$$

$$t_i = T\, r_3 \tag{13}$$

Volume assigned to the simulated drops

The falling point of each simulated drop was obtained with the ballistic theory, its associated volume was given by the volumetric drop size distribution and finally the volume of water was accumulated in its respective ground cell.

In this research, ULLN and Weibull distributions were considered (Equations 1 and 2). The performance of both distributions was analyzed for each sprinkler type and operation condition.

The associated volume of a drop entering a cell was accumulated following:

$$V_i = \left(1 - WDEL_j\right) Q_j\, T\, \frac{f(d_i)/p(d_i, \varphi_i, t_i)}{\sum_i f(d_i)/p(d_i, \varphi_i, t_i)} \tag{14}$$

where V_i and d_i are the associated volume and diameter, respectively, of the i-th drop, Q_j and $WDEL_j$ are the sprinkler application rate and the wind drift and evaporation losses, respectively, of the j-th nozzle, T is the irrigation time of the experiment, $f(d_i)$ is the volumetric drop size distribution (Equations 1 and 2) and $p(d_i, \varphi_i, t_i)$ is the sampling density function for RSS, UMCS and BMCS methods (Equations 9, 11 and 12, respectively).

Note that the associated volume to the simulated drops V_i (Equation 14) has no relationship with the real volume of a spherical drop.

Database of field experiments

Table 11 summarizes the field experiments that were considered for calibration and validation of the proposed model. All these experiments were performed following international standards (Merriam and Keller, 1978) and were accomplished by the RAMA research group (RAMA, 2018). Six types of impact sprinklers equipped with different nozzle sizes and operating pressures were available in the database.

Two types of field experiments were reported in the database for each sprinkler type: isolated sprinkler and solid-set layouts.

Table 11. *Summary of field experiments analyzed. The features of each sprinkler are shown for nozzle size and operating pressure for both experiment types. The reference of the research works where each sprinkler type was used is also reported.*

Reference	Sprinkler - abbreviation	Nozzles size (mm)	Pressure (kPa)	Experiment type			
				Isolated sprinkler	Solid-set configuration		
				Tests	Spacing (m)	Wind velocity rank (m s^{-1})	Tests
Playán et al. (2006)	Riegos Costa 130H - RC130	4.0 + 2.4 4.4 + 2.4	200 300 400	6	18 x 15	1.0 – 7.6	20
	Vyrsa 70 - VYR70	4.0 + 2.4 4.4 + 2.4	200 300 400	6	18 x 15	0.4 – 9.3	21
Sánchez et al. (2011)	Somlo 30C - SOM30C	4.0 + 2.4 4.4 + 2.4 4.8 + 2.4	240 320 420	10	15 x 15	0.4 – 8.0	55
Stambouli et al. (2014)	Riegos Costa 130 H - RC130BY	4.0 + 2.5 4.5 + 2.5 5.16 + 2.5	200 300 400	10	18 x 18	0.4 – 7.5	49
Paniagua P. (2015)	Naandanjain 5035 - NAAN	5.16 + 2.5	200 300	4	18 x 18	0.8 – 7.1	11
Robles et al. (2017)	Riegos Costa 130H - RC130p	5.16 + 2.4	200 300	4	18 x 18	0.6 – 5.0	11

The isolated sprinkler experiments were performed in a wind protected plot and the radial pluviometry was determined under no wind conditions. A set of catch-cans were located around the sprinkler in four radii at 90º each (oriented to the cardinal points); the catch cans were spaced every 0.5 m. The height of the sprinkler was 2 m and the irrigations lasted 2 h for all the experiments. The water application pattern of the isolated sprinklers was used to calibrate the parameters of the volumetric drop size distribution functions (Equations 1 and 2).

The experiments on solid-set covers different sprinkler layouts as rectangular and square with distances of 18 m and 15 m between sprinkler lines and 18 m and 15 m between sprinklers. All the solid-set experiments lasted 2 h. The solid-set layout was composed by 16 sprinklers. A 25 catch-can network was homogeneously distributed between the four central sprinklers of the solid-set layouts. Catch-can network allowed measuring the irrigation deep and determinate the irrigation performance indexes as the *CUC* and the *WDEL*. Each sprinkler type arranged in a solid-set configuration was evaluated under different working pressures from 200 kPa to 400 kPa and under different wind velocities ranging from a minimum of 0.4 m s^{-1} to a maximum of 9.3 m s^{-1}. The meteorological conditions of each experiment were measured every 5 or 10 seconds and monitored every 5 min with an automatic meteorological station located in the experimental plot. The solid-set experiments provided data to calibrate the parameters of

the model describing the drag coefficient, K_1 and K_2 (Equation 4). The experiments were also used to validate the solid-set irrigation model.

A new set of field experiments were performed in this research (RC130p) to include in the database (Table 11). Using the same impact sprinkler, Riegos Costa 130 H, from Playán et al. (2006) and Stambouli et al. (2014), different nozzles made of plastic and threaded to the sprinkler were tested. The RC130p sprinkler has the same features than the one introduced in the Chapter III, but operating at 200 kPa and 300 kPa. The nozzles used in Playán et al. (2006) were made of brass threaded to the sprinkler, while those of Stambouli et al. (2011) were of bayonet coupled and made of plastic. Further details of the experiments could be found in their respective references in Table 11.

For the RC130p sprinkler, the principal nozzle size was 5.2 mm and the auxiliary nozzle was 2.4 mm. The experiments of RC130p sprinkler were performed under low pressure, 200 kPa. The objective of this set of experiments was to include in the database an alternative configuration to operate at low pressure (200 kPa) but maintaining the discharge of the sprinklers working at the standard pressure (300 kPa) (Robles et al., 2017). Four experiments were performed on isolated sprinkler configuration under no wind conditions. Eleven experiments were performed on a rectangular 18 m by 18 m solid-set configuration, with wind velocities ranging from 0.6 m s^{-1} to 5.0 m s^{-1}. The features of both experiment types were in accordance to the procedures of the other field experiments included in the database.

Totalizing, the database was integrated by 40 experiments on isolated sprinkler configurations and 167 experiments on solid-set layouts.

Calibration process

Terrain cell size

The dimension of the cells (where the drops are accumulated) for calibrating the parameters of the Equations 1 and 2 was fixed in 0.5 m x 0.5 m in accordance with the spacing of the pluviometers in isolated sprinkler.

While for the calibration of the parameters of the Equation 4 (K_1 and K_2), an analysis to define the optimal cell size was performed. Different cell sizes were analyzed (0.5 m, 1.2 m and 3.6 m) considering the *CUC* correlation and the corresponding computational time. It is necessary to take into account that reducing the cell size increases the number of simulated drops in order to control the sampling error.

Objective function

An adequate sprinkler irrigation model should provide a good estimation of the averaged applied irrigation depth and also a good approximation of its spatial variability. The most common index to describe the variability of the irrigation performance in

sprinkler irrigation is the *CUC*. The objective function of the proposed model included both variables by minimizing the error between measured and simulated values. The error norm usually includes parameters as the *RMSE*, the coefficient of determination (r^2) or correlation (r) and a combination between *RMSE* and the other two coefficients (r^2 or r). This error norm has been established as the objective function in previous irrigation simulation models (Dechmi et al., 2004; Playán et al., 2006). In this research, the objective function to minimize was:

$$RMSE + \Omega\,(CUC_{mea} - CUC_{sim})^2 \quad (15)$$

where Ω = 0.05 mm hr^{-1} is a weight coefficient, and CUC_{mea} and CUC_{sim} are the *CUC* measured and the *CUC* simulated, respectively.

Optimization algorithms

The Multiple-Purposes Calibration and Optimization Tool (MPCOTool) has been used to compute the optimal parameters of the ballistic simulation model in sprinkler irrigation. MPCOTool is a free calibration module that allows computing the input empirical parameters used in physical models once the objective function is defined (Burguete and Latorre, 2018).

The module implements different optimization algorithms such as: regular systematic sampling, Monte-Carlo, hill climbing and genetic algorithms (Burguete et al., 201Xa).

A combination of three algorithms has been used to optimize the parameters of Equations 1, 2 and 4. An iterative method was applied to the Monte-Carlo algorithm selecting a given number of simulations (10 in this research) with the lowest values of the objective function. These candidates define the extreme values of the next iteration where Monte-Carlo algorithm is again performed. Moreover, the best result by Monte-Carlo algorithm is refined in each iteration using the hill climbing search method. This process will be repeated as many times as iterations are established. An exhaustive description of these methods can be consulted in the user manual of the MPCOTool.

For the calibration of the 2 parameters of the Weibull distribution (Equation 2) and the *C'* distribution (Equation 4), a total of 348 simulations were performed: 100 Monte-Carlo simulations plus 16 simulations for hill climbing search were repeated 3 times. For the calibration of the 3 parameters of the ULLN distribution (Equation 1) the number of simulations and iterations, 896, increased because one additional dimension has to be explored. In this case 200 Monte-Carlo simulations plus 24 simulations for hill climbing search were repeated 4 times. A schematic description of the convergence of the algorithms was represented for the Weibull distribution, *C'* and ULLN distribution using one sprinkler as example.

Optimal parameters and the simulated pluviometry were obtained for all irrigation events. Moreover, for solid-set experiments the *CUC* of the simulated pluviometry was computed and a set of equations for the empirical parameters of *C'* model was established for the whole database.

Validation process

Cross-validation was used to assess the predictive performance of the model. This approach splits the available data into two parts, a training set and a validation set. The first set was used to fit the regression model and the test set provides an error estimate. We focus on a particular form of cross-validation, called leave-one-out cross-validation (LOOCV). In this case, only one point was selected as the test set. The regression model was built on all the remaining data, evaluating its error on the single-point held out. A global error estimate was obtained by repeating this procedure for each of the training points available. Despite the LOOCV increases the computational costs, since a number of iterations were performed, the error was minimized and estimated for all data points. Comparisons of pluviometry and *CUC* of simulated and measured values were performed for the experiments. From the 167 experiments, 40 of them were not considered for validation because predictions with high wind velocities produce important errors. The predictive ability of the model was assessed in terms of *CUC* and *RMSE*. Both Weibull and ULLN distributions were validated independently and the results were compared.

Results and Discussions

Analysis of computational efficiency

Numerical comparisons between Runge-Kutta methods were presented (Figure 21) to select the optimal numerical method, including variable and constant time step. The filled symbols in Figure 21 represent the first to four order Runge-Kutta methods with a constant time step (Δt), while the empty symbols represent the same Runge-Kutta methods but with variable time step, with k_t between 0 and 1 (Equation 7). The computational efficiency, inversely proportional to the steps number, depends on the required accuracy, being the low order methods more efficient for low accuracy. In all cases, it is noticeable that considering a variable Δt reduces the number of steps with respect to any constant Δt. In this research, a maximum error of 10 cm was allowed in the numerical drop trajectories. The method of third order Runge-Kutta with $k_t = 0.3$ was the most efficient to solve the drops dynamics within the required accuracy. Fourth order Runge-Kutta method (RK4), commonly used to solve the drops dynamics, with variable time step is the most efficient technique for errors less than 5 cm. Nevertheless, for the desired accuracy, the calculation time of RK4 increases in 8.5% with respect to the RK3.

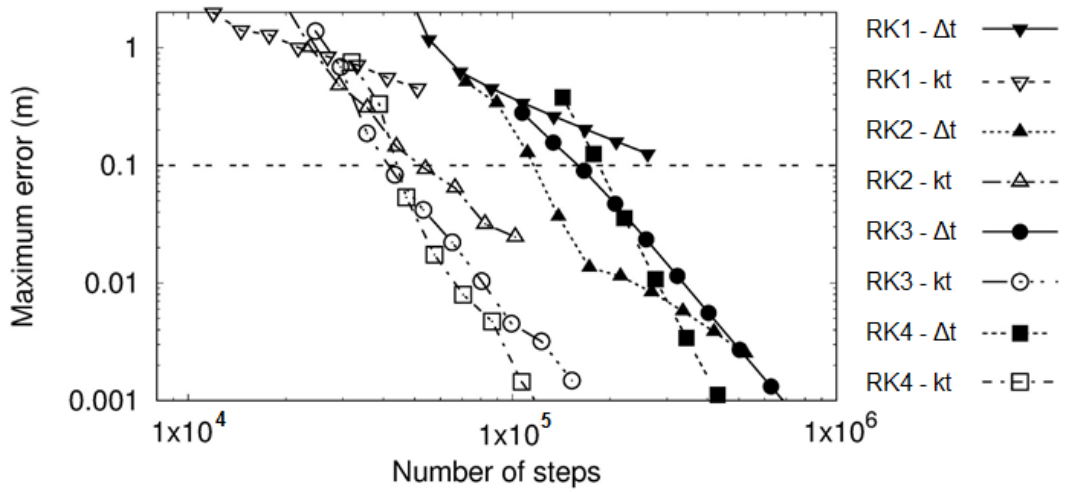

Figure 21. *Computational efficiency analysis for different Runge-Kutta methods with constant (Δt) and variable time steps (kt). The number of steps is showed in logarithmic scale. The dotted line represents the maximum error established of 10 cm in drops trajectory.*

Wind measurement interval

Figure 22a shows the analysis of the CUC_{mea} and the *CUC* simulated (CUC_{Wvfreq}) considering different wind measurement intervals (5 min, 10 min, 30 min and 120 min). The simulations of these analyses have been performed using both ULLN (Equation 1) and Weibull (Equation 2) drop size distributions. The results indicate an increase in the *CUC* differences with the wind measurement frequency. These differences reached its maximum values when the wind is considered as a constant value in the simulations (frequency of 120 min) and reach minimum values for the 5 min measurement interval. The *CUC* differences generally increases with the wind velocity. The average of *CUC* differences for all measurement intervals was less than 4% particularly for calm wind conditions ($< 2\ m\ s^{-1}$). Analyzing all data, the differences between CUC_{mea} and CUC_{Wvfreq} for measurement intervals of 5 min, 10 min, 30 min and 120 min reached average values of 5.5%, 5.6%, 6.0% and 9.0%, respectively.

The *RMSE* of the pluviometry simulated with the four measurement intervals ($RMSE_{Wvfreq}$) was obtained and summarized in Figure 22b. Maximum, minimum and average values are shown for each interval. Statistically, there is a significant difference at 95% confidence level (Fisher´s LSD test) of the means of *RMSE* for the interval of 120 min with respect the other three. Larger values of $RMSE_{Wvfreq}$ for 120 min were observed, particularly for the average and the maximum value.

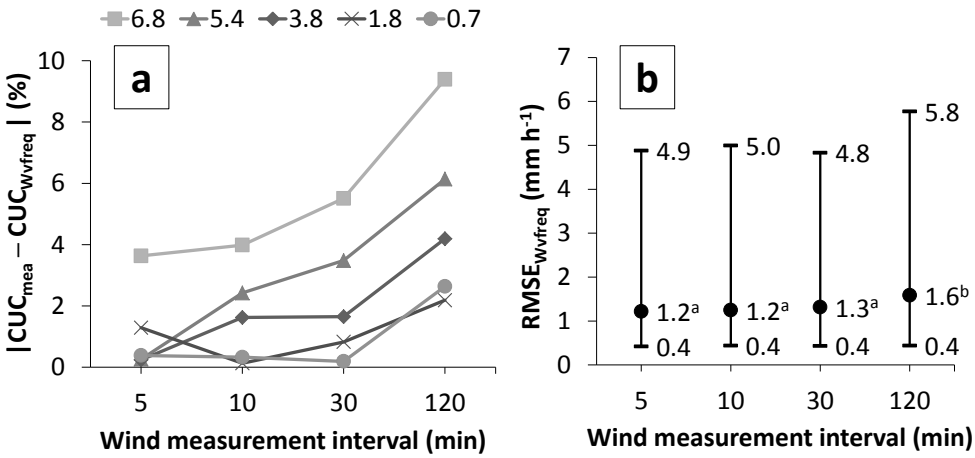

Figure 22. *CUC differences and RMSE for different wind velocity frequencies. Absolute differences of CUC measured (CUC_{mea}) and CUC simulated (CUC_{sim}) with respect the wind velocity frequencies (Figure 22a). RMSE of the simulations for every wind velocity frequency is shown in Figure 22b. Each line in Figure 22a corresponds to the simulation of a solid-set experiment with a different average of the wind velocity (m s^{-1}). In Figure 22b, the numbers followed by different letters are significantly different after ANOVA according to a Fisher´s Protected LSD test at 95% confidence level.*

From the analysis of the differences in *CUC* and *RMSE* of pluviometry for the four wind measurement intervals, there is no significant difference of considering the wind velocity frequency at intervals lower than 30 min for all the simulations. Considering a constant average (120 min), as commonly used in the previous works, significantly increases the errors on the estimated pluviometry.

Wind drift and evaporation losses

The 167 solid-set experiments (Table 11) were analyzed to compute the *WDEL* as a percentage of the water collected in the pluviometers and the water emitted by the sprinklers. The application rate of the sprinklers was considered using the flow-pressure curves reported by the authors or obtained from the manufacturers catalog. Maximum losses of 45% and minimum of 0.14% were obtained. It is important to mention that these losses are subjected to the uncertainty of the experimental measurements.

The *WDEL* model was formulated as a multiple linear regression considering a number of factors:

$$WDEL = 35.44 + 3.13\,W + 0.26\,T - 0.08\,Rh - 7.45\,\text{x}10^{-3}\,Ed + 3.65\,\text{x}10^{-10}\,P \quad (16)$$

with $Ed = (d_m^3+d_a^3) / (d_m^2+d_a^2)$, *Ed* (m) is the diameter equivalent. *WDEL* is expressed in %, *W* is the wind velocity (m s^{-1}), *T* is the temperature (°C), *Rh* is the relative humidity

(%), P is the operating pressure (Pa), and d_m and d_a are the main and auxiliary nozzles (m), respectively.

The performed statistical analysis suggests that wind velocity is the most significant meteorological factor contributing in 35% to the losses variability. In previous research works, wind velocity is reported as the most important factor in *WDEL* (Yazar, 1984; Tarjuelo, 1999; Dechmi et al., 2003; Playán et al., 2005). In contrast, the operating pressure was the lowest significant factor, contributing only to 1% of the *WDEL* variability.

The coefficients of the Equation 16 represents the physics of *WDEL*, which increases with the wind velocity, temperature and pressure, and decreases with relative humidity and nozzle diameter. The uncertainty of the individual measurements is reduced by the model since a high number of experimental tests are considered. The proposed model represents the experimental *WDEL* variability in 60% for the solid-set experiments analyzed.

Effect of slope on irrigation performance

The effect of the slope on *CUC* is presented in Figure 23 for different wind velocities. The maximum and minimum *CUC* differences of the eight simulated slopes directions (every 45º) in each experiment is represented with a different line. The consideration of the slope in the terrain increases or decreases the *CUC*, to a greater or less extent, depending on the wind velocity, the wind direction and the slope direction. In general, there is a tendency in *CUC* differences to overpass 5% when the wind velocity is higher than 4 m s^{-1}. On the contrary, at wind velocities lower than 4 m s^{-1} the *CUC* differences barely reach 5%. The largest *CUC* differences of 11% are found for maximum and minimum values. The differences are more noticeable when the slope is in the same direction of the predominant wind direction of the experiment because drops trajectory is lengthened or cut depending on the slope sense and the water application pattern is modified. On the other hand, this effect is less important when the slope is perpendicular to the wind direction.

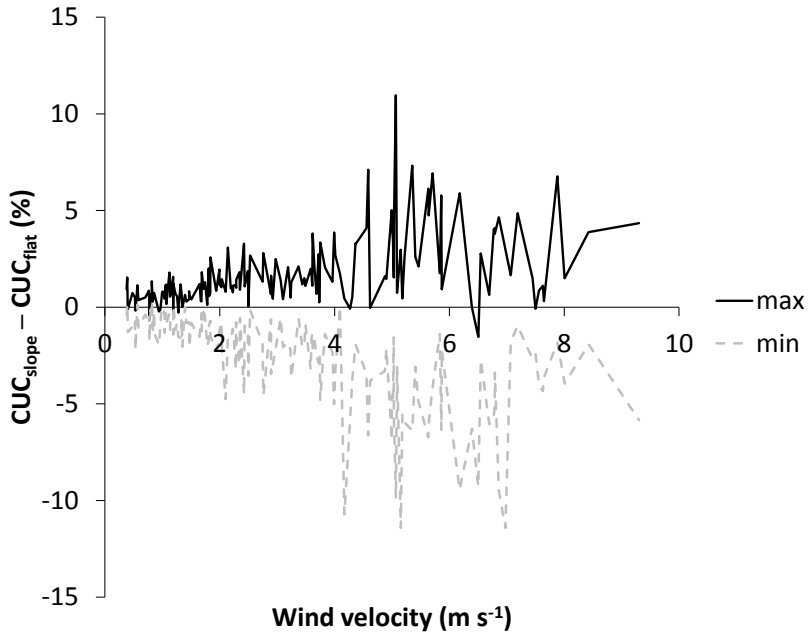

Figure 23. *Differences in CUC simulated considering different slopes (CUC_{slope}) and without slope (CUC_{flat}) as function of wind velocity. Each line with a symbol represents maximum and minimum CUC differences for all solid-set experiments.*

Drops generation

The spatial distribution of the simulated drops falling points for an isolated sprinkler is shown in Figure 24a, 24b and 24c for the three sampling methods RSS, UMCS and BMCS, respectively. The number of simulated drops falling in a terrain cell with respect to the distance between the cell center and the sprinkler is presented in Figure 24d, 24e and 24f for its respective sampling method RSS, UMCS and BMCS.

Figure 24a and 24d shows the drops generated with the RSS method by Playán et al. (2006) using 180 horizontal angles (radially distributed) and 180 drop diameters. It is observed a high concentration of simulated drops in the center of the sprinkler that decreases with the distance of the sprinkler. The average number of drops generated in the simulated cells is around 10, with a coefficient of variation (*CV*) of 37%.

The same behavior has been observed in the UMCS method (Figure 24b and 24e) but the number of simulated drops increases to an average of 2071 with a *CV* of 25%.

The parameters *a* and *b* (Equations 12 and 13) of the BMCS method have been calibrated to minimize the *CV*, resulting in optimal values *a*=0.39 and *b*=1.30. Using these values, the BMCS method simulates the drops more homogeneously (Figure 24c and 24f), the *CV* is reduced to 10% and the average number of drops is increased to 2120.

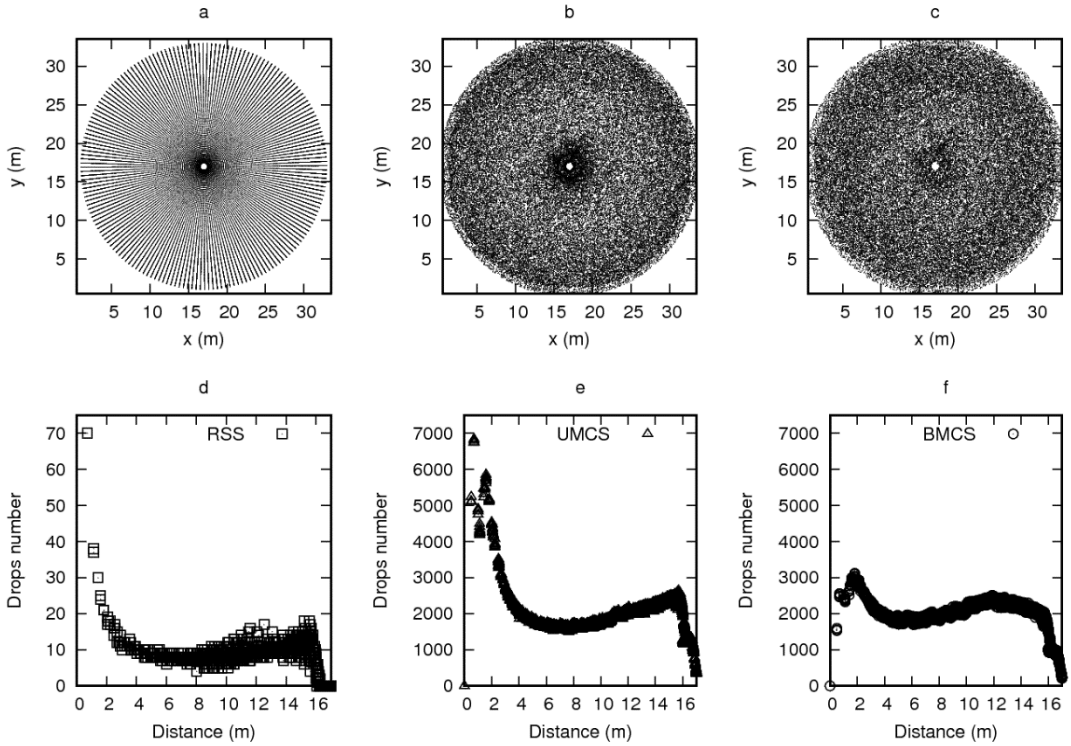

Figure 24. *Schemes and histograms of drops generation in an isolated sprinkler under calm wind conditions based on RSS method (Figure 24a and 24d), UMCS method (Figure 24b and 24e) and BMCS method (Figure 24c and 24f).*

Model calibration

Size of simulation cells

Figure 25 shows the relationships between CUC_{mea} and CUC_{sim} for the three terrain cell sizes analyzed. The relationships shown in the Figure 25 were performed for the Weibull distribution since no differences were observed with respect to the ULLN distribution. The coefficient of determination (r^2) was 0.75 approximately for the three cell sizes analyzed. The slope of the regression line for the 3.6 m cell size was the most different from the 1:1 line (Figure 25c), and therefore a large variability of the CUC_{sim} was observed. Simulating with a cell size of 3.6 m slightly overestimate the *CUC* compared with the other cell sizes, particularly for the high wind velocity events (lower values of *CUC*).

As expected, the computing time increases as the cell size decreases. At smaller cell size, larger number of drops has to be simulated per nozzle to maintain the sampling error. Decreasing the cell size from 3.6 m to 1.2 m increases the computing time in 9 times with respect to the 3.6 m cell size; whereas, for the 0.5 m cell size the computing time

increases in 49 times with respect to the 3.6 m cell size. In order to achieve the best fit of *CUC*, avoiding a time consuming process, the 1.2 m cell size has been selected for calibration and validation.

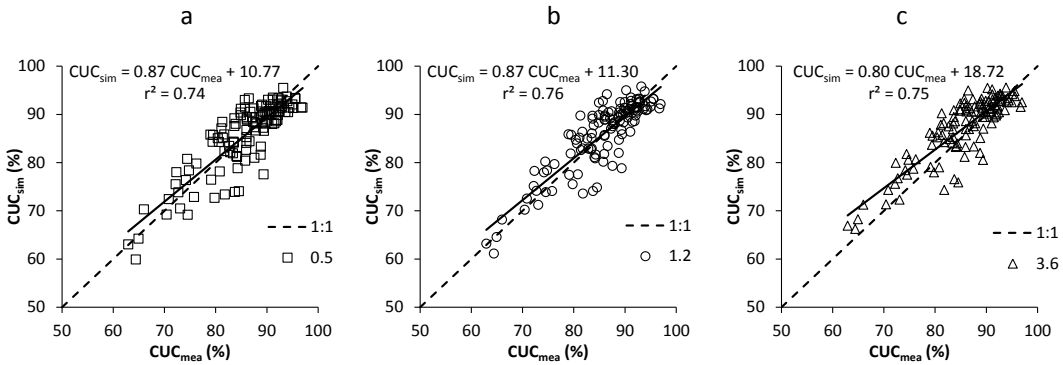

Figure 25. *Relationships of CUC simulated (CUC_{sim}) with respect CUC measured (CUC_{mea}) for 0.5 m, 1.2 m and 3.6 m cell size. Each relationship is shown with different lines.*

Optimization algorithms

The convergence of the algorithms for each model (Weibull, *C'* and ULLN) is reflected in Figure 26. The models with two parameters to calibrate (Weibull and *C'*) simulate 116 times for iteration Figure 26a (Weibull) and Figure 26b (*C'*), while the ULLN distribution (Figure 26c) simulates 224 times for iteration. The optimum values of each model are those combinations of the parameters of the models that produce the minimum value of the objective function.

The boundary values for Weibull distribution (Weibull Figure 26a) are: 0.2-7.0 mm (d_{50}) and 0-5 (n). The drag coefficient thresholds (*C'* Figure 26b) are: 0-4 (K_1) and 0-1 (K_2). Finally, ULLN distribution (Figure 26c) is bounded by: 0.5-7.0 mm (α), -3 to 1 (μ) and 0.3-1.4 (σ). The optimal parameters could exceed these values since a tolerance of 10% has been established for each iteration. Further details of algorithms and tolerances could be found in the MPCOTool manuals (Burguete and Latorre, 2018).

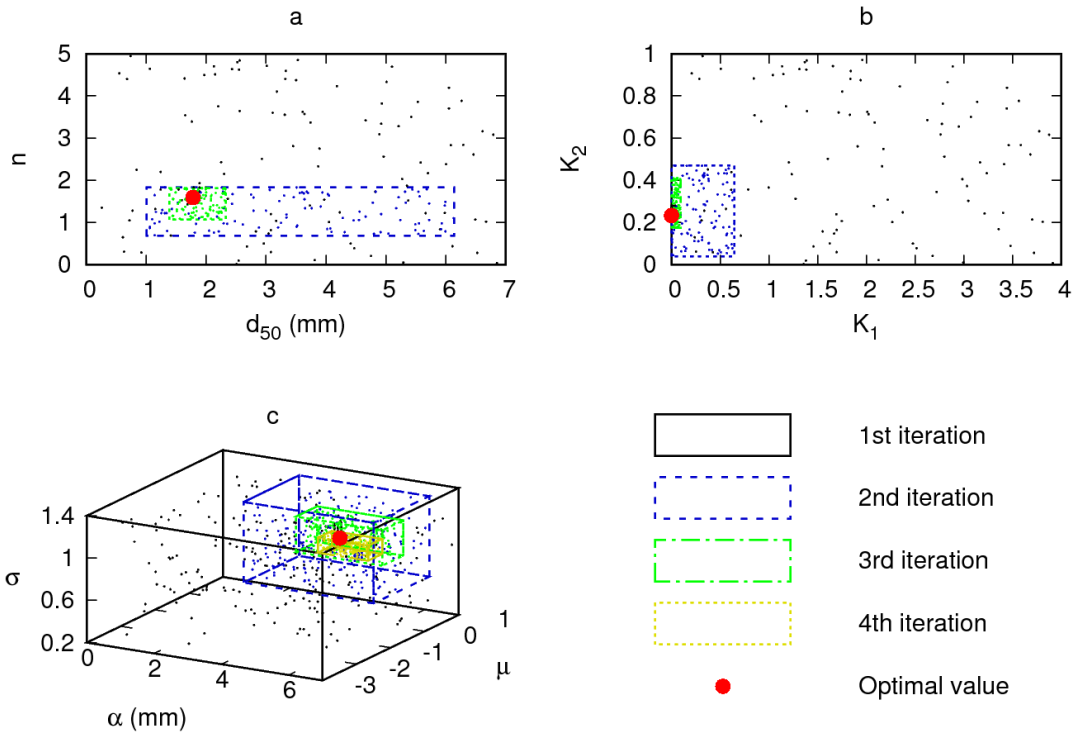

Figure 26. *Convergence of the optimized parameters of the models. a) Weibull, b) C' and c) ULLN. Application case to NAAN sprinkler at 200 kPa. Every point in the subfigures represents a simulation and every delimitation line represents the number of iterations depending on the model.*

ULLN and Weibull distributions in isolated sprinklers

The 40 experiments performed on isolated sprinkler (Table 11) were used to calibrate the volumetric drop size distribution using the Equation 1 (ULLN) and Equation 2 (Weibull). The results of calibrations with both distributions are shown in Table 12. The experiments were performed with wind velocities ranging from 0.39 m s^{-1} to 2.8 m s^{-1} with a minimum pressure of 173 kPa to a maximum of 420 kPa.

According to Table 12, there is no significant difference of *RMSE* between Weibull and ULLN distributions. The average *RMSE* was 0.7 mm hr^{-1} for both distributions. The minimum and maximum values of *RMSE* were similar for both distributions with an average of 0.37 mm hr^{-1} and 1.3 mm hr^{-1}, respectively. The correlation coefficients were also similar ranging from 0.75 to 0.97. In 90% from the 40 cases analyzed the *RMSE* is below 1 mm hr^{-1} for the Weibull as much for ULLN distribution. The *RMSE* average of the other 10% reaches 1.12 mm hr^{-1} for the two distributions. In the Table 12, the maximum values of *RMSE* for both distributions (1.29 mm hr^{-1} and 1.33 mm hr^{-1}, respectively) were found for the same sprinkler type, nozzle size and operating pressure: sprinkler RC130BY, main nozzle size of 5.16 mm and an operating pressure of 385 kPa. Despite low values of *RMSE*, ULLN distribution

requires a large calibration time. For further research to calibrate new irrigation material the recommendation is to establish a target *RMSE* and/or r values to choose the most adequate volumetric drop size distribution.

In this research work, the metrics *RMSE* and *r* were improved using different values of d_{50} and *n* than those by Playán et al. (2006) with the same distribution (Weibull– Equation 2) for the sprinklers RC130 and VYR70. The *RMSE* decreases with the new version of the model from an average value of 2.1 mm h^{-1} to 0.68 mm h^{-1} for the RC130 sprinkler and from an average value of 1.77 mm h^{-1} to 0.55 mm h^{-1} for the VYR70 sprinkler. Also the values of the correlation coefficient were improved from 0.66 to 0.90 for the RC130 sprinkler, and from 0.75 to 0.95 for the VYR70 sprinkler. In agreement with the findings of Playán et al. (2006), our d_{50} optimum parameters (acting as the volume median diameter) show a moderately strong relationship (r^2= 52%) with respect to the operating pressure and nozzle diameters but the optimum values of *n* shown a weak relationship (r^2 < 1%) with respect to the pressure. Although the effect of d_{50} with the pressure is clear for the RC130, RC130BY, SOM30C and VYR70 sprinklers, was not for the rest of sprinkler types. The differences in the optimization methods used in both research works could explain the differences. Since Playán et al. (2006) used a supervised method to select the optimum values of the parameters; the new model uses automatic algorithms (MPCOTool) to select the optimum values.

Moreover, the *EV* (Equation 3) that acts as the mean drop diameter indicates a moderately strong relationship with respect to the operating pressure for both volumetric drop sizes distributions (*r*=0.56). Nevertheless, the *EV* using ULLN and Weibull distributions are statistically different at 95% confidence level after a t-test since the ULLN distribution is more susceptible identifying drop small diameters compared with Weibull distribution. As it is expected, the drop diameter decreases as the operating pressure increases (at higher pressure smaller drop sizes) and as the nozzle size decreases.

In the research work of Zapata et al. (2018) (Chapter III), the authors measured the drop sizes in solid-set plots with different sprinklers using an optical disdrometer. The sprinklers analyzed, also included in our research work (Table 11), were: RC130 (nozzles 4.4 mm + 2.4 mm, pressure 300 kPa), RC130p (pressure of 200 kPa) and NAAN (pressure of 200 kPa). They found smaller drops in the experiments with the sprinkler RC130 (300 kPa) and in the sprinkler NAAN (200 kPa) compared with the sprinkler RC130p (200 kPa). In agreement, they found the larger *WDEL* for the sprinkler NAAN (200 kPa) and lowest losses for RC130p (200kPa). Our semi-empirical results of Weibull distribution confirm their results since the *EV* and d_{50} values (Table 12) indicated larger drop sizes for the sprinkler RC130p (200 kPa) compared with the other two sprinklers. The ULLN distribution indicates the larger drops for RC130p (200 kPa) and also for NAAN (200 kPa).

Table 12. *Calibrations of the Weibull and ULLN parameters for drop size distribution in isolated sprinklers.*

Sprinkler	Main	Pressure	Wind	Weibull					ULLN					
	Nozzle size (mm)	(kPa)	Velocity ($m\ s^{-1}$)	d_{50} (m)	n	RMSE ($mm\ hr^{-1}$)	r	EV (mm)	α (m)	μ	σ	RMSE ($mm\ hr^{-1}$)	r	EV (mm)
NAAN	5.16	173	1.30	0.0018	1.61	0.65	0.91	0.0022	0.0070	-1.02	1.02	0.66	0.90	0.0020
		191	0.79	0.0018	1.54	0.61	0.91	0.0022	0.0068	-0.96	1.10	0.62	0.90	0.0022
		200	1.13	0.0017	1.66	0.49	0.95	0.0020	0.0068	-1.08	0.98	0.43	0.97	0.0019
		303	1.38	0.0017	1.74	0.76	0.93	0.0019	0.0067	-1.09	0.94	0.71	0.93	0.0019
RC130	4.0	200	0.97	0.0017	1.86	0.54	0.88	0.0019	0.0042	-0.40	1.03	0.62	0.85	0.0018
		300	1.17	0.0015	1.82	0.91	0.85	0.0017	0.0051	-0.89	0.93	0.91	0.85	0.0016
		401	0.78	0.0014	1.72	0.67	0.93	0.0016	0.0028	0.07	1.35	0.57	0.95	0.0014
	4.4	200	2.40	0.0017	1.76	0.59	0.92	0.0019	0.0067	-1.10	0.89	0.59	0.92	0.0019
		300	2.80	0.0016	1.75	0.73	0.90	0.0018	0.0061	-1.03	0.90	0.72	0.91	0.0018
		400	1.07	0.0015	2.10	0.65	0.91	0.0016	0.0033	-0.24	1.01	0.68	0.90	0.0015
RC130p	5.16	180	0.61	0.0018	1.64	0.89	0.77	0.0021	0.0038	-0.04	1.33	0.86	0.79	0.0018
		200	0.99	0.0018	1.68	0.57	0.91	0.0021	0.0040	-0.16	1.24	0.57	0.91	0.0019
		220	0.57	0.0018	1.64	0.95	0.78	0.0021	0.0037	-0.02	1.33	0.92	0.79	0.0018
		308	1.20	0.0015	1.65	0.64	0.94	0.0018	0.0036	-0.30	1.17	0.62	0.94	0.0016
RC130BY	4.0	200	1.08	0.0021	1.96	0.37	0.86	0.0023	0.0045	-0.19	1.06	0.38	0.87	0.0021
		285	0.60	0.0016	2.15	0.49	0.90	0.0018	0.0038	-0.29	0.96	0.51	0.90	0.0017
		382	1.12	0.0014	2.28	0.54	0.93	0.0015	0.0040	-0.62	0.81	0.53	0.94	0.0015
	4.5	183	1.18	0.0019	2.09	0.41	0.91	0.0021	0.0049	-0.46	0.94	0.41	0.91	0.0020
		291	1.08	0.0016	2.17	0.44	0.93	0.0018	0.0058	-0.94	0.80	0.42	0.93	0.0018
		400	1.08	0.0016	2.07	0.76	0.84	0.0018	0.0057	-0.90	0.85	0.78	0.83	0.0018
	5.16	201	0.96	0.0018	2.16	0.56	0.93	0.0035	0.0042	-0.27	0.97	0.62	0.92	0.0018
		215	0.62	0.0019	1.75	0.98	0.79	0.0021	0.0042	-0.21	1.19	0.96	0.80	0.0019
		299	1.02	0.0017	1.79	0.93	0.85	0.0019	0.0043	-0.43	1.07	0.94	0.85	0.0018
		385	1.57	0.0017	1.60	1.29	0.76	0.0020	0.0062	-0.95	1.05	1.33	0.75	0.0020
SOM30C	4.0	240	0.63	0.0015	1.33	0.60	0.94	0.0019	0.0040	-0.48	1.34	0.61	0.94	0.0017
		320	0.77	0.0016	1.40	0.55	0.94	0.0020	0.0039	-0.39	1.31	0.53	0.95	0.0017
		420	1.23	0.0014	1.53	0.58	0.95	0.0017	0.0046	-0.80	1.11	0.61	0.94	0.0016
	4.4	240	0.97	0.0017	1.42	0.82	0.90	0.0021	0.0044	-0.50	1.25	0.83	0.90	0.0018
		340	0.44	0.0015	1.46	0.76	0.93	0.0019	0.0039	-0.41	1.28	0.80	0.92	0.0016
		420	0.62	0.0014	1.49	1.01	0.90	0.0017	0.0031	-0.12	1.36	1.00	0.90	0.0015
	4.8	240	0.41	0.0017	1.41	1.14	0.81	0.0021	0.0038	-0.15	1.44	1.07	0.83	0.0018
		330	0.79	0.0016	1.44	0.97	0.88	0.0019	0.0033	-0.11	1.43	0.86	0.90	0.0016
		384	0.69	0.0014	1.27	1.12	0.92	0.0018	0.0033	-0.22	1.54	1.01	0.93	0.0015
		420	0.94	0.0017	1.44	0.65	0.93	0.0021	0.0054	-0.69	1.22	0.69	0.92	0.0020
VYR70	4.0	200	1.95	0.0016	1.50	0.53	0.93	0.0019	0.0053	-0.81	1.11	0.51	0.94	0.0018
		300	1.68	0.0013	1.89	0.52	0.96	0.0015	0.0032	-0.33	1.07	0.53	0.96	0.0014
		400	0.39	0.0014	1.68	0.67	0.93	0.0017	0.0038	-0.47	1.13	0.67	0.93	0.0016
	4.4	200	1.57	0.0016	1.63	0.49	0.95	0.0019	0.0048	-0.65	1.09	0.49	0.95	0.0018
		300	1.06	0.0015	1.71	0.43	0.97	0.0018	0.0056	-0.96	0.99	0.41	0.97	0.0017
		400	1.30	0.0014	1.79	0.68	0.95	0.0016	0.0040	-0.61	1.02	0.66	0.95	0.0015

Calibration of drag coefficient

The optimum parameters of *C'* (K_1 and K_2) obtained from the solid-set experiments of the database (a total of 167) are shown in Appendix A. The presented values are divided in two groups: optimized values for the Weibull distribution and optimized values for the ULLN distribution. Appendix A shows K_1 and K_2 and the reference wind velocity average value of each experiment. Depending on the wind velocity, the uniformity values ranged from 60% to 97%. With respect to the parameters of the drag coefficient *C'*, minimum values of 0.0 and maximum of 4.89 were found for K_1 using the Weibull distribution and values from 0.0 to 4.0 for the ULLN distribution. The values of K_2 remain between 0.0 and 1.2 for Weibull distribution and between 0.0 and 1.0 for ULLN distribution. There is a statistically significant relationship between wind velocity and the *K* parameters of the two distributions. The relationship is weak for K_1, wind speed explains <10% of the K_1 variability for both distributions, while for K_2

parameter there is a moderately strong relationship with respect to wind velocity (wind velocity explains an average of 33% of the K_2 variability for both distributions). Montero et al. (2001) and Playán et al. (2006) showed similar results. The optimum parameters of K_1 and K_2 for both Weibull and ULLN distributions were used to simulate the pluviometry and uniformity of each irrigation event. The *RMSE*, the correlation coefficient *r* and the *CUC* from the calibrations (CUC_{cal}) of both distributions were obtained. The optimum values of K_1 and K_2 of the ULLN and Weibull distribution resulted with the same average value of *RMSE* with 1.0 mm hr $^{-1}$, respectively. In both distributions the standard deviation of RMSE was similar with an average of 0.43 mm hr^{-1}. The correlation coefficients ranged from 0.0 to 0.91 for Weibull distribution while for ULLN ranged from 0.0 to 0.90. In general, low values of the correlation coefficient correspond to high values of irrigation uniformity (*CUC* > 84%) reached under low wind velocity conditions.

For the NAAN, RC130p and VYR70 sprinkler types, the ULLN distribution showed lower values of *RMSE* than the Weibull distribution with an average of 4% for the three sprinklers. Weibull distribution showed lower *RMSE* values than ULLN with an average of 0.8% for the sprinklers RC130, RC130BY and SOM30C. Statistically, there is no significant difference between the mean of *RMSE* for both distributions at 95% confidence level. Statistically, three outlier values of *RMSE* were found for the RC130BY sprinkler equipped with a 5.16 mm main nozzle operating at a pressure of 400 kPa under calm wind conditions had a possible experimental uncertainty.

Analyzing low pressure, just as observed by Li et al. (1994), ULLN and Weibull distributions were quite similar for the sprinklers RC130, VYR70 and SOM30C indistinctly of working pressure and nozzle size. Nevertheless, ULLN distribution reduced the *RMSE* compared Weibull distribution for the NAAN sprinkler using low pressure. Even when the *RMSE* differences are small (0.13 mm hr^{-1}), represents an important amount of the total sprinkler discharge (13%). The modification of the sprinkler suggested by Kincaid (1991) changes the water application profile being necessary to adjust the curve by a more robust distribution as ULLN.

The predictive ability of the proposed ballistic model was also assessed comparing the CUC_{mea} with the calibrated CUC_{cal} (Figure 27). The ballistic model explains 99% of the variability of the CUC_{mea} for both Weibull (Figure 27a) and ULLN (Figure 27b) distributions. Summarizing, the new ballistic simulation model, independently of the volumetric drop size distribution selected, showed a good capacity to reproduce the irrigation uniformity.

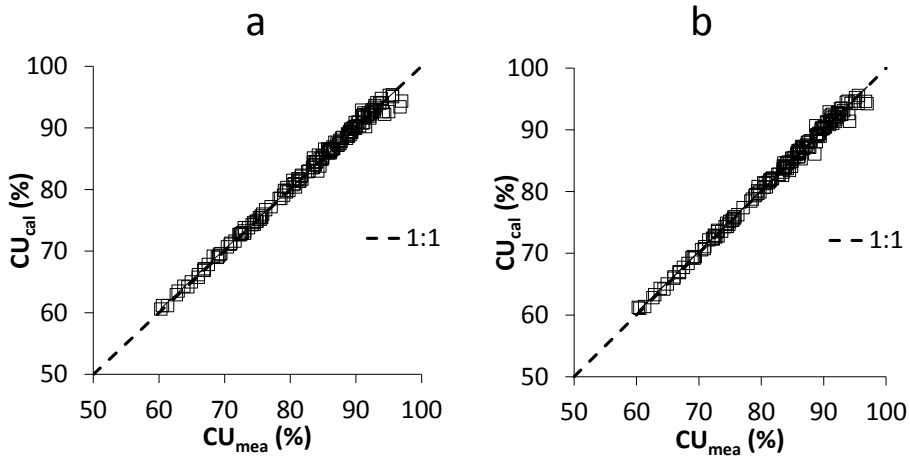

Figure 27. *Relationship between CUC measured (CUC_{mea}) and CUC calibrated (CUC_{cal}) for the whole 167 solid-set experiments database for ULLN (Figure 27a) and Weibull model (Figure 27b). The dotted line represents the 1:1 relationship.*

The K_1 and K_2 values showed in Appendix A were formulated in equations for both distributions Weibull (Table 13) and ULLN (Table 14). The equations were integrated as a function of the operating Pressure (kPa) using linear and quadratic regressions as a function of the Wind velocity (m s^{-1}). The dependent variables *c* and *b* of Tables 13 and 14 were computed through the expression: $x + y\ (Pressure\text{-}z)$; once *c* and *b* are computed, the K_1 and K_2 values are given by the expression: $c * Wind\ velocity^2 + b * Wind\ velocity$, for each sprinkler type. The maximum operating pressure analyzed was 300 kPa for the sprinklers NAAN and RC130p, 420 kPa for the sprinkler SOM30C and 400 kPa for the rest of sprinkler types.

Model validation

The predictive ability of the model was assessed comparing measured *CUC* with simulated *CUC* using LOOCV for both drop size distributions, Weibull (Figure 28a) and ULLN (Figure 28b). The Weibull and ULLN distributions provide a similar coefficient of determination (r^2=0.75). Differences between CUC measured (CUC_{mea}) and *CUC* validated (CUC_{val}) averaged 2.9% and 2.7%, for the Weibull and ULLN distributions, respectively. Again as in the calibration process, the largest differences between CUC_{mea} and CUC_{val} occurred for the high values of CUC_{mea} (low spatial variability of the irrigation pluviometry). Attending to the *RMSE*, the same differences were found for both distributions just as in the calibration process (averages of 1 mm hr^{-1}). In a particular analysis of *RMSE* per sprinkler type, ULLN distribution minimized the *RMSE* for the NAAN and RC130p sprinklers with respect to the Weibull distribution (6.5% and 7.2%, respectively). No differences were observed in *RMSE* for the rest of sprinklers between using one or another distribution.

Table 13. *Coefficients to predict K_1 and K_2 for the solid-set sprinklers analyzed using Weibull distribution.*

Sprinkler	Nozzle size (mm)	**K_1**											
		Pressure ≤ 300						**Pressure > 300**					
		c			b			c			b		
		x	y	z	x	y	z	x	y	z	x	y	z
NAAN	5.16 + 2.5	-0.0085			0.1068	0.0002							
RC130	4.0 + 2.4	-0.0232	-0.0017		0.4787	0.0059		-0.1975	-0.0008		1.0657	0.0069	
	4.4 + 2.4	-0.0679	-0.0005		0.7402	0.0042		-0.1138	0.0001		1.1597	-0.0010	
RC130	5.16 + 2.4	0.0435	-0.0019		0.2971	0.0051							
RC130BY	4.0 + 2.4	-0.0818	-0.0014		0.6922	0.0082		-0.2178	0.0011		1.5115	-0.0072	
	4.5 + 2.4	-0.0031	-0.0014	200	0.3275	0.0071	200	-0.1369		300	0.9968	0.0019	300
	5.16 + 2.5	-0.0162	0.0004		0.2347	-0.0005		0.0282	-0.0080		0.1827	0.0442	
SOM30C	4.0 + 2.4	0.0150	-0.0010		0.3541	0.0034		-0.0640	0.0001		0.6225	0.0012	
	4.4 + 2.4	-0.0042	-0.0001		0.4826	-0.0033		-0.0109	-0.0008		0.2292	0.0074	
	4.8 + 2.4	-0.2264	0.0004		1.5171	0.0024		-0.1965	0.0010		1.7063	-0.0062	
VYR70	4.0 + 2.4	-0.0576	0.0001		0.5511	-0.0015		-0.0428	0.0005		0.4008	-0.0013	
	4.4 + 2.4	-0.0160	0.0003		0.1660	-0.0011		0.0117	0.0004		0.0598	0.0007	

Sprinkler	Nozzle size (mm)	**K_2**											
		Pressure ≤ 300						**Pressure > 300**					
		c			b			c			b		
		x	y	z	x	y	z	x	y	z	x	y	z
NAAN	5.16 + 2.5	-0.0382	0.0003		0.3873	-0.0025							
RC130	4.0 + 2.4	-0.0393	-0.0001		0.2690	-0.0002		-0.0531	0.0004		0.2442	-0.0016	
	4.4 + 2.4	0.0172			0.0027	0.0003		0.0142			0.0281	-0.0003	
RC130	5.16 + 2.4	-0.0829	0.0009		0.5150	-0.0030							
RC130BY	4.0 + 2.4	-0.0113	0.0001		0.2249	-0.0008		-0.0013	-0.0002		0.1405	0.0009	
	4.5 + 2.4	-0.0918	0.0010	200	0.4471	-0.0037	200	0.0006		300	0.0925	0.0004	300
	5.16 + 2.5	0.0096	-0.0004		0.0444	0.0019		-0.0285	-0.0025		0.2383	0.0146	
SOM30C	4.0 + 2.4	-0.0378	0.0002		0.3164	-0.0007		-0.0212	0.0002		0.2627	-0.0012	
	4.4 + 2.4	-0.0471	0.0005		0.3846	-0.0028		-0.0103	-0.0002		0.1740	0.0007	
	4.8 + 2.4	-0.0334	-0.0001		0.3517	0.0004		-0.0439			0.3803	-0.0001	
VYR70	4.0 + 2.4	-0.0240	0.0001		0.2952	-0.0011		-0.0116	-0.0001		0.1884	0.0011	
	4.4 + 2.4	-0.0251	0.0001		0.3083	-0.0011		-0.0108	0.0002		0.1943	-0.0009	

c/b = x+ y (Pressure - z)

*ki = c * Wind velocity^2 + b * Wind velocity*

Table 14. *Coefficients to predict K_1 and K_2* for the solid-set spr*inklers analyzed using ULLN distribution.*

Sprinkler	Nozzle size (mm)	K_1											
		Pressure ≤ 300						**Pressure > 300**					
		c			b			c			b		
		x	y	z	x	y	z	x	y	z	x	y	z
NAAN	5.16 + 2.5	-0.0247	0.0002		0.2210	-0.0005							
RC130	4.0 + 2.4	-0.0550	-0.0009		0.6066	0.0026		-0.1439	-0.0029		0.8651	0.0139	
	4.4 + 2.4	-0.0666			0.7188	0.0018		-0.0715	-0.0004		0.9012	0.0026	
RC130	5.16 + 2.4	-0.0051	-0.0015		0.4000	0.0059							
RC130BY	4.0 + 2.4	-0.1502	-0.0008		1.0756	0.0043		-0.2252	0.0013		1.5064	-0.0082	
	4.5 + 2.4	-0.0118	-0.0012	200	0.3897	0.0057	200	-0.1293	-0.0001	300	0.9333	0.0034	300
	5.16 + 2.5	-0.0469	-0.0004		0.4172	0.0037		-0.0863	-0.0058		0.7830	0.0341	
SOM30C	4.0 + 2.4	-0.0268	-0.0019		0.4802	0.0102		-0.1825	-0.0006		1.2997	0.0053	
	4.4 + 2.4	-0.0303	-0.0013		0.5152	0.0059		-0.1271	-0.0008		0.9658	0.0036	
	4.8 + 2.4	-0.1656	0.0007		1.1364	-0.0034		-0.1085	-0.0012		0.8659	0.0082	
VYR70	4.0 + 2.4	-0.0388			0.3954	0.0004		-0.0435	0.0003		0.4350	0.0004	
	4.4 + 2.4	-0.0075	0.0002		0.0985	-0.0004		0.0118	0.0001		0.0547	0.0021	

Sprinkler	Nozzle size (mm)	K_2											
		Pressure ≤ 300						**Pressure > 300**					
		c			b			c			b		
		x	y	z	x	y	z	x	y	z	x	y	z
NAAN	5.16 + 2.5	-0.0281	0.0002		0.3079	-0.0016							
RC130	4.0 + 2.4	-0.0197			0.1783			-0.0241	0.0007		0.1738	-0.0017	
	4.4 + 2.4	0.0066	0.0001		0.0844	-0.0005		0.0116			0.0378	-0.0004	
RC130	5.16 + 2.4	-0.0654	0.0006		0.4333	-0.0021							
RC130BY	4.0 + 2.4	0.0084	-0.0001		0.1019	0.0003		-0.0007	-0.0003		0.1368	0.0010	
	4.5 + 2.4	-0.0781	0.0008	200	0.4120	-0.0029	200	-0.0043	-0.0001	300	0.1371	0.0008	300
	5.16 + 2.5	0.0061	-0.0003		0.0609	0.0013		-0.0214	-0.0028		0.1891	0.0159	
SOM30C	4.0 + 2.4	-0.0151	-0.0002		0.2182	0.0007		-0.0275	0.0001		0.2746	-0.0003	
	4.4 + 2.4	-0.0398	0.0004		0.3128	-0.0019		-0.0107	-0.0002		0.1655	0.0006	
	4.8 + 2.4	-0.0222	-0.0002		0.2573	0.0006		-0.0360			0.3064	0.0008	
VYR70	4.0 + 2.4	-0.0300	0.0002		0.3368	-0.0014		-0.0130	0.0001		0.1975	-0.0003	
	4.4 + 2.4	-0.0223	0.0002		0.2857	-0.0013		-0.0031	0.0001		0.1581	-0.0003	

c/b = x+ y (Pressure - z)

*ki = c * Wind velocity^2 + b * Wind velocity*

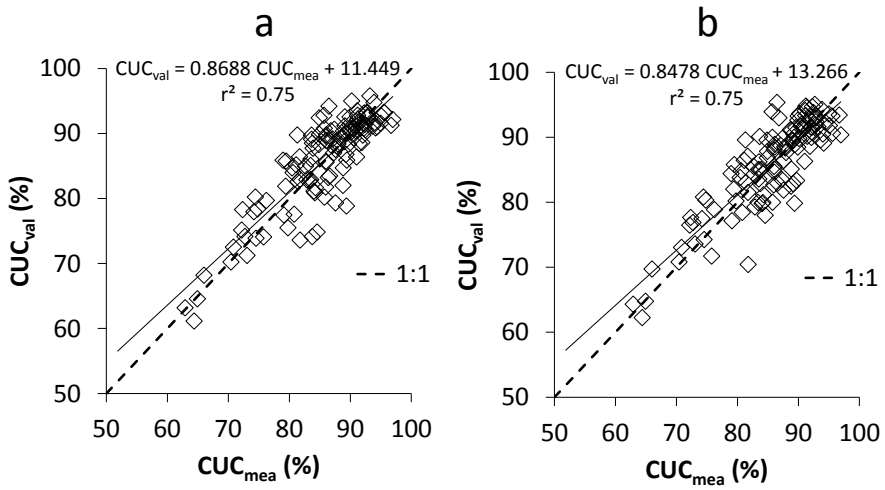

Figure 28. *Relationship between CUC measured (CUC_{mea}) and CUC validated (CUC_{val}) for the whole 167 solid-set experiments database for ULLN (Figure 28a) and Weibull model (Figure 28b). The dotted line represents the 1:1 relationship.*

Computational efficiency

Another feature of the proposed model is that the calibrator MPCOTool enables to perform in parallel all the simulations from the calibrations and validation processes by using a computers cluster. With this parallelization it was possible to perform the calibrations of the 167 solid-set experiments in 11 h using the Weibull distributions while 36 h were required for ULLN distribution using the cluster Trueno (CSIC– Ministry of Economy, Industry and Competitiveness). The previous processes cost around 4 months in a conventional computer.

Conclusions

An improved ballistic sprinkler simulation model with a self-calibration tool and a database of field experiments was presented. The database covers a wide range of experimental conditions with different sprinkler types and layouts, nozzle sizes, operating pressures and meteorological conditions that were used for calibration and validation of the model parameters.

The third order Runge-Kutta method has been the most efficient computationally compared with the commonly used fourth order Runge-Kutta method establishing a maximum error of 10 cm in the drops trajectory calculations.

A wind velocity measurement interval of 30 minutes (just as the information provided by the agrometeorological services in Spain, SIAR network) has been enough to reproduce adequately the water distribution pattern of an irrigation event, when is not possible to measure at lower intervals.

The effect of considering the plot with slope was not very important in terms of the uniformity, particularly for wind velocities lower than 4 m s^{-1} (*CUC* < 5%). This effect was more relevant when the slope is in the direction of the wind velocity and at winds higher than 4 m s^{-1}.

The numerical efforts made in drops generation suggested that bimodal Monte-Carlo sampling method simulated the drops more homogenously minimizing the sampling error and increasing the accuracy with respect to regular systematic sampling and uniform Monte-Carlo sampling methods. The cell size of the terrain where the drops fall, has been defined in 1.2 m reaching an agreement between accuracy and calculation time.

The upper limit lognormal was the most efficient model to reproduce the drop size distribution of the sprinklers especially designed to operate at low pressure. Not differences were found for the rest of the sprinklers using the Weibull or the Upper Limit Lognormal distributions. The predictive ability of the model in terms of Christiansen´s uniformity coefficient in calibration and validation stages was satisfactory (99% and 75%, respectively).

The parallelization of the MPCOTool with the Trueno cluster allowed speeding up the calibrations and simulations processes, minimizing the computing time with respect to a conventional computer (40 times faster).

The auto-calibration procedure incorporated in the model provides a valuable tool for the actualization of the model parameters under new field experiments or under changes in the mathematical definition of the model.

The information provided in tables could be useful in the management irrigation arena at a farm level and irrigation scheduling.

Acknowledgments

This paper applies the “first-last-author-emphasis” approach for the sequence of authors. This research was funded by MICINN of the Government of Spain through grant AGL2013-48728-C2-1-R and AGL2017-89407-R. Octavio Robles received a scholarship granted by the Minister of Economy and Competitiveness of the Spanish Government.

References

Bautista-Capetillo, C., Robles, O., Salinas, H., Playán, E., 2014. A particle tracking velocimetry technique for drop characterization in agricultural sprinklers. Irrig. Sci. 32 (6), 437–447.

Bergstra, J., Bengio, Y., 2012. Random search for hyper-parameter optimization. J. Mach. Learn. Res. 13, 281–305.

Burguete, J., Latorre, B., 2018. MPCOTool: The multi-purposes calibration and optimization tool. Spain: GitHub. http://github.com/jburguete/mpcotool.

Burguete, J., Lacasta, A., Latorre, B., Ambroj, S., Ouazaa, S., Zapata, N., García-Navarro, P., 201Xa. MPCOTool: an open source software to supply empirical parameters required in simulation models. I: model and tests. Submitted to Computers and Electronics in Agriculture.

Burguete, J. Playán, E., Montero, J., Zapata, N., 2007. Improving drop size and velocity estimates of an optical disdrometer: implications for sprinkler irrigation simulation. Trans. ASAE. 50 (6), 2103–2116.

Christiansen, J.E., 1942. Irrigation by Sprinkling. Agricultural Experimental Station Bulletin 670, University of California Berkeley, Berkeley, Calif.

Carrión, P., Tarjuelo, J.M., Montero, J., 2001. SIRIAS: a simulation model for sprinkler irrigation: I. Description of the model. Irrig. Sci. 20, 73–84.

Dechmi, F., Playán, E., Cavero, J., Faci, J.M., Martínez-Cob, A., 2003. Wind effects on solid set sprinkler irrigation depth and yield of maize (Zea mays). Irrig. Sci. 22, 67–77.

Dechmi, F., Playán, E., Cavero, J., Martínez-Cob, A., Faci, J.M., 2004. A coupled crop and solid-set sprinkler simulation model: I. Model development. J. Irrig. Drain. Eng. ASCE. 130 (6), 499–510.

Fukui, Y., Nakanishi, K., Okamura, S., 1980. Computer evaluation of sprinkler irrigation uniformity. Irrig. Sci. 2, 23–32.

Hills, D., Gu, Y., 1989. Sprinkler volume mean droplet diameter as a function of pressure. Trans. ASAE. 32, 471–476.

Kincaid, D.C., 1991. Impact sprinkler pattern modification. Trans. ASAE. 34 (6), 2397–2403.

Kincaid, D.C., Solomon, K.H., Oliphant, J.C., 1996. Drop size distributions for irrigation sprinklers. Trans. ASAE. 39 (3), 839–845.

King, B. A., Winward, T. W., Bjorneberg, D.L., 2010. Laser precipitation monitor for measurement of drop size and velocity of moving spray-plate sprinklers. App. Eng. Agric. 26 (2), 263–271.

Li, J.S., Kawano, H., 1995. Simulating water-drop movement from noncircular sprinkler nozzles. J. Irrig. Drain. Eng. ASCE. 121(2), 152–158.

Li, J., Kawano, H., Yu, K., 1994. Droplet size distributions from different shaped sprinkler nozzles. Trans. ASAE. 37 (6), 1871–1878.

Merriam, L., Keller, J., 1978. Farm irrigation system evaluation: a guide for management. Utah State University, Logan Utah, 271 p.

Montero, J., 1999. Análisis de la distribución de agua en sistemas de riego por aspersión estacionario. Desarrollo del modelo de simulación de riego por aspersión (SIRIAS). PhD dissertation. Universidad de Castilla-la Mancha, Albacete, Spain.

Montero, J., Tarjuelo, J.M., Carrión, P., 2001. SIRIAS: a simulation model for sprinkler irrigation. II. Calibration and validation of the model. Irrig. Sci. 20, 85–98.

Montero, J., Tarjuelo, J.M., Carrión, P., 2003. Sprinkler droplet size distribution measured with an optical spectropluviometer. Irrig. Sci. 22 (2), 47–56.

Mugele, R.A., Evans H.D., 1951. Droplet size distribution in sprays. Industrial and Eng. Chem. 43 (6), 1317–1324.

Playán, E., Salvador, R., Faci, J.M., Zapata, N., Martínez-Cob, A., Sánchez, I., 2005. Day and night wind drift and evaporation losses in sprinkler solid-sets and moving laterals. Agric. Water Manage. 76, 139–159.

Playán, E., Zapata, N., Faci, J. M., Tolosa, D., Lacueva, J.L., Pelegrín, J., Salvador, R., Sánchez, I., Lafita, A., 2006. Assessing sprinkler irrigation uniformity using a ballistic simulation model. Agric. Water Manage. 84 (1–2), 89–100.

RAMA, 2018. Grupo de investigación en Riego, Agronomía y Medio Ambiente. CITA – EEAD-CSIC. Zaragoza España. http://grupo-rama.es/es/.

Robles, O., Cavero, J., Playán, E., Zapata, N., 2017. Assessing low-pressure solid-set sprinkler irrigation in maize. Agric. Water Manage. 191, 37–49.

Salvador, R., Bautista-Capetillo, C., Burguete, J., Zapata, N., Playán, E., 2009. A photographic methodology for drop characterization in agricultural sprinklers. Irrig. Sci. 27 (4), 307–317.

Seginer, I., Nir, D., von Bernuth, D., 1991. Simulation of wind distorted sprinkler patterns. J. Irrig. Drain. Eng., ASCE. 117 (2), 285–306.

Solomon, K.H., Kincaid, D.C., Bezdek, J.C., 1985. Drop size distribution for irrigation spray nozzles, Trans. of ASAE. 28 (6), 1966–1974.

Stambouli, T., Zapata, N., Faci, J.M., 2014. Performance of new agricultural impact sprinkler fitted with plastic nozzles. Biosystems Engineering. 118 (1), 39–51.

Tarjuelo, J. M., Carrión, P., Valiente, M., 1994. Simulación de la distribución del riego por aspersión en condiciones de viento. Invest. Agrar., Prod. Prot. Veg. 9 (2), 255–272 (in Spanish).

Tarjuelo, J.M, 1999. El riego por aspersión y su tecnología. Mundiprensa, Madrid, Spain.

von Bernuth, R.D., Gilley, J.R., 1984. Sprinkler Droplet Size Distribution Estimation from Single Leg Test Data, Trans. of ASAE. 27, 1435–1441.

Vories, E.D., von Bernuth, R.D., Mickelson, R.H., 1987. Simulating sprinkler performance in wind. J. Irrig. Drain. Eng. 113 (1), 119–130.

Yazar, A., 1984. Evaporation and drift losses from sprinkler irrigation systems under various operating conditions. Agric. Water Manage. 8, 439–449.

Zapata, N., Playán, E., Skhiri, A., Burguete, J., 2009. Simulation of a collective solid-set sprinkler irrigation controller for optimum water productivity. J. Irrig. Drain. Eng. ASCE. 135 (1), 13–24.

Zapata, N., Robles, O., Playán, E., Paniagua, P. Romano, C., Salvador, R., Montoya, F., 2018. Low-Pressure sprinkler irrigation in maize: Differences in water distribution above and below the crop canopy. Agric. Water Manage. 203, 353–365.

Zerihun, D., Sanchez, C.A., 2014. Sprinkler irrigation precipitation pattern simulation model: Development and evaluation. USBR.

Zerihun, D., Sanchez, C.A., Warrick, A.W., 2016. Sprinkler irrigation droplet dynamics. I: Review and theoretical development. J. Irrig. Drain. Eng. 142 (5), 04016007.

CHAPTER V. CHARACTERIZATION AND SIMULATION OF THE IRRIGATION OF A ROTATOR LOW-PRESSURE SPRINKLER FOR CENTER PIVOT IRRIGATION SYSTEMS

CHARACTERIZATION AND SIMULATION OF A ROTATOR LOW-PRESSURE SPRINKLER FOR CENTER PIVOT IRRIGATION SYSTEMS[4]

Resumen

Los aspersores de impacto han sido reemplazados por los aspersores tipo spray como una alternativa para reducir los requerimientos de presión en máquinas de riego autopropulsadas y, por lo tanto, reducir la tarifa eléctrica. Además, los modelos de simulación en riego son otra herramienta que permiten mejorar el riego por aspersión en la fase de diseño. En este trabajo de investigación, diversos experimentos fueron realizados para caracterizar el patrón de aplicación de agua de un aspersor rotator aislado de tipo spray bajo diferentes condiciones experimentales. Las evaluaciones se realizaron a dos bajas presiones para seis boquillas bajo diferentes condiciones meteorológicas. Se implementó un modelo balístico para simular el riego modificando su coeficiente de resistencia aerodinámica para la dinámica de gotas. Esta modificación al coeficiente de arrastre consistió en la no dependencia de la velocidad del viento y su cálculo durante la frecuencia de tiempo de las mediciones meteorológicas. Como parámetros de entrada al modelo balístico, se obtuvieron las pérdidas de energía debido al impacto de chorro con la placa del aspersor mediante una técnica óptica. Además, como otro parámetro de entrada, dos distribuciones de gotas fueron calculadas y comparadas en base al mejor ajuste. Para valorar el riego simulado, tres diferentes coeficientes de arrastre fueron evaluados y comparados en ambos procesos de calibración y validación. Las calibraciones se realizaron usando un software libre de optimización. Los modelos de arrastre evaluados fueron: un modelo en función del número de Reynolds para gotas esféricas, un coeficiente de arrastre comúnmente utilizado y el propuesto en este trabajo. Los resultados indican una precisión en las pérdidas de energía (menores del 60%) para ambas presiones de operación con el análisis de cerca de 16500 pequeñas gotas comparado con otros trabajos de investigación. El modelo seleccionado para la distribución de gotas, simuló con precisión la aplicación de agua con un RMSE máximo de 19%. Diferencias significativas se observaron en el riego simulado en la fase de validación comparando los tres modelos de arrastre evaluados. En el peor escenario, el RMSE se disminuyó en 28 % con el modelo propuesto con respecto al modelo convencional, y disminuyó un 4% con respecto al modelo en función del número de Reynolds. Se requiere de más trabajo para evaluar la metodología propuesta para aspersores fijos tipo spray y aspersores de impacto.

Palabras clave: aspersor rotator tipo spray, simulación balística, modelo de arrastre modificado, pérdidas de energía.

[4] Robles, O., Burguete, J., Zapata, N., Félix-Félix, R., Latorre, B., 201X. Characterization and simulation of a rotator low-pressure sprinkler for center pivot irrigation systems. (*In press*)

Abstract

The impact sprinklers had been replaced by spray sprinklers as an alternative to reduce the pressure requirements in self-propelled irrigation machines and, therefore, reduce the energy bills. Moreover, the simulation models are another tool that allows improving the sprinkler irrigation in the designs arena. In this research work, a number of experiments were performed to characterize the water application pattern of an isolated rotator spray plate sprinkler under different experimental features. The evaluations were performed at two low-pressures for six nozzle sizes under different meteorological conditions. A ballistic model was used to simulate the irrigation performance modifying its aerodynamic drag coefficient for drop dynamics. This modification to the drag coefficient consisted in a no-dependence on the wind velocity and its calculation during the frequency time of the meteorological measurements. As input parameters to the ballistic model, the energy losses due the impact of the out-going jet with the sprinkler plate were obtained using an optical technique. Moreover, as another input, two drop size distributions were computed and compared based on its best performance. In order to assess the irrigation performance, three different drag coefficients were evaluated and compared in both calibration and validation phases. The calibrations were performed using a free tool for optimization. The drag models evaluated were as a function of Reynolds number for spherical drops, a drag coefficient commonly used and the one proposed in this work. The results indicate an accuracy of the energy losses (lower that 60%) for both operating pressures with the analysis of over a 16500 droplets compared with other research works. The model selected for the drop size distribution, reproduced accurately the water application with maximum RMSE´s of 19%. Significant differences were observed in the irrigation performance in the validation phase comparing the three drag models evaluated. In the worst scenario, 28% of the RMSE could be decreased using the proposed drag model with respect to the conventional model and decrease 4% with respect the Reynolds model. Further work is needed in order to assess the methodology proposed for fixed spray and impact sprinklers.

Keywords: Rotator spray sprinkler, ballistic simulation, modified drag model, energy losses.

Introduction

Self-propelled sprinkler irrigation systems, lateral move and center pivot systems have become an alternative for irrigation modernization, particularly for large scale landholding (Keller and Bliesner, 1990; Tarjuelo, 1999; Playán et al., 2004). According to the last update of the census of agriculture in Spain, the irrigated land with self-propelled systems has increased approximately in 7% over the last five years (ESYRCE 2012 and 2017). In the same way, in the USA the increment reached 9% between 2008 and 2013 (USDA, 2013).

At the end of the twenty century, fixed spray plate sprinklers (FSPS) and rotating spray plate sprinklers (RSPS) supposed an important improvement on irrigation performance and a reduction of pressure requirements (Faci et al., 2001; Playán et al., 2004) compared with the previous impact sprinklers that equipped the irrigation machines. Currently FSPS and RSPS are the most common sprinkler used in self-propeller irrigation machines. In Spain, the escalating electricity cost and consumption in the last ten years (Moreno et al., 2010; Tarjuelo et al., 2015) is forcing to look for more efficient alternatives from the energy point of view. Low-pressure devices (with pressure requirements between 69 kPa and 103 kPa) have been commercialized in the last years as an alternative to reduce the energy bill.

A number of simulation models have been developed based on experimental data in order to improve the sprinkler irrigation designs. The characterization of the water distributions patterns, the energy losses, the drop size distribution and the wind drift and evaporation losses for FSPS and RSPS have been subject of numerous research (Mugele and Evans, 1951; Solomon et al., 1985; Molle and Le Gat, 2000; Ouazaa et al., 2014; Zhang et al., 2018).

Mugele and Evans (1951) and Solomon et al. (1985) proposed the ULLN model to characterize drop size distributions for impact sprinklers used in sprinkler irrigation machines as pivot or linear-move. Li et al. (1994) and Kincaid et al. (1996) proposed the Weibull model to describe the drop size distribution for impact sprinkler of solid-set systems. Both models are based on the measurement of the drop sizes emitted by the sprinklers. The first methodologies to characterize the drop sizes have been replaced by non-intrusive methods such as the disdrometer (Montero et al., 2003), the photographic method (Salvador et al., 2009) and the particle image velocimetry (PIV, Zhang et al., 2018) or particle tracking velocimetry (PTV, Bautista et al., 2014).

A semi-empirical model to predict the water application pattern in sprinkler irrigation machines was presented by Molle and Le Gat (2000). The authors used a combination of the beta function for adjusting the radial water application of a two nozzle sprinkler used in center pivot system. Their analysis was based on their previous theoretical work. They proposed two models: one for indoor and a second for windy

conditions (up to 6 m s^{-1}). In order to obtain the distributions curves, they divided the drops population into three groups: the ones generated by the deflecting plate of impact sprinkler (to break the main jet) and the two of the jet nozzles. Moreover, they performed a large number of calibrations: each of the two models (indoor and windy conditions) had three parameters to calibrate for the three drop population by experiment. Their results indicated almost negligible differences between measured and simulated values in the validation process and their statistical indexes also indicated a satisfactory predictive ability.

Recently, Zhang et al. (2018) used the PIV technique to characterize the initial drop velocity of a FSPS and simulated the velocities with a computational fluid dynamics software. One of their results indicates an important energy loss of the FSPS jets when impacting the deflecting plate for operating pressures lower than 100 kPa (between 28% and 51% of energy losses). Higher energy losses were presented by Ouazaa et al. (2014) measuring initial drop velocities with the photographic method (Salvador et al., 2009), ranging from 35% to 75%. The differences could be attributed to the methodologies used in each research work.

Ballistic theory has been commonly used to describe drop movements in solid-set sprinkler irrigation models (Fukui et al., 1980; Tarjuelo et al., 1994; Carrión et al., 2001; Dechmi et al., 2003; Playán et al., 2006; Zerihun et al., 2016). To simulate the dynamics of the center pivot sprinklers droplets, first it is necessary to know where the drops are formed, its initial velocity, and its volumetric drop size distribution (Ouazaa et al., 2014).

In the ballistic model proposed by Fukui et al. (1980), the drops trajectories are subjected to a drag coefficient (*C*) that for spherical drops depends on the Reynolds number (Re). This proposal was later modified by Tarjuelo et al. (1994) in order to modeling the effect of the two jets for impact sprinklers. Their studies were based on the findings of Seginer et al. (1991). Tarjuelo et al. (1994) introduced two factors, K_1 and K_2, affecting the drag coefficient (*C'*), describing the effect of the wind velocity and the direction of the drop movement:

$$C' = C\ (1 + K_1 \cdot \sin\alpha - K_2 \cdot \cos\ \beta) \tag{17}$$

with *C*:

$$\begin{aligned} 100 \leq Re \quad & C = -0.0033\, Re + 1.2\ \frac{33.3}{Re} \\ 100 \leq Re \leq 1000 \quad & C = -0.0000556\, Re + 0.48\ \frac{72.2}{Re} \\ Re \geq 1000 \quad & C = 0.45 \end{aligned} \tag{18}$$

where α is the angle formed by the drop velocity vector with respect to the air (**V**) and drop velocity respect to the ground, and β is the angle formed by the vectors **V** and the wind velocity.

Ouazaa (2015) reproduced the water application pattern of RSPS and FSPS using the ballistic model of Fukui et al. (1980) considering the drag coefficient of Tarjuelo et al. (1994). Ouazaa (2015) did not find a significant relationship of Tarjuelo´s drag coefficients and the wind velocity. The author adjusted the *K* parameters to force their relationships with the wind velocity by introducing the Rayleigh distribution functions for each sprinkler type RSPS and FSPS. They found that both models *K* and *K'*, reproduced accurately the RSPS but not the FSPS.

Another problem is that for low wind conditions, the effect of K_1 in the water distribution patter is not important because the factor "$sin \bullet \alpha$" tends to zero (effect on the perpendicular direction of the wind), while the effect of K_2 is more relevant in the leeward direction of the wind producing important changes in the water distribution of RSPS and FSPS.

The objectives of this research are: 1) to characterize the water distribution of a low-pressure RSPS under different combination of nozzle sizes, working pressures and meteorological conditions; 2) to characterize the drops velocities emitted by the sprinkler with these combinations in order to compute the energy losses of the jet impact with the plate using an optical technique; 3) to improve the Tarjuelo´s drag coefficient to reproduce the water application patterns of the experiments as a function of the wind velocity, 4) to calibrate and validate the model addressing the improvements of the new proposed drag coefficient.

Materials and Methods

The RSPS analyzed in this research was the Nutator N3000, equipped with the green plate. The number of nozzle sizes experimentally measured were 6 of the 42 listed in the catalogue 3000 Series 3TN Nozzle System (use of trademarks does not imply endorsement). The sprinkler and nozzles were manufactured by Nelson Irrigation Co. (Walla Walla, WA USA). The sprinkler operates at low-pressures, between 69 kPa and 103 kPa, both tested in this research, and it combines spinning action with a continuously offset plate axis. The green plate has a total of nine grooves (three different grooves repeated three times). The grooves are formed from the center of the plate and have depth and curvature. The jet impacts with the plate dividing it into nine smallest jets. The energy of the impact is used by the plate to rotate and to do precession-nutation movements; throwing the nine jet drops with different horizontal angle up to 21º (no information about the lower horizontal angle is given by the brand).

Experimental set up to characterize the water application patterns

The field experiments were carried out at the facilities of the Agrifood Research and Technology Centre of Aragón located in Zaragoza, Spain. The water application patterns were measured for the Nutator N3000 isolated sprinkler, locating the plate to a height of 2 m from the soil. The experiments were performed under two working pressures of 69 kPa and 103 kPa for the following nozzles size: 2.4, 3.8, 5.2, 6.7, 7.9 and 8.7 mm (N12, N19, N26, N34, N40 and N44, respectively).

The sprinkler was hold to a metallic structure that locates the nozzle at 2 m from the soil. A flow meter was installed before the Nutator sprinkler to verify the discharge. A pressure regulator was installed just before the nozzle. Also a pressure transducer was installed after the regulator and before the nozzle to register the working pressure every minute. A number of experiments were performed for each nozzle size and working pressures, trying to evaluate a range of wind velocities up to 10 m s^{-1}.

The catch can configuration was a square network of 1 m side for the 4 m closest to the nozzle and of 2 m side from 4 m to 20 m from the nozzle location (Figure 29). This configuration was similar to that presented in Faci et al. (2001) for the RSPS evaluations. The range of the network was increased from 20 m to 24 m in the Southeast direction due to the predominant Northwest wind direction in the area. The installed network had a total of 189 catch cans covering an area of 576 m^2 (Figure 29). The catch-cans had a conical shape, with a height of 0.40 m each, a total capacity of 45 mm and they were placed at 0.5 m above the ground.

Meteorological conditions were recorded every minute with a weather station located in situ. Air temperature, air relative humidity, and wind velocity and wind direction were measured. The experiments with the isolated Nutator sprinkler were classified according to its wind velocity. The field data was used for calibrating the optimal parameters and simulate its water application patterns using a ballistic model. Irrigation performance comparisons between calm and windy conditions and between nozzle sizes were performed.

Radial application patterns of the Nutator sprinkler were compared with radial application patterns of FSPS from Ouazaa et al. (2014) for the same nozzle sizes and working pressure (103 kPa).

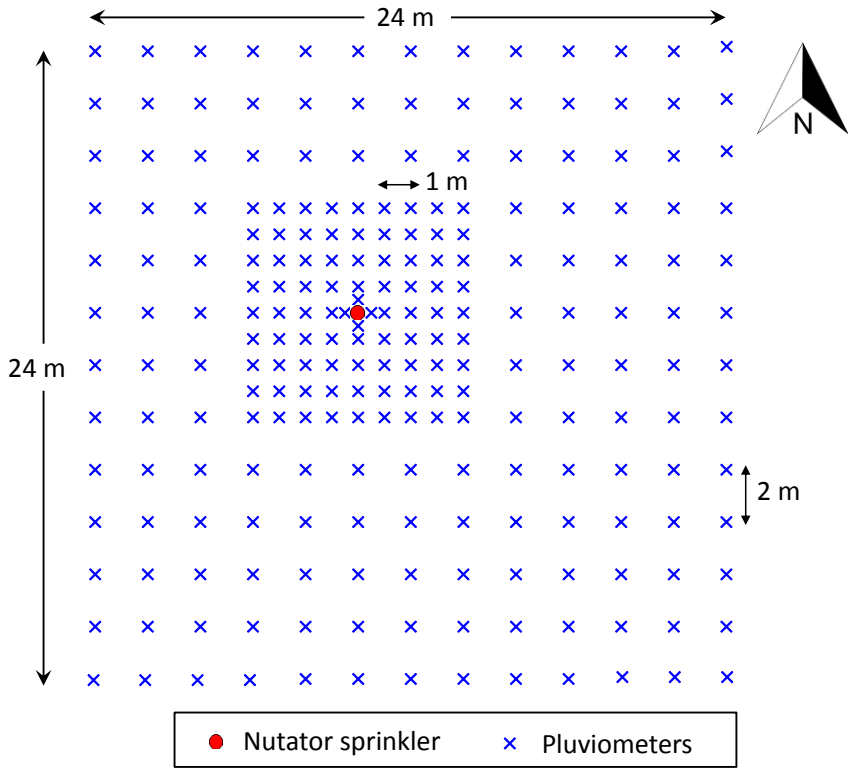

Figure 29. *Experimental set-up for characterize the water application patterns of the isolated sprinkler.*

Experimental set up for drops characterization

The Particle Tracking Velocimetry (PTV) technique of Bautista et al. (2014) modified by Félix-Félix et al. (2017) was used in order to characterize sprinkler nozzle drops. The objective was to quantify the energy losses due the impact of the jet with the sprinkler´s plate. The experiments were carried out under indoor conditions at the laboratory of flow visualization of the Inter-American Institute of Technology and Water Sciences of the Autonomous University of Mexico State in Toluca, Mexico.

The experimental set-up is shown in Figure 30. The installation was composed by a pressurized irrigation system and the optical PTV system. The pressurized system was integrated by: a water tank with a capacity of 0.80 m^3, a hydropneumatic pump with a power of 0.37 kW with a pressure regulating tank, one 400 kPa glycerin manometers, two pressure regulators of 69 kPa and 103 kPa, 22 mm PVC pipeline, Nutator N3000 sprinkler located at an elevation of 1 m above the soil and alternating the nozzles sizes 2.4, 3.8, 5.2, 6.7, 7.9 and 8.7 mm. The sprinkler was surrounded with a plastic sheet for watering a minimum area leaving a zone enough for the outgoing jet.

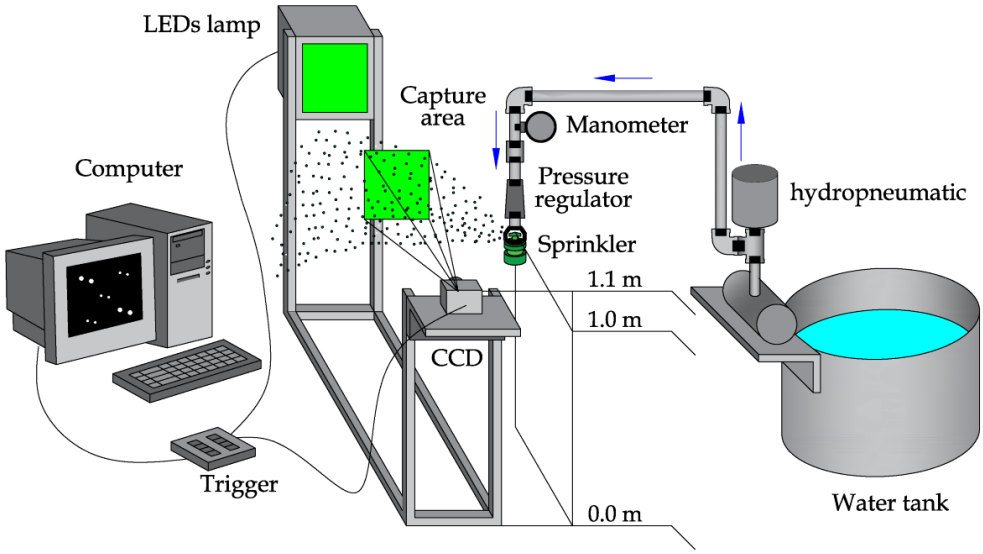

Figure 30. *Experimental set-up for drops characterization. Spacings and components of the hydraulic and optical systems are shown.*

The PTV system with in-line volumetric illumination was integrated by: an illumination system composed by high-power LEDs, a high-speed CCD camera with a temporal resolution of 250 frames per second and a spatial resolution of 1024 by 1040 pixels (the CCD pixel size was 7.4 μm) equipped with a 50 mm lens, optical accessories, a synchronizer NI (trigger) to control the image acquisition sequence and the light. The software for imaging processing PTV SED v2.1 algorithm (Salinas-Tapia et al., 2006) was used. Tests were performed at night, illuminating the capture zone with the LEDs system. Every time that the shutter camera opens, the lamp is activated in two pulses with the trigger, illuminating the drops, then the shutter is closed originating a photograph with a group of drops: the ones captured in the first pulse and its respective pairs in the second pulse. PTV SED was used to obtain drops diameters, drops velocities (both horizontal and vertical components) and drops angles taking into account the coordinates of the drops centroids and the time frequency. With the irrigation system working, pictures were taken at a distance of 0.30 m from the sprinkler at a height of 1.10 m for characterizing the drops (Figure 30). The capture zone in each height was 0.14 m x 0.11 m.

The PTV technique could identify an incorrect drop in the second pulse either because of the high density of particles in an image or the high velocity of the drops (lower than the theoretical velocity of a spherical drop 14 m s^{-1}). Based on the previous post-processing, an analysis was performed to the data in order to guarantee valid drops. In a first stage, the drops that do not follow a consistent behavior in the relationship of drops velocity and angle were rejected. And the second analysis was to apply the inverse trajectory of the drops following the methodology of Sánchez-Burillo et al. (2013). The

drops were returned to the sprinkler position (drops captured at 0.30 m from the sprinkler) using the ballistic theory with a negative time step, the distance and the camera height with respect to the sprinkler. Drops differing 0.05 m of the sprinkler position were neglected.

Finally, the energy losses were computed for each nozzle as the difference between the theoretical velocity (Torricelli's equation) and the drops velocities after the two post-processing analysis. Power regressions were obtained to predict any energy losses for a nozzle size up to 9.9 mm (# 50 of the catalogue) for both operating pressures 69 kPa and 103 kPa.

Further information about PTV technique and image processing could be found in Bautista et al. (2014) and Félix-Félix et al. (2017) and the research work of Sánchez-Burillo et al. (2013) for the inverse simulation.

Simulation of the water application patterns

Ballistic simulation

Considering weight, buoyancy and drag forces; the trajectory of a spherical drop is given by:

$$\mathbf{A} = \left(1 - \frac{\rho_a}{\rho_w}\right) \mathbf{g} - \frac{3\,\rho_a\, C'|\mathbf{U} - \mathbf{W}|}{4\,\rho_w\, d}\,(\mathbf{U} - \mathbf{W}) \tag{19}$$

where **A** is the drop acceleration vector, **g** is the gravity vector, ρ_a and ρ_w are the air and water density, respectively, **U** is the drop velocity vector with respect to the ground and **W** is the wind velocity vector.

Among the numerical methods to solve droplet dynamics, the fourth order Runge-Kutta (RK4) is the most used (Fukui et al., 1980; Vories et al., 1987, Carrión et al., 2001, Dechmi et al., 2003, Playán et al., 2006). In the Chapter IV, the third order Runge-Kutta for solving the Equation 19 was used, establishing an error of 10 cm in drops trajectories and a variable time step demonstrating a decrease of 8.5 % in the calculation time using this RK3 with respect to the RK4 method. Therefore, this methodology was also applied in this Chapter. The following procedures regarding drops generation, drop size distributions and the calibration processes were performed based on the results of the Chapter IV.

Drop size distribution

The experiments of the isolated sprinkler under the lowest wind velocity (<1.5 m s $^{-1}$) for each nozzle size and under two working pressures were used to calibrate two volumetric drop size distributions, ULLN (Equation 20) and Weibull (Equation 21):

$$f(d) = \frac{\alpha \exp\left[-\frac{1}{2}\left(\frac{\beta - \mu}{\sigma}\right)^2\right]}{\sigma\, d\, (\alpha - d)\sqrt{2\pi}} \quad (20)$$

were α is the maximum drop diameter and $\beta(d) = \ln [d/(\alpha\text{-}d)]$

$$f(d) = 0.639\, n \frac{d^{n-1}}{d_{50}^{n}} \exp\left[-0.693\left(\frac{d}{d_{50}}\right)^{n}\right] \quad (21)$$

where *f(d)* is the volumetric probability density function of the total discharge from the sprinkler, d is the drop diameter, μ and σ are the mean and the standard deviation of β, respectively, and d_{50} is the volume mean drop diameter. The ULLN distribution has three parameters α, μ and σ. The Weibull distribution has two parameters, d_{50} and n.

The parameters of both distributions were calibrated using the free software MPCOTool (Burguete and Latorre, 2018). Implements a number of optimization algorithms: regular systematic sampling, Monte-Carlo, orthogonal sampling, hill climbing and genetic algorithms. The explanation of the optimization algorithms, its delimitation, the cell size and the drops simulated, were described in the Chapter IV.

After the calibration process for both distributions, the water application pattern was simulated with the ballistic model. The Root Mean Square Error (RMSE) and the coefficient of correlation (r) of the measured and simulated pluviometry were obtained for ULLN and Weibull, and both RMSE and r were compared. The best model was selected to simulate water distribution pattern of the Nutator sprinklers. Relationships between the model parameters and the nozzle size were established.

Drag model, calibration and validation

In this research, a modification to the Tarjuelo´s equation has been performed. The proposal was made to the K_1 and K_2 parameters of the Equation 17, replacing them with $L_1 \cdot W$ and $L_2 \cdot W$, respectively:

$$C' = C \cdot G \quad (22)$$

with C is the Fukui´s drag coefficient; $G = \max(1 + L_1 \cdot W \cdot \sin\alpha - L_2 \cdot W \cdot \cos\beta, 0.1)$; L_1 and L_2 are dimensionless parameters and W is the wind velocity module (m s $^{-1}$), and the 0.1 constant was used in order to avoid non-physical results (too small or negative drag resistance values).

L_1 and L_2 are now independent of the wind velocity and they were calibrated for each group of experiments of the same nozzle size. In comparison with the Equation 17

where the *K* parameters are constant values during the whole trajectory of drops for each experiment; with the new proposal (Equation 22), *C'* can change with the Reynolds number and computed during the time frequency that the meteorological conditions were measured. Since the meteorology of each experiment was recorded every minute with a weather station located in situ, the value of *C´* can change depending on the experimental conditions.

A simplification on the definition of the *K* parameters has been commonly practiced in order to obtain the drag coefficient for impact sprinklers, RSPS or FSPS (Tarjuelo et al., 1994; Carrión et al., 2001; Dechmi et al., 2003; Playán et al., 2006; Ouazaa et al., 2014; Ouazaa, 2015). This simplification was based on considering the *K* parameters as constant values for experiment generalizing the effects of variable meteorology. In this Chapter V, the meteorological variability of an experiment could be analyzed since the model incorporates the possibility of its simulation.

For assessing the simulation performance of the isolated RSPS, three different drag models were evaluated and compared based on the RMSE of the calibration and validation phases. The drag models assessed were: 1) a function of Reynolds number as proposed by Fukui et al. (1980); 2) *K* coefficients as proposed by Tarjuelo et al. (1994); and 3) *L* coefficients, the new model proposed in this Chapter. The results of the drag models 2 and 3 were compared with the results of the Fukui et al. (1980) model for spherical drops.

In the Fukui et al. (1980) drag model, no parameters needs to be calibrated, since Reynolds number is dependent on the drop size. The RMSE was computed in every experiment for both pressures between measured and simulated, and compared with the RMSE of the calibrations and the validations process of the drag models 2 and 3.

The parameters of the Tarjuelo´s drag model were calibrated for each individual experiment of the isolated sprinkler for both pressures. On the contrary, the parameters of the new model *L* were calibrated by nozzle size groups and working pressure. The methodology commonly used, calibrating each individual experiment, could introduce an overfitting problem because of its failure to predict an experiment with different conditions On the other hand, considering the optimum parameters of a calibration by groups (more data), represents an advantage for validate any case under the range of sizes analyzed generalizing the model and minimizing the errors with less probability to overfit (Burnham and Anderson, 2002).

MPCOTool was used for the calibrations of both drag models, with *K* and *L* parameters. Once the calibration is done, the water application patter was simulated for each nozzle size and working pressure with the ballistic model and the RMSE between measured and simulated was computed for both models.

The validation phase for both drag models was based on the leaving-one-out-cross validation (LOOCV) method (As in the Chapter IV). In LOOCV only one experiment is selected as the validation set and the rest of experiments are used to calibrate. The process is systematically repeated to validate every case. In the Tarjuelo´s model, a linear interpolation between the closest points is used to estimate the coefficients of the validation case. In the *L* model, the constant parameters of the group calibration are introduced in the validation case. The predicted ability of both models was assessed in terms of RMSE (between measured and simulated) and r in validation phase.

Results and Discussion

Water application patterns

Table 15 shows the features of the experiments performed with the isolated sprinkler. The wind velocity of the experiments ranged between 0.6 m s^{-1} and 9.7 m s^{-1}. A total of 33 tests and 7447 pluviometer readings were performed for both operating pressures (69 kPa and 103 kPa). The experiments of the isolated sprinkler under the working pressure of 69 kPa (total of 3774 readings) were performed in 2016 (between May-September) while the ones for 103 kPa (total of 3673 readings) were carried out between October-December 2017 and January-February 2018.

An average of 5 experiments were performed per nozzle size and operating pressure in order to obtain the water application patterns covering calm, medium and high wind conditions. The average wind velocity of the experiments performed on the 103 kPa experiments was higher than for 69 kPa working pressure (Table 15). Maximum wind velocities of 7.7 m s^{-1} and 9.7 m s^{-1} were evaluated for both operating pressures and minimum wind velocities of 0.9 m s^{-1} and 0.6 m s^{-1} were observed for 69 kPa and 103 kPa, respectively.

Depending on the nozzle size and working pressure, the experiments lasted from a minimum of 1 h to a maximum of 3.4 h. The measurements of the operating pressure along an irrigation event, registered with the Dickson pressure transducer, presents small variations, indicating a correct operation of the pressure regulators and a proper functioning of the sprinklers. The maximum standard deviation (SD) of the working pressure was 0.7 kPa and 1.0 kPa for 69 kPa and 103 kPa, respectively. These values represent 1% of the corresponding operating pressure.

Table 15. *Experimental features of the measured pluviometry of the isolated Nutator sprinkler*

Nozzle size (mm)	Pressure (kPa)							
	69				103			
	Tests	Wind velocity range (m s^{-1})	Irrigation time range (h)	Pressure SD (kPa)$^{\Psi}$	Tests	Wind velocity range (m s^{-1})	Irrigation time range (h)	Pressure SD (kPa)$^{\Psi}$
2.4	4	1.1 - 6.9	1.8 - 3.0	0.4	6	0.7 - 8.3	2.8 - 3.4	0.7
3.8	5	1.6 - 6.1	1.8 - 3.0	0.7	6	0.9 - 6.1	2.1 - 3.1	1.0
5.2	5	1.3 - 7.7	1.0 - 2.8	0.4	6	0.4 - 9.4	1.5 - 2.1	0.7
6.7	4	0.9 - 7.4	1.0 - 1.9	0.5	5	0.8 - 8.5	1.0 - 1.1	0.8
7.9	7	0.9 - 5.7	1.0 - 1.3	0.5	6	0.6 - 8.2	1.0 - 1.1	0.9
8.7	8	1.2 - 7.6	1.0 - 1.4	0.5	4	0.6 - 9.7	1.0	0.9

$^{\Psi}$ mean standard deviation-SD- of the pressure measured with the Dickson per nozzle size experiment

The Figure 31 shows measured water distribution patterns for two nozzle sizes, N12 and N44, and two wind conditions, calm and windy, working at 103 kPa. The diameter watered by the N12 was up to 12 m (Figure 31a) while the one for the N44 nozzle was 16 m (Figure31b) under low wind velocity. The experiments under low wind velocity were performed with the wind velocity lower than 1 m s^{-1}, and the high velocity experiments were performed at 6 m s^{-1} for N12 (Figure31c) and at 9 m s^{-1} for the N44 nozzle (Figure 31d). The maximum irrigation depth measured for the N12 nozzle was 6.4 mm hr^{-1} and 3.3 mm hr^{-1} for calm and windy conditions, respectively. While the maximum irrigation depth measured for the N44 was 49 mm hr^{-1} and 25 mm hr^{-1} for calm and windy conditions, respectively. Wind speed is one of the most important environmental factors affecting the quality of sprinkler irrigation (Trimmer 1987; Vories et al. 1987; Playán et al., 2005). The influence of wind speed is related to the type of spray sprinkler, nozzle diameter, working pressure, and nozzle height above the soil surface (Tarjuelo et al. 1999, Faci et al., 2001).

Wind produced a displacement of the water distribution of Nutator in the direction of the predominant wind direction (Figure 31). This displacement was proportional to the wind speed. Under medium wind conditions (data not presented in the figures), water application by the Nutator often resulted in smoothing by the random drift produced by wind blows. Under these conditions the irrigation uniformity could even be improved in the presence of wind (Faci et al., 2001).

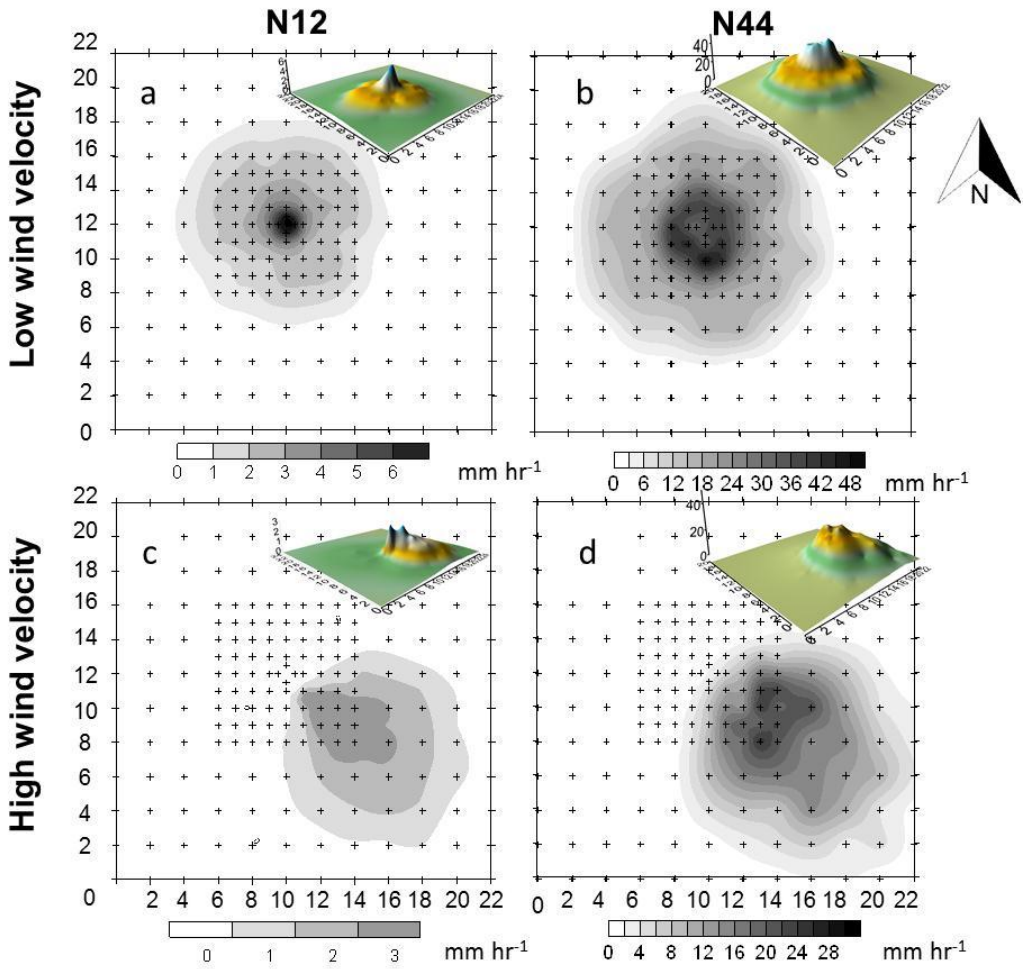

Figure 31. *Measured water distribution patterns at 103 kPa for the nozzle N12 (2.4 mm) and nozzle N44 (8.7 mm) for calm and windy conditions.*

The radial application pattern of the Nutator has a conical distribution shape. This triangular shape in cross section is similar to the impact sprinklers commonly used in solid-set sprinkler irrigation systems. Figure 32 shows the comparison between the radial application patterns of the Nutator sprinkler and the FSPS at the same operating pressure of 103 kPa. The comparison was performed for two nozzle sizes, N26 and N44. The data of the FSPS was obtained from Ouazaa et al. (2014). According to Christiansen (1942), theoretically, the triangular shape as that of the Nutator sprinkler could produce a better uniformity distribution considering the overlapping of the nozzles along the center pivot lateral. On the contrary, the uniformity at overlapping the doughnut/ring shape of the FSPS, resulted in a large variability decreasing the irrigation uniformity. There is a difference in the wetted radius between the two sprinklers at the N26 nozzle of 1.5 m and a difference of 1 m with N44, with the largest wetted area for the Nutator sprinkler. The water distribution pattern of the Nutator sprinkler was similar in shape to the RSPS

sprinkler. The important difference is that the RSPS operates at pressures above 138 kPa while the Nutator can operate at lower pressures, since 69 kPa.

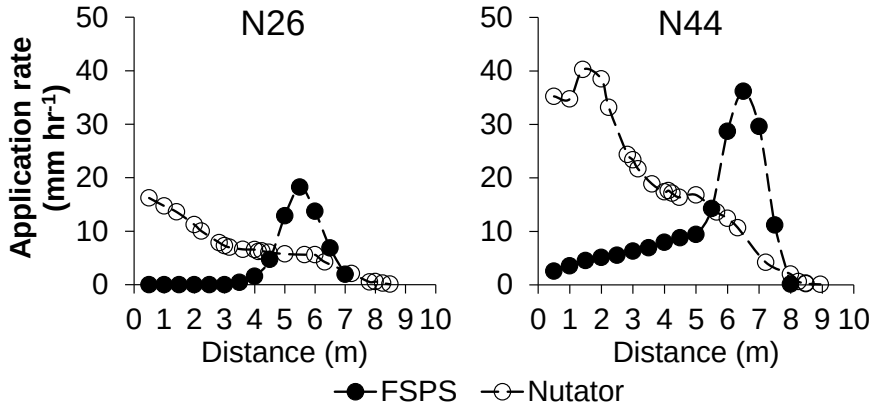

Figure 32. *Measured radial water distribution patterns at 103 kPa for the nozzle sizes N26 (5.2 mm) and nozzle N44 (8.7 mm) for the Nutator sprinkler and the FSPS sprinkler from Ouazaa et al., (2014).*

Energy losses

With the PTV technique, considering the drops of the upper jet a total of 10227 droplets were characterized for the 69 kPa pressure and 6475 for the pressure of 103 kPa. After the post-processing between 30% and 50% of drops were neglected in both operating pressures. Considering all the nozzle sizes for the operating pressure of 69 kPa, the drops flew to an average of 9.1 m s^{-1} (standard deviation -SD- of 0.5 m s^{-1}) and to an average of 17.1º with respect to the horizontal line (SD = 0.2º). For the pressure of 103 kPa the drops had an average velocity of 11.0 m s^{-1} (SD = 1.3 m s^{-1}) and an average of 16.9º (SD = 0.5º). A considerably large drops number was analyzed with the semiautomatic process of PTV technique compared with the labor-intensive low-speed photographic technique (Salvador et al., 2009).

The energy losses of the RSPS are presented in the Figure 33. Power regressions are shown for both operating pressures. For the pressure tests of 69 kPa, minimum losses of 29% and maximum of 50% were observed and for the experiments of 103 kPa the energy losses ranging between 19% and 60%.

Ouazaa et al. (2015) found higher energy losses for FSPS working at 69 kPa (from 40% to 70%). The energy losses observed in this research work are similar to those obtained by other authors using fixed spray late sprinklers (FSPS). Zhang et al. (2018) characterized the drops using an optical technique (PTV) and they found energy losses ranging between 28% and 50% for a pressure of 100 kPa. Sánchez-Burillo et al. (2013) characterized the drops using the photographic technique of Salvador et al. (2009) and after returning the drops to its initial position; they found energy losses between 33% and 74% using an operating pressure of 138 kPa for nozzles diameters between 3.75 mm and

7.97 mm. In agreement with Zhang et al. (2018) and Ouazaa et al. (2015) and the results of this research, sprinkler design should be reviewed for FSPS, RSPS and for Nutator sprinklers to minimize the energy losses, mainly for the smaller nozzle sizes.

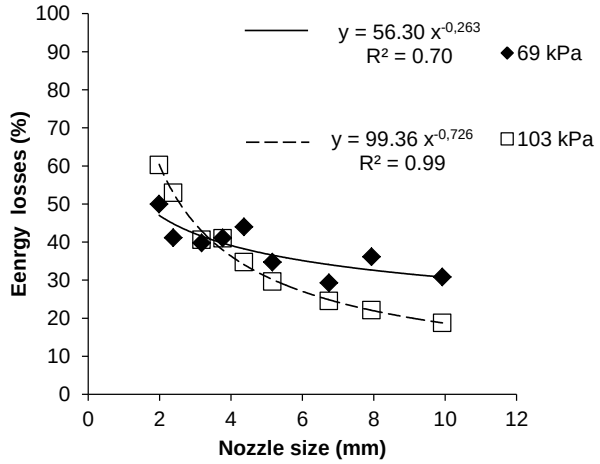

Figure 33. *Estimated energy losses in function of the nozzle size. The energy losses obtained from the initial drops velocity using the PTV technique.*

Ballistic model

Drop size distribution

A total of six experiments (one per nozzle size) of the isolated Nutator sprinkler under low wind conditions (<1.5 m s^{-1}) were selected to calibrate the optimal parameters of both drop size distributions (Weibull and ULLN) for both operating pressures.

A comparison was performed for both drop size distributions in Figure 34 assessing the RMSE between the measured and simulated pluviometry. Each relationship is presented with different symbol for each pressure. The 1:1 line is also represented in the figure. Although slightly higher RMSE was observed using the Weibull model for both pressures, the statistical difference between ULLN and Weibull RMSE´s was not significant at the 95.0% level. Based on previous comparisons and considering the computational costs, Weibull drop size distribution was selected to reproduce the water application patterns of the experiments.

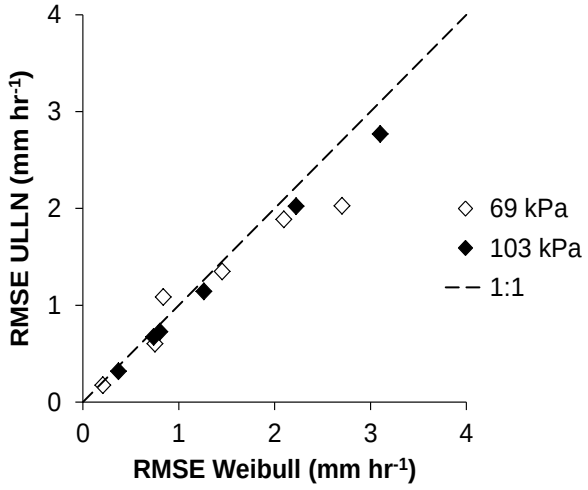

Figure 34. *Comparisons of the RMSE for both drop size distributions ULLN and Weibull for 103 kPa and 69 kPa. Both operating pressures are represented with a different symbol. The dashed line represents the 1:1 relationship.*

Table 16 shows the optimal parameters of the Weibull distribution (d_{50} and n) for both operating pressures and for each nozzle size evaluated. The maximum RMSE was found for 8.7 mm nozzle size, with 2.7 mm hr^{-1} and 3.1 mm hr^{-1} for the pressure of 69 kPa and 103 kPa, respectively. According to our measurements, the maximum RMSE reaches 19% of the total amount of water applied in one hour for both pressures. The Weibull model presents good adjustments with correlation coefficients between 0.93 and 0.99.

Table 16. *Optimal parameters of Weibull drop size distribution model for both operating pressures.*

Pressure (kPa)	Nozzle size (mm)	Flow (LPM)	d_{50} (mm)	n	RMSE (mm hr^{-1})	r
69	2.4	3.0	1.35	1.33	0.21	0.96
	3.8	7.5	1.34	1.51	0.75	0.93
	5.2	14.0	1.47	1.47	0.84	0.97
	6.7	24.1	1.47	1.41	1.45	0.96
	7.9	33.5	1.45	1.45	2.10	0.97
	8.7	40.7	1.45	1.21	2.70	0.98
103	2.4	3.6	0.92	1.34	0.37	0.95
	3.8	9.1	1.09	1.53	0.74	0.96
	5.2	17.1	1.15	1.63	0.80	0.99
	6.7	29.6	1.12	1.58	1.26	0.99
	7.9	41.0	1.14	1.76	2.22	0.98
	8.7	49.8	1.14	1.76	3.10	0.97

The relationship between nozzle size and model parameters was presented on Figure 35. A linear regression model was adjusted between nozzle sizes and parameters d_{50} and n, for pressure of 69 kPa (Figure 35a and 35b) and for pressure of 103 kPa (Fig. 35c and 35d). As expected, the tendency of d_{50} is to increase with the nozzle size, because

larger nozzle generates larger drops, and to decrease with the working pressure. The averages values of d_{50} were 1.42 mm and 1.10 mm for 69 kPa and 103 kPa, respectively. There is a statistically significant difference between the values of *n* for the two working pressures at the 95.0% confidence level after a Fisher´s LSD procedure. Average values of 1.4 and 1.6 were found for *n* at 69 kPa and 103 kPa, respectively. Kincaid et al. (1996) and Ouazaa (2015) working with RSPS, obtained a similar relationship between the model parameters, d_{50} and *n*, and the nozzle size and the working pressure.

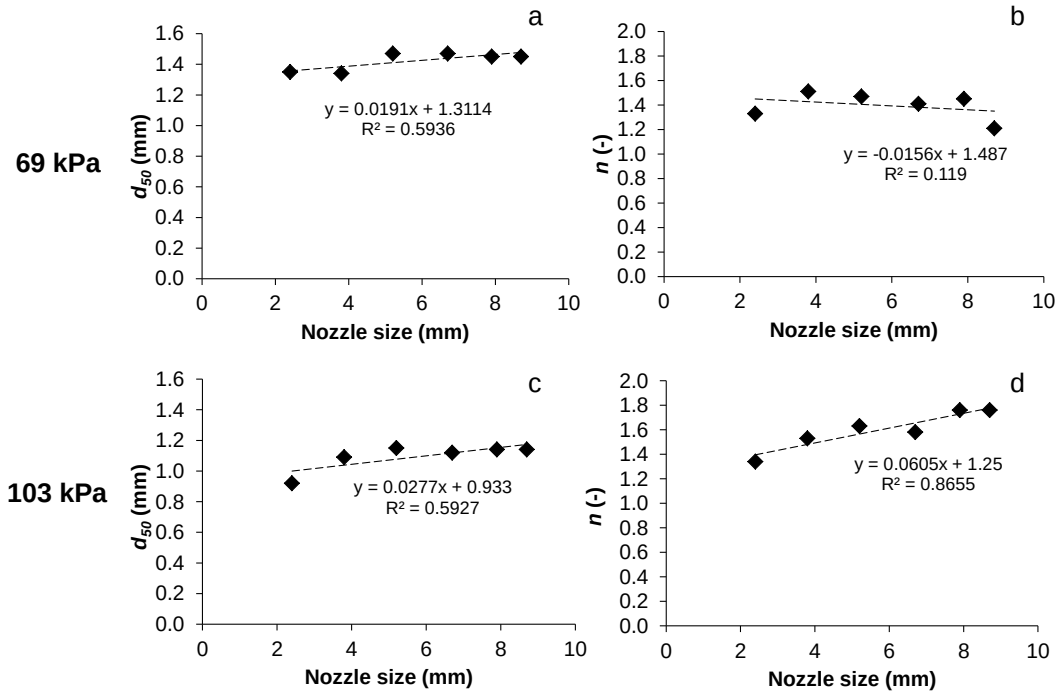

Figure 35. *Optimal parameters of Weibull drop size distribution (d_{50} and n) for both operating pressures 69 kPa (Fig. 35a and 35b) and 103 kPa (Figure 35c and 35d). Dashed line represents the linear regressions for each case.*

Drag coefficient improvements, calibration and validation

The values of RMSE for the calibrations of the drag model of Fukui et al. (1980) was related with the one of Tarjuelo et al. (1994) and with the *L* model for both pressures, the comparisons are showed on Figure 36a for 69 kPa and Figure 36b for 103 kPa. The irrigation was well simulated in the calibration phase using both drag models. The values of RMSE for the three models ranged between 0.18 mm hr^{-1} and 5.10 mm hr^{-1} for the pressure of 69 kPa, while for the pressure of 103 kPa the rank was 0.3 mm hr^{-1} to 6.2 mm hr^{-1}. There are not statistically differences on the RMSE of the three models for both pressures. For the pressure of 69 kPa the RMSE of the *L* model were slightly lower compared with the Fukui et al. (1980) model. The Figure 36b (103 kPa) shows more variability of the RMSE´s between the three models compared with the lowest pressure 69

kPa (Figure 36a). For both pressures, the largest RMSE occurred in the larger nozzle sizes (8.7 mm) using any model, the highest errors are associated to high wind velocities (>5 m s^{-1}) and with the higher water application rate of the large nozzles. For the pressure of 69 kPa the maximums RMSE were 4.5 mm hr^{-1} (*K* model), 4.6 mm hr^{-1} (*L* model) and 5.1 mm hr^{-1} (Fukui´s model), representing 28% and 32% of the water application rate for the 8.7 mm nozzle size. For the pressure of 103 kPa the maximums RMSE were 5.1 mm hr^{-1} (*K* model), 5.2 mm hr^{-1} (*L* model) and 6.2 mm hr^{-1} (Fukui´s model), representing 22% and 27% of the water application rate for the 8.7 mm nozzle size. Both models *K* and *L* computed the calibrations and validations in similar time, 5 days and 5 hours using the *L* model and 5 days and 7 hours with the *K* model.

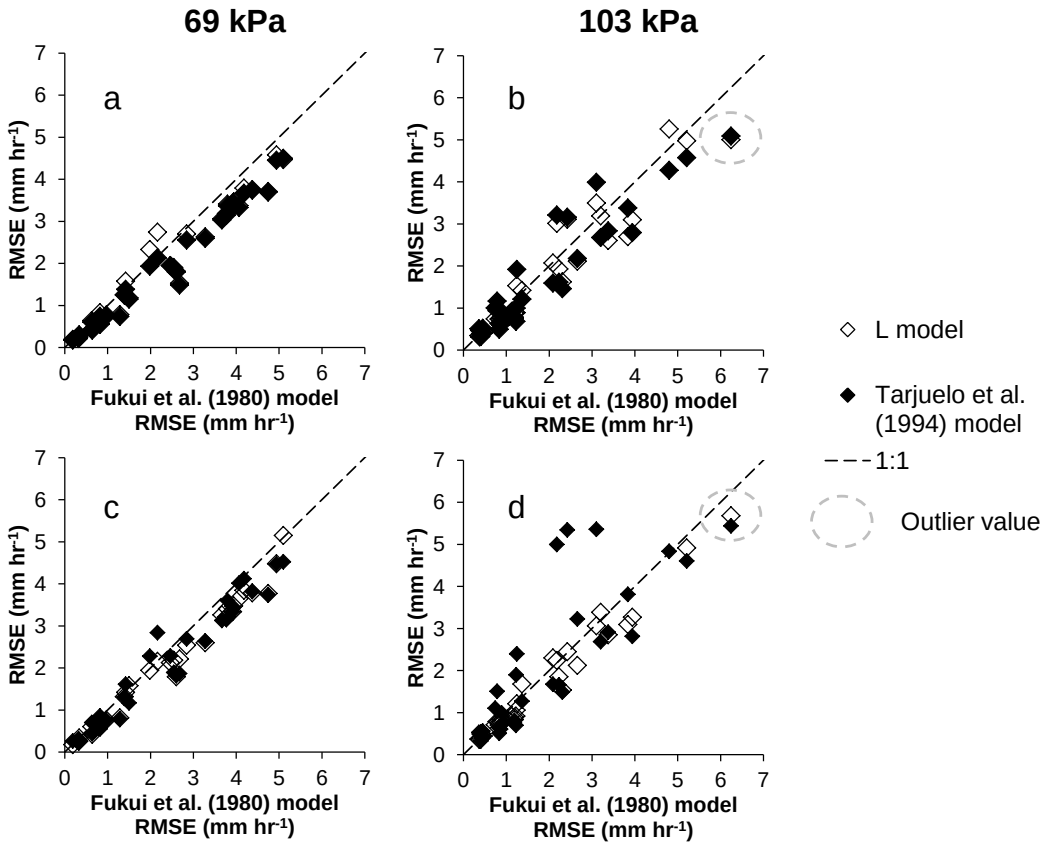

Figure 36. *RMSE comparisons from the calibration (Fig. 36a and 36b) and validation (Fig. 36c and 36d) phases. RMSE of the Fukui et al. (1980) drag model vs. RMSE of the L drag model and Tarjuelo et al. (1994) drag model for both pressures are shown in each figure. Each model compared is shown with different symbol. The 1:1 relationship is represented with a dashed line.*

Although no significant differences were observed between the three models in the calibration phase, slightly larger differences were found in validation. The Figure 36c and 36d shows the 33 experiments validated with the methodology LOOCV for both pressures 69 kPa (Fig. 36c) and 103 kPa (Fig. 36d). The assessment in validation phase is more

relevant than in calibration phase since the blind simulations represents the goodness of a model in a real scenario under unknown conditions. There is not statistically significant difference on the RMSE of the Fukui et al. (1980) model and the *K* model for both pressures at 95.0% confidence level. However, for the pressure of 103 kPa, there are three validations found as the larger differences in the irrigation simulated using the *K* model (Figure 36d). The worst of these was found for the 8.7 mm nozzle size with a RMSE of 5.4 mm hr^{-1} (with the *K* model), and a RMSE of 3.1 mm hr^{-1} (with *L* model and Fukui´s model). These differences represent 24% (*K* model) and 13% (with *L* model and Fukui´s model) of the total amount of water applied in one hour.

Moreover, there is not statistically significant difference between both RMSE of the Fukui et al. (1980) model and the *L* model for both pressures at 95.0% confidence level in the validation phase. However, slightly higher RMSE´s were observed using the Fukui et al. (1980) model with respect to the *L* model for 31 cases in the pressure of 69 kPa and for 24 cases for the pressure of 103 kPa. The maximum RMSE, 6.2 mm hr^{-1}, was found for the 8.7 mm nozzle size working at 103 kPa using Fukui´s model which represents 29% of the total amount of water applied. For same pressure of 103 kPa, the maximum RMSE value with the *L* model is 5.7 mm hr^{-1}, which represents 25% of the total amount of water applied in one hour.

There is an unexpected value (outlier) observed in the Figure 36d it´s also observed in the calibration phase (Fig. 36b). This could be attributed to some experimental problems during the irrigation time of the experiment: 103 kPa, nozzle size of 8.7 mm, wind velocity 4.4 m s^{-1}, irrigation time of 1 h.

The worst cases reproduced in the validation phase with the *K* model (Figure 8d), were under wind velocities lower than 1 m s^{-1}, which indicate a failure in the model of Tarjuelo et al. (1994) at null wind velocities. It is common to establish the k parameters as zero but is not clear where the limit is. On the other hand, the *L* model has a natural transition to the Fukui´s model.

Summarizing, at the validation phase, in the worst scenario, the *L* model improves the irrigation performance on 11% with respect to the *K* model and 4% respect to the Fukui et al. (1980) model.

Figure 37 shows the relationship (adjusted to linear regressions) between nozzle size and the parameters L_1 and L_2 for the working pressure of 69 kPa (Fig. 37a and 37b) and for the working pressure of 103 kPa (Fig. 37c and 37d). The resulting linear regression models showed that there is not a clear effect of the operating pressure on the values of the L_1 parameters. Moreover, the optimal values of the parameters L_1 for both pressures can be considered as zero (Fig. 37a and 37c). As the L_2 values increase the drag coefficient of the drops decreases. The values of the parameter L_2 decreases as the nozzle size increases for the low pressure (Fig. 37b). For the 103 kPa working pressure the relationship between

nozzle size and L_2 parameter is very weak and L_2 can be considered a constant with an average value of 0.06. The previous recommendations given for the Nutator sprinkler used in this researcher could differ in values and/or tendencies against other different sprinklers as RSPS or FSPS.

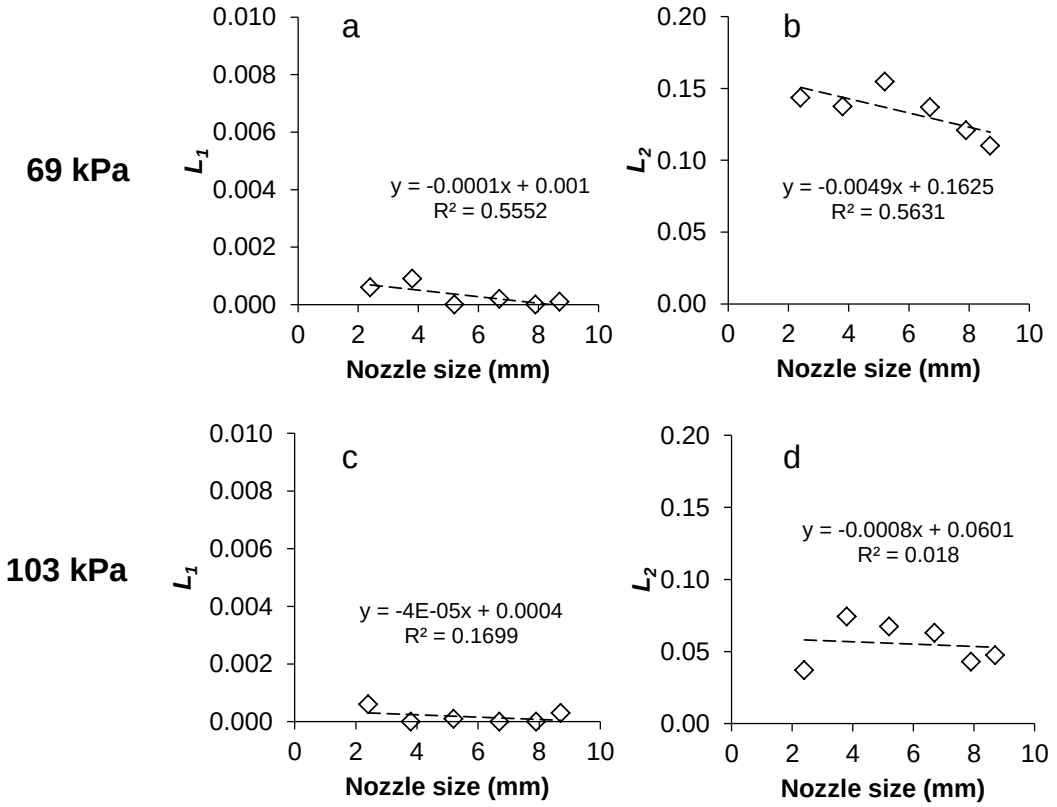

Figure 37. *Optimal values of the L model related with the nozzle size for both operating pressures 69 kPa (Fig. 37a and 9b) and 103 kPa (Fig. 37c and 37d). Linear regressions are shown for each parameter.*

Conclusions

The experimental characterization of a low-pressure rotator spray plate sprinkler was performed covering a wide range of meteorological conditions, nozzle sizes and working pressures.

The radial application pattern of the Nutator sprinkler was observed in triangular shape that could increase the uniform distribution compared with the doughnut/ring-shaped of the FSPS.

The PTV technique allowed to obtained the features of 16702 droplets originated from the sprinkler that were post-processed in order to obtain reliable data for energy losses characterization. This semiautomatic technique represents an advantage in the

number of drops analyzed vs. calculation time with respect to the low-speed photographic technique.

The PTV technique resulted adequate to estimate the energy losses of the Nutator sprinklers. The values of energy losses ranged from 19% to 60% of the total applied.

ULLN drop size distribution reproduced accurately the water application pattern of the RSPS at low pressure as much as the Weibull model, the last one was used for saving computational cost.

A new model has been proposed in this research to simulate the irrigation of a low-pressure rotator spray plate sprinkler based in the modification of the drag coefficient equation.

The properties of the *L* model, as the calibrations/validations by nozzle size and pressure groups (avoiding overfitting), the computation of the drag force within a variable meteorology, the continuous transition of this model to the Fukui´s model for low winds and the possibility of considering any experiment either with low or high wind velocity, represents an advantage over other models improving the drops physics and generalize its use for unknown conditions and new irrigation material.

At the validation phase, the *L* model resulted in lower errors than the *K* model (28%). The *K* model was not accurately for this kind of sprinklers, even compared with the simple drag ballistic model of Fukui without correcting the wind. The *L* model resulted also in slightly lower errors than the Fukui´s drag model (4%).

Five regressions per operating pressure were proposed (energy losses, d_{50}, n, L_1 and L_2) in order to obtain the parameters model for the non-evaluated nozzle sizes in between the minimum (2.4 mm) and the maximum (8.7 mm) evaluated.

The methodology proposed in this research represents an opportunity for reproduce the irrigation of other spray plate sprinklers, RSPS and FSPS. Further work is necessary in order to assess the improved model for impact sprinklers.

Acknowledges

This paper applies the “first-last-author-emphasis” approach for the sequence of authors. This research was funded by MICINN of the Government of Spain through grant AGL2013-48728-C2-1-R and AGL2017-89407-R. Octavio Robles received a scholarship granted by the Minister of Economy and Competitiveness of the Spanish Government. The authors would like to thank to the Inter-American Institute of Technology and Water Sciences in Toluca Mexico for providing the facilities of the flow visualization laboratory and to the Dr. Humberto Salinas-Tapia and Boris López for their support.

References

Bautista-Capetillo, C., Robles, O., Salinas-Tapia, H., Playán, E., 2014. A particle tracking velocimetry technique for drop characterization in agricultural sprinklers. Irrig. Sci. 32 (6), 437–447.

Burguete, J., Latorre, B., 2018. MPCOTool: The multi-purposes calibration and optimization tool. Spain: GitHub. http://github.com/jburguete/mpcotool.

Burnham, K.P.; Anderson, D.R., 2002. Model selection and multimodel inference (2nd ed.). Springer-Verlag, New York. pp. 488.

Carrión, P., Tarjuelo, J.M., Montero, J., 2001. SIRIAS: a simulation model for sprinkler irrigation: I. Description of the model. Irrig. Sci. 20, 73–84.

Dechmi, F., Playán, E., Cavero, J., Faci, J.M., Martínez-Cob, A., 2003. Wind effects on solid set sprinkler irrigation depth and yield of maize (Zea mays). Irrig. Sci. 22, 67–77.

ESYRCE, 2012 and 2017. Encuesta de Superficies y Rendimientos de Cultivos en España. Ministerio de Agricultura Pesca y Alimentación. pp. 101.

Faci, J.M., Salvador, R., Playán, E., Sourell, H., 2001. A comparison of fixed and rotating spray plate sprinklers. J. Irrig. Drain. Eng. ASCE. 127(4), 224–233.

Félix-Félix, J.R., Salinas-Tapia, H., Bautista-Capetillo, C., García-Aragón, J., Burguete, J., Playán, E., 2017. A modified particle tracking velocimetry technique to characterize sprinkler irrigation drops. Irrig. Sci. 35, 515–531.

Fukui, Y., Nakanishi, K., Okamura, S., 1980. Computer evaluation of sprinkler irrigation uniformity. Irrig. Sci. 2, 23–32.

Keller, J., Bliesner, R.D., 1991. Sprinkle and trickle irrigation. Van Nostrand Reinhold, New York.

Kincaid, D.C., Solomon, K.H., Oliphant, J.C., 1996. Drop size distributions for irrigation sprinklers. Trans. ASAE. 39 (3), 839–845.

Li, J., Kawano, H., Yu, K., 1994. Droplet size distributions from different shaped sprinkler nozzles. Trans. ASAE. 37 (6), 1871–1878.

Molle, B., Le Gat, Y., 2000. Model of water application under pivot sprinkler: II. Calibration and results. J. Irrig. Drain. Eng. 126(6), 348–354.

Montero, J., Tarjuelo, J.M., Carrión, P., 2003. Sprinkler droplet size distribution measured with an optical spectropluviometer. Irrig. Sci. 22 (2), 47–56.

Moreno, M.A., Ortega, J.F., Córcoles, J.I., Martínez, A., Tarjuelo, J.M., 2010. Energy analysis of irrigation delivery systems: monitoring and evaluation of proposed measures for improving energy efficiency. Irrig. Sci. 28, 445–460.

Mugele, R.A., Evans, H.D., 1951. Droplet size distribution in sprays. Industrial and Eng. Chem. 43 (6), 1317–1324.

Ouazaa, S., Burguete, J., Paniagua, P., Salvador, R., Zapata, N., 2014. Simulating water distribution patterns for fixed spray plate sprinkler using the ballistic theory. Spanish Journal of Agricultural Research. 12(3), 850–863.

Ouazaa, S., 2015. Development of models for solid-set and center-pivot sprinkler irrigation systems. PhD dissertation. Zaragoza, Spain (http://digital.csic.es/handle/10261/117636).

Playán, E., Garrido, S., Faci, J.M., Galán A., 2004. Characterizing pivot sprinklers using an experimental irrigation machine. Agric. Water Manage. 70, 177–193.

Playán, E., Salvador, R., Faci, J.M., Zapata, N., Martínez-Cob, A., Sánchez, I., 2005. Day and night wind drift and evaporation losses in sprinkler solid-sets and moving laterals. Agric. Water Manage. 76, 139–159.

Playán, E., Zapata, N., Faci, J.M., Tolosa, D., Lacueva, J.L., Pelegrín, J., Salvador, R., Sánchez, I., Lafita, A., 2006. Assessing sprinkler irrigation uniformity using a ballistic simulation model. Agric. Water Manage. 84 (1–2), 89–100.

Salinas-Tapia, H., García, A.J., Moreno, H.D., Barrientos, G.B., 2006. Particle tracking velocimetry (PTV) algorithm for non-uniform and nonspherical particles. Proc. Electron Robot Automot. Mech. Conf. CERMA. 2, 322–327.

Salvador, R., Bautista-Capetillo, C., Burguete, J., Zapata, N., Playán, E., 2009. A photographic methodology for drop characterization in agricultural sprinklers. Irrig. Sci. 27 (4), 307–317.

Sánchez-Burillo, G., Delirhasannia, R., Playán, E., Paniagua, P., Latorre, B., Burguete, J., 2013. Initial drop velocity in a fixed spray plate sprinkler. J. Irrig. Drain. Eng. 139 (7), 521–531.

Seginer, I., Nir, D., von Bernuth, D., 1991. Simulation of wind distorted sprinkler patterns. J. Irrig. Drain. Eng., ASCE. 117 (2), 285–306.

Solomon, K.H., Kincaid, D.C., Bezdek, J.C., 1985. Drop size distribution for irrigation spray nozzles, Trans. of ASAE. 28 (6), 1966–1974.

Tarjuelo, J.M., Carrión, P., Valiente, M., 1994. Simulación de la distribución del riego por aspersión en condiciones de viento. Invest. Agrar. Prod. Prot. Veg. 9 (2), 255–272 (in Spanish).

Tarjuelo, J.M., 1999. El riego por aspersión y su tecnología, 3a Edición. Ediciones Mundi-Prensa, Madrid, España.

Tarjuelo, J.M., Rodríguez-Díaz, J.A., Abadía, R., Camacho, E., Rocamora, C., Moreno, M.A., 2015. Efficient water and energy use in irrigation modernization: Lessons from Spanish case studies. Agric. Water Manage. 162, 67–77.

Trimmer, W.L., 1987. Sprinkler evaporation loss equation. J. Irrig. Drain. Eng., ASCE 113 (4), 616–620.

USDA, 2013. United States Department of Agriculture. National Agricultural Statistics Service. 2014 Census of agriculture. Farm and ranch irrigation survey. Vol. 3, special studies, part 1. Issued November 2014. pp. 100–103.

Vories, E.D., Von Bernuth, R.D., Mickelson, R.H., 1987. Simulating sprinkler performance in wind. J. Irrig. Drain. Eng. 113 (1), 119–130.

Zerihun, D., Sanchez, C.A., Warrick, A.W., 2016. Sprinkler irrigation droplet dynamics. I: Review and theoretical development. J. Irrig. Drain. Eng. 142 (5), 04016007.

Zhang, Y., Sun, B., Fang, H., Zhu, D., Yang, L., Li, Z., 2018. Experimental and simulation investigation on the kinetic energy dissipation rate of a fixed spray-plate sprinkler. Water MDPI. 10, 1365. doi:10.3390/w10101365.

CAPÍTULO VI. CONCLUSIONES GENERALES

De los ensayos agronómicos sobre maíz durante tres campañas de cultivo en los que se comparan tratamientos de presión en boquilla de riego por aspersión se concluye que las diferencias en la uniformidad de riego entre tratamientos de presión no resultan significativas cuando se miden con pluviómetros a 1 m sobre el suelo. La uniformidad de riego de los tratamientos de baja presión decrece rápidamente a medida que se incrementa la altura del pluviómetro, mientras que los tratamientos de presión estándar no muestran ese descenso con la altura del cultivo. Estos resultados indican que, hay que valorar la viabilidad de la metodología en la determinación de los índices de calidad de riego por aspersión cuando la altura de los pluviómetros está próxima al plano horizontal de la boquilla del aspersor.

La diferencia del coeficiente de uniformidad de Christiansen (CUC) estacional entre los tratamientos de baja presión y el de presión estándar es de un 12% de media, superior para el tratamiento de presión estándar. La diferencia del CUC estacional entre ambos tratamientos de baja presión, aspersor convencional y aspersor con placa deflectora en la pala, es despreciable.

La arquitectura foliar de cultivos de porte alto como el maíz tiene un papel importante en la distribución de agua del riego por aspersión. Este papel es más relevante en los tratamientos de baja presión. Las diferencias entre tratamientos de presión en la uniformidad medida sobre el dosel vegetal, se reducen cuando ésta se mide bajo el dosel. Esto explica que no existan diferencias de rendimiento entre tratamientos de presión convencional (300 kPa) y baja presión (200 kPa).

Tras tres años de cultivo de maíz, se puede concluir que el riego con baja presión permite reducir los requerimientos energéticos mientras se mantiene el rendimiento de maíz y el uso del agua. Todo ello sin modificar los espaciamientos convencionales entre aspersores.

Se desarrolló una base de datos de ensayos experimentales de aspersores de impacto que consta de 40 ensayos de aspersor aislado y de 167 ensayos en cobertura total. Ambos tipos de ensayos bajo diferentes características de operación, permitieron desarrollar una herramienta de auto-calibración para la reproducción del riego con la simulación balística. Asimismo los ensayos de cobertura total permitieron establecer una regresión lineal múltiple que estima las pérdidas por evaporación y arrastre de forma más eficaz y general que los modelos anteriores.

Se ha introducido la topografía del terreno en la simulación del riego por aspersión y se han analizado pendientes del 5% en diferentes ángulos con respecto a la dirección del viento. El efecto de la topografía ha resultado mínimo excepto para velocidades de viento superiores a 4 m s^{-1}.

Para la resolución numérica de las trayectorias de las gotas, el método de Runge-Kutta de tercer orden reduce el tiempo de cálculo en 8.5% comparado con el de cuarto

orden (comúnmente usado), admitiendo un error numérico máximo de 10 cm. El paso de tiempo variable basado en la condición de estabilidad reduce los tiempos de cálculo en un orden de magnitud con respecto al paso de tiempo fijo.

Se ha caracterizado un aspersor de baja presión con plato giratorio de movimiento de precesión-nutación (Nutator). El patrón de aplicación de agua es de forma triangular, lo que potencialmente da lugar a mayores uniformidades en su solape comparado con los aspersores de plato fijo.

La técnica óptica PTV, utilizada para caracterizar las pérdidas de carga debidas al choque del chorro con el plato deflector, permite la medida de la velocidad, diámetro y ángulo de miles de gotas de forma rápida por lo que representa una ventaja frente a la laboriosa técnica de fotografía a baja velocidad.

Los nuevos coeficientes del modelo de resistencia aerodinámica en condiciones de viento son constantes, por tanto suponen una mejora porque no interfieren con la variación de la meteorología a lo largo del riego. Además, no modifican la resistencia de una gota esférica para vientos muy bajos. Los coeficientes propuestos reducen los errores de validación en el aspersor Nutator, en el que cabe destacar el mal comportamiento de los coeficientes comúnmente usados.

Líneas futuras

Continuar con los esfuerzos para demostrar a las partes interesadas, agricultores, comunidades de regantes, ingenierías y administraciones públicas, la viabilidad del riego a baja presión en coberturas totales en parcelas comerciales. Incidir en los aspectos del diseño en parcela.

En el tema de modelización, incorporar las novedades y características de los aspersores de baja presión para la simulación, gestión y diseño de una zona regable para operar a baja presión. Hacer especial énfasis en el análisis económico del ahorro energético y en las diferencias en el diseño.

En cuanto al modelo de autocalibración, en aspersores de impacto resultaría interesante incorporar a la base de datos los aspersores de borde comúnmente utilizados en los diseños de la red parcelaria, permitiendo así la simulación completa de la parcela.

Una línea más es en la fase de simulación, es analizar la viabilidad del modelo de modificado de arrastre, para su uso generalizado en aspersores fijos (FSPS) y de rotación (RSPS) de máquinas de riego así como para aspersores de impacto.

Analizar las máquinas de riego tipo pivote o avance frontal equipados con aspersores tipo Nutator, su diseño, las pluviometrías, y sobre todo la calidad del riego. Comparar estos índices de calidad del riego y el consumo energético de las máquinas equipadas con Nutator frente a las equipadas con boquillas FSPS y RSPS para varias campañas de riego con meteorología diversa.

APPENDIX

Sprinkler	Main nozzle size (mm)	Pressure (kPa)	Wind velocity (m s^{-1})	CUC_{mea} (%)	Weibull					ULLN				
					K_1	K_2	CUC_{cal} (%)	RMSE (mm hr^{-1})	r	K_1	K_2	CUC_{cal} (%)	RMSE (mm hr^{-1})	r
NAAN	5.16	200	1.04	89	0.414	0.373	89	0.88	0.07	0.005	0.000	91	0.52	0.74
			2.10	85	0.253	0.446	85	0.75	0.65	0.760	0.433	85	0.72	0.66
			3.59	69	0.055	1.017	69	1.23	0.67	0.217	0.922	69	1.19	0.71
			7.07	67	0.374	0.838	67	1.32	0.71	0.385	0.748	67	1.22	0.74
		300	0.78	93	0.279	0.000	93	0.88	0.13	0.763	0.000	93	0.81	0.07
			1.28	94	0.129	0.017	94	0.57	0.39	0.053	0.016	93	0.59	0.49
			1.84	89	0.098	0.208	90	0.60	0.72	0.056	0.244	89	0.64	0.70
			2.24	86	0.069	0.326	86	0.74	0.72	0.189	0.305	86	0.76	0.71
			4.36	76	0.365	0.579	77	1.05	0.78	0.768	0.494	76	1.05	0.80
			5.00	73	0.686	0.552	73	0.89	0.88	0.803	0.562	73	0.92	0.86
			6.18	74	0.342	0.586	74	1.20	0.82	0.787	0.428	74	1.23	0.79
RC130	4.0	200	3.75	82	1.409	0.460	82	0.45	0.79	1.461	0.385	82	0.44	0.80
			5.35	75	1.858	0.339	75	0.50	0.86	1.665	0.395	75	0.49	0.87
		300	1.23	92	0.776	0.216	92	0.63	0.13	0.701	0.154	92	0.63	0.10
			1.81	85	1.777	0.218	85	0.82	0.51	1.424	0.206	85	0.88	0.40
			2.76	89	0.600	0.345	89	0.49	0.78	0.648	0.355	89	0.45	0.80
			3.23	85	1.894	0.205	85	0.61	0.69	1.677	0.268	85	0.51	0.79
		400	1.65	91	2.706	0.002	92	0.54	0.55	3.982	0.163	92	0.73	0.18
			2.04	88	2.382	0.116	88	0.40	0.85	2.752	0.093	88	0.42	0.81
			2.42	91	1.812	0.197	91	1.53	0.66	1.338	0.260	91	1.51	0.70
			3.83	79	2.826	0.075	79	0.92	0.73	2.773	0.684	79	0.97	0.70
	4.4	200	1.26	86	2.616	0.013	87	0.96	0.02	2.448	0.000	87	0.94	0.02
			2.14	91	0.036	0.087	92	0.46	0.54	0.091	0.270	92	0.54	0.32
			7.56	72	1.821	0.954	72	0.74	0.81	1.728	0.977	72	0.73	0.82
		300	1.07	90	1.975	0.041	91	0.93	0.02	0.211	0.340	90	0.94	0.04
			1.47	92	1.621	0.117	92	0.63	0.32	1.454	0.027	93	0.62	0.36
			3.57	84	2.039	0.225	84	0.75	0.72	2.242	0.165	84	0.68	0.77
			7.63	69	2.433	1.000	70	1.07	0.76	2.740	0.941	69	1.08	0.75
		400	1.06	91	1.707	0.001	91	0.77	0.45	1.889	0.000	92	0.63	0.59
			4.26	76	2.291	0.031	75	1.35	0.67	2.411	0.055	76	1.35	0.67
			7.19	69	2.632	0.798	69	1.55	0.66	2.658	0.729	69	1.62	0.63
RC130p	5.16	200	0.87	86	0.134	0.492	86	1.16	0.00	0.042	0.460	86	1.20	0.01
			1.99	82	1.086	0.563	82	1.19	0.29	1.252	0.461	82	1.15	0.28
			3.19	72	1.046	0.857	73	1.06	0.72	0.823	0.766	72	0.98	0.78

Sprinkler	Main nozzle size (mm)	Pressure (kPa)	Wind velocity (m s^{-1})	CUC_{mea} (%)	Weibull					ULLN				
					K_1	K_2	CUC_{cal} (%)	RMSE (mm hr^{-1})	r	K_1	K_2	CUC_{cal} (%)	RMSE (mm hr^{-1})	r
			4.56	68	2.258	0.646	68	1.15	0.74	1.773	0.631	68	1.14	0.77
		300	0.57	90	0.308	0.165	91	1.18	0.22	0.227	0.194	91	1.05	0.13
			0.77	86	2.090	0.266	87	1.39	0.03	1.137	0.401	86	1.38	0.12
			1.99	81	1.429	0.555	82	1.33	0.47	1.494	0.494	81	1.26	0.49
			2.28	86	0.700	0.352	86	0.89	0.62	1.745	0.270	86	0.85	0.66
			2.34	84	0.335	0.444	84	1.12	0.42	0.880	0.382	85	0.96	0.54
			5.00	63	0.497	1.096	63	1.42	0.79	0.545	0.988	63	1.37	0.83
			5.02	64	0.776	1.200	64	1.33	0.77	1.822	0.759	64	1.34	0.80
RC130BY	4.0	200	1.47	85	0.458	0.385	85	0.56	0.56	2.438	0.000	85	0.48	0.69
			3.06	80	1.767	0.497	80	0.46	0.82	1.475	0.440	80	0.42	0.86
			3.72	71	1.356	0.709	71	0.68	0.79	1.417	0.578	71	0.67	0.80
			5.46	65	1.164	0.888	65	0.68	0.86	1.352	0.809	65	0.70	0.85
			5.86	67	1.349	0.939	67	0.54	0.90	1.423	0.848	67	0.55	0.90
		300	1.42	90	1.710	0.055	90	0.49	0.79	1.903	0.021	90	0.52	0.78
			1.69	87	2.000	0.321	88	0.49	0.77	2.135	0.234	87	0.46	0.81
			2.53	75	2.363	0.377	74	1.03	0.73	2.006	0.464	74	1.03	0.71
			5.64	61	1.718	0.824	61	1.12	0.79	1.344	0.824	61	1.08	0.81
			5.71	66	1.421	0.683	66	0.85	0.83	1.287	0.672	66	0.79	0.86
		400	1.02	90	0.892	0.028	90	0.50	0.69	0.356	0.031	91	0.43	0.79
			4.59	66	1.487	0.518	66	0.75	0.91	1.616	0.532	66	0.77	0.90
			5.63	64	0.861	0.572	64	1.18	0.83	0.702	0.571	64	1.14	0.83
			7.50	75	0.087	0.206	75	1.93	0.55	0.114	0.218	75	1.89	0.59
	4.5	200	0.48	82	0.829	0.993	82	1.85	0.35	0.342	0.995	82	1.86	0.35
			1.14	81	0.121	0.582	82	1.21	0.17	0.000	0.548	82	1.19	0.21
			2.89	79	0.559	0.415	80	0.68	0.72	1.199	0.493	80	0.79	0.64
			3.23	72	1.237	0.577	73	0.78	0.82	0.950	0.590	72	0.85	0.79
			3.61	74	0.698	0.537	74	0.84	0.76	1.134	0.547	74	0.90	0.74
			4.01	73	1.695	0.427	73	1.20	0.55	1.534	0.534	73	1.21	0.55
			2.29	87	1.096	0.126	87	0.62	0.60	1.276	0.102	87	0.69	0.49
			3.25	79	0.837	0.326	80	0.60	0.81	0.924	0.346	80	0.69	0.76
		300	1.05	87	0.096	0.112	88	0.81	0.67	0.133	0.321	87	1.08	0.31
			1.68	90	1.488	0.100	90	0.74	0.34	1.182	0.121	90	0.74	0.25
			2.29	87	1.096	0.126	87	0.62	0.60	1.276	0.102	87	0.69	0.49
			2.43	79	1.911	0.406	79	1.07	0.57	1.262	0.491	79	1.13	0.53
			2.97	79	2.154	0.194	80	0.77	0.79	2.163	0.349	80	0.94	0.70
			5.77	67	1.111	0.560	67	1.05	0.88	1.011	0.653	67	1.11	0.86
			1.33	93	1.188	0.176	93	0.37	0.85	1.466	0.168	93	0.42	0.70

Sprinkler	Main nozzle size (mm)	Pressure (kPa)	Wind velocity (m s^{-1})	CUC_{mea} (%)	Weibull					ULLN				
					K_1	K_2	CUC_{cal} (%)	RMSE (mm hr^{-1})	r	K_1	K_2	CUC_{cal} (%)	RMSE (mm hr^{-1})	r
		400	0.59	91	1.006	0.012	92	0.87	0.65	0.000	0.019	92	0.87	0.65
			2.19	81	0.989	0.456	81	1.72	0.16	2.042	0.452	82	1.72	0.19
			2.35	80	2.730	0.155	81	1.54	0.40	2.570	0.357	81	1.47	0.43
			4.09	77	2.478	0.516	77	0.85	0.82	2.727	0.546	77	0.81	0.82
	5.16	200	0.94	84	0.064	0.016	85	1.11	0.59	0.053	0.020	84	1.08	0.58
			1.04	84	0.051	0.044	85	1.26	0.54	0.000	0.000	84	1.24	0.56
			1.13	84	0.246	0.142	84	1.15	0.54	0.002	0.174	83	1.08	0.60
			1.19	83	0.348	0.112	84	0.80	0.75	0.641	0.102	83	0.79	0.76
			1.35	84	0.487	0.024	83	0.91	0.71	1.262	0.137	84	1.15	0.47
			4.27	76	0.665	0.332	76	0.86	0.83	0.829	0.286	76	0.81	0.85
			5.07	72	0.797	0.493	73	0.90	0.87	0.959	0.521	73	0.89	0.90
		300	1.32	91	0.077	0.236	90	0.94	0.48	0.093	0.232	91	0.99	0.45
			1.78	91	0.073	0.002	93	0.73	0.40	0.000	0.005	93	0.67	0.53
			2.21	83	0.150	0.450	83	1.41	0.51	2.035	0.399	83	1.56	0.33
			2.90	76	1.654	0.723	76	1.55	0.66	2.490	0.514	76	1.57	0.65
			5.03	75	1.473	0.419	75	0.78	0.90	1.495	0.376	75	0.81	0.89
		400	0.40	79	2.423	1.000	80	2.81	0.03	3.761	1.000	81	2.89	0.07
			0.53	81	4.775	0.853	81	2.41	0.35	4.000	0.949	81	2.56	0.30
			0.80	80	0.993	0.951	81	3.23	0.16	0.344	0.985	81	3.27	0.08
			5.22	61	2.950	1.179	61	1.51	0.86	3.746	0.986	61	1.85	0.78
SOM30C	4.0	240	0.39	87	0.120	0.066	87	1.16	0.26	3.700	0.086	88	0.95	0.49
			1.06	91	0.073	0.000	90	0.84	0.40	0.224	0.025	91	0.79	0.60
			1.19	92	0.111	0.005	92	0.63	0.28	0.902	0.002	92	0.65	0.24
			1.47	92	1.226	0.185	93	0.65	0.18	0.269	0.088	92	0.60	0.38
			2.89	90	1.625	0.689	90	0.58	0.57	1.484	0.632	90	0.56	0.71
			4.31	84	1.254	0.988	84	0.72	0.80	0.773	0.857	84	0.79	0.71
			8.01	78	3.881	0.023	79	1.26	0.22	2.315	0.722	78	1.19	0.23
		320	0.52	92	0.516	0.018	92	0.83	0.22	3.743	0.009	92	0.59	0.58
			0.83	91	0.061	0.268	92	0.80	0.34	0.372	0.134	91	0.67	0.55
			0.99	97	0.107	0.017	93	0.53	0.26	1.686	0.168	95	0.47	0.26
			3.49	85	2.314	0.790	85	0.75	0.80	2.557	0.638	85	0.73	0.84
			5.18	90	0.565	0.738	90	0.97	0.48	0.013	0.798	90	0.98	0.51
			6.50	86	1.704	0.814	86	0.72	0.77	1.797	0.549	86	0.82	0.68
		420	0.77	94	0.003	0.002	93	0.78	0.21	3.934	0.232	91	0.87	0.00
			0.82	97	0.013	0.000	94	0.70	0.21	3.724	0.015	94	0.66	0.24
			3.10	89	1.684	0.552	89	1.47	0.61	1.501	0.619	89	1.49	0.63
			5.83	84	2.193	0.771	84	0.82	0.74	2.920	0.725	84	0.85	0.75

Sprinkler	Main nozzle size (mm)	Pressure (kPa)	Wind velocity (m s^{-1})	CUC_{mea} (%)	Weibull					ULLN				
					K_1	K_2	CUC_{cal} (%)	RMSE (mm hr^{-1})	r	K_1	K_2	CUC_{cal} (%)	RMSE (mm hr^{-1})	r
			3.47	89	2.437	0.423	90	0.78	0.53	2.875	0.599	89	0.69	0.65
	4.4	240	0.82	90	0.869	0.337	91	0.92	0.44	0.674	0.005	90	0.63	0.79
			1.84	87	2.379	0.918	87	1.10	0.33	3.455	0.776	88	1.03	0.38
			3.44	86	0.398	0.946	86	0.67	0.72	1.148	0.837	86	0.72	0.68
			3.69	84	2.658	0.026	84	1.40	0.12	0.659	0.017	85	1.17	0.45
			3.74	89	1.104	0.779	89	0.86	0.41	0.212	0.721	89	0.86	0.42
			4.90	84	1.110	1.064	84	0.73	0.76	1.551	0.673	84	0.51	0.88
			5.87	81	3.576	0.625	81	1.15	0.37	2.808	0.486	82	1.20	0.32
		300	1.00	92	0.096	0.306	93	0.74	0.34	2.605	0.239	93	0.77	0.27
			6.39	86	0.512	0.677	86	0.86	0.61	0.663	0.574	85	1.12	0.43
			0.86	94	1.453	0.076	92	0.76	0.18	2.497	0.093	94	0.57	0.44
			2.75	93	0.229	0.361	94	0.63	0.50	0.196	0.363	94	0.79	0.24
			7.14	85	1.520	0.731	84	0.60	0.85	0.837	0.671	83	0.85	0.68
		400	2.50	93	1.983	0.454	94	0.85	0.72	3.652	0.272	93	0.98	0.26
			6.79	89	1.793	0.455	88	1.05	0.33	0.072	0.253	86	1.80	0.52
			0.97	95	1.074	0.125	93	0.90	0.00	1.149	0.221	95	0.62	0.43
			1.50	92	0.436	0.419	92	0.92	0.31	0.047	0.343	92	0.90	0.35
			3.65	89	1.566	0.671	89	0.93	0.64	2.550	0.407	88	1.10	0.53
			5.09	86	3.479	0.117	86	1.28	0.53	0.007	0.553	87	1.26	0.37
	4.8	240	1.14	91	2.264	0.223	92	0.88	0.20	1.119	0.094	91	0.61	0.65
			1.74	89	2.286	0.877	89	1.25	0.11	1.760	0.207	89	1.13	0.28
			4.37	84	0.054	1.012	86	1.37	0.28	0.026	0.808	85	1.40	0.31
			4.88	88	3.687	0.532	88	1.20	0.13	3.341	0.892	87	1.22	0.18
			6.69	85	0.034	0.997	85	1.42	0.07	0.000	0.608	84	1.59	0.00
		320	1.26	93	0.115	0.230	93	1.06	0.06	0.501	0.162	93	1.00	0.22
			1.67	92	2.998	0.247	92	0.91	0.35	2.677	0.296	93	0.85	0.40
			3.62	89	3.481	0.761	89	0.96	0.49	0.362	0.682	89	1.20	0.21
			3.73	86	4.180	1.156	86	1.17	0.54	2.290	0.747	86	1.66	0.12
			7.45	86	2.235	0.125	86	1.56	0.20	0.032	0.499	86	1.75	0.16
			7.65	85	1.059	0.543	87	1.69	0.00	0.756	0.012	86	1.52	0.19
		420	0.80	96	4.891	0.525	95	0.95	0.02	3.577	0.591	96	0.90	0.30
			0.85	96	3.075	0.013	95	0.90	0.18	3.928	0.566	94	0.97	0.13
			1.94	95	0.556	0.355	95	0.90	0.05	0.038	0.548	95	0.82	0.15
			3.60	92	2.022	0.531	92	0.73	0.62	2.930	0.658	91	0.71	0.69
			4.62	86	2.115	0.988	86	1.42	0.46	2.921	1.000	87	1.60	0.31
			5.03	86	2.459	1.006	86	1.49	0.41	2.544	0.893	86	1.52	0.39
			6.55	88	2.628	0.522	88	1.45	0.12	1.104	0.819	88	1.54	0.05
			6.79	86	3.880	0.341	86	1.75	0.16	1.168	0.832	87	1.78	0.06

Sprinkler	Main nozzle size (mm)	Pressure (kPa)	Wind velocity (m s^{-1})	CUC_{mea} (%)	Weibull					ULLN				
					K_1	K_2	CUC_{cal} (%)	RMSE (mm hr^{-1})	r	K_1	K_2	CUC_{cal} (%)	RMSE (mm hr^{-1})	r
VYR70	4.0	200	2.03	86	0.859	0.304	86	0.71	0.50	0.264	0.433	86	0.73	0.49
			2.49	83	0.399	0.612	83	0.88	0.43	0.785	0.565	83	0.87	0.45
			3.37	73	1.755	0.838	74	0.99	0.61	1.142	0.954	74	0.98	0.65
			6.86	69	1.048	0.884	69	0.75	0.79	0.870	0.887	69	0.69	0.82
		300	1.81	88	0.286	0.143	87	0.72	0.52	0.556	0.168	87	0.74	0.47
			2.92	73	0.997	0.550	73	1.39	0.59	0.933	0.555	73	1.29	0.63
			8.42	68	0.384	0.758	69	0.76	0.84	0.625	0.741	68	0.87	0.80
		400	0.38	93	0.589	0.029	93	0.72	0.11	0.425	0.056	93	0.74	0.18
			4.17	75	1.132	0.901	75	1.10	0.74	1.663	0.570	75	1.13	0.73
			9.30	60	3.054	1.075	61	1.49	0.72	3.154	1.000	61	1.57	0.70
	4.4	200	1.19	88	0.931	0.267	88	0.98	0.07	0.401	0.242	88	0.90	0.19
			1.72	89	0.066	0.237	89	0.63	0.52	0.111	0.225	89	0.64	0.49
			3.96	74	0.135	0.979	75	1.00	0.68	0.141	0.922	75	0.95	0.70
			7.88	71	0.383	0.856	71	0.73	0.85	0.339	0.847	71	0.61	0.89
		300	1.39	94	0.058	0.188	94	0.68	0.23	0.053	0.001	94	0.54	0.55
			2.23	89	0.214	0.406	89	0.92	0.40	0.202	0.475	89	0.83	0.49
			6.77	73	0.913	0.813	73	1.04	0.76	0.881	0.905	74	1.03	0.75
		400	0.70	94	0.753	0.025	95	0.95	0.14	0.262	0.006	95	0.85	0.38
			3.99	81	1.082	0.530	80	1.23	0.63	1.275	0.535	81	1.20	0.67
			5.15	70	2.004	0.694	71	1.66	0.70	2.190	0.730	71	1.56	0.75
			6.98	63	3.420	1.002	63	1.62	0.75	2.999	0.966	63	1.53	0.78